Incorporating Flow-Accelerated Corrosion Effects into Probabilistic Risk Assessment

by

Tsu-Mu Kao

B.S., Nuclear Engineering (1980), National Tsing-Hua University, Taiwan, R.O.C.
M.S., Nuclear Engineering (1982), National Tsing-Hua University, Taiwan, R.O.C.

Submitted to the Department of Nuclear Engineering
in Partial Fulfillment of the Requirements for the Degree of

DOCTOR OF PHILOSOPHY

at the

MASSACHUSETTS INSTITUTE OF TECHNOLOGY

September 1998

Signature of Author _____
Department of Nuclear Engineering
July 9, 1998

Certified by _____
George E. Apostolakis
Professor of Nuclear Engineering
Thesis Supervisor

Certified by _____
Ronald G. Ballinger
Associate Professor of Nuclear Engineering
Thesis Reader

Accepted by _____
Lawrence M. Lidsky
Chairman, Departmental Committee on Graduate Students

Incorporating Flow-Accelerated Corrosion Effects into Probabilistic Risk Assessment

by

Tsu-Mu Kao

Submitted to the Department of Nuclear Engineering on July 9,1998
in Partial Fulfillment of the Requirements for the Degree of
DOCTOR OF PHILOSOPHY

Abstract

Traditional probabilistic risk assessments (PRAs), in general, do not include passive SSCs (systems, structures, and components), since they are much more reliable than the active components modeled in PRAs routinely. Aging phenomena, however, may make passive SSCs less reliable than assumed. This thesis investigates the impact of flow-accelerated corrosion (FAC) on carbon steel piping on the secondary cooling system of a PWR.

A stress-strength interference (or reliability physics) model based on physical FAC phenomena (rather than estimating distribution parameters from expert opinions) is proposed. We determined the capacity probability distribution using the KWU-Kastner-Riedle (KWU-KR) FAC model. The uncertainties associated with the KWU-KR model itself are assessed.

The Surry IPE (Individual Plant Examination) has been used as a case study. We calculate the core damage probability (CDP) due to FAC for a 10-year period of time.

The failure probability due to the steady-state pressure is dominated by epistemic uncertainties. Since the hazard function is meaningful for aleatory failures only, it cannot be calculated in this case. However, the failure rate due to transients can be calculated, because they involve aleatory uncertainties. Our calculations show that the failure rate due to transients can be approximated by a straight line, as the linear aging model postulates. We point out that this is not the total impact of FAC, since the failure due to the steady-state pressure is not included.

FAC has some impact on the probability of the accident sequence initiated by the LMFW (Loss of Main Feedwater). However, the CDP due to FAC has insignificant impact on the 10-year total CDP. The main reason is that the contribution to the total core damage frequency from LMFW in Surry is small.

Thesis Supervisor: George E. Apostolakis
Title: Professor of Nuclear Engineering

Acknowledgments

I would like to thank Professor George Apostolakis, a great advisor who opened the door of PRA for me and let me see the beauty of this science. Ten times of discussing and correcting my thesis in the last stage and three times of practicing my thesis defense in front of him were unforgettable experiences.

I thank Professor Ronald Ballinger who served as my thesis reader and Professor Michael Driscoll who reviewed the English in my whole thesis. I also thank Professor Sow-Hsin Chen, who not only served as my thesis committee member, but also gave me much advice during my study.

This thesis would not have been written without the help of many people to whom I am indebted. Mr. Curtis Smith in SAPHIERE code aspect and Dr. Vikram Shah in material aspect at INEEL (Idaho National Engineering and Environmental Laboratory) were most helpful in the whole period of this thesis work. Dr. Jya-Syin Wu and Dr. Nathan Siu provided very good suggestions in the early stage of my thesis that were appreciated.

I also thank the support from friends during my study. Those friends are Dr. John Bernard, Dr. Robert Mulvihill, Ms. Mary McPeak, Ms. Clare Egan, Ms. Emanuela Binello, Mr. Christopher Garrett, Ms. Vicentica Valdes, Ms. Sarah Abdelkader, Ms. Suchandra Tina Ghosh, Mr. Mark van der Helm, Dr. Wen-Yih Tseng, Dr. Chi Kao, Dr. Jec-Kong Gone, Dr. Lin-Wen Hu, Dr. Xinhui Chen, Mr. C. C. Chen, Mr. Rai-Fong Su, Mr. C, C. Niu, Dr. Li-Fu Lin, Dr. J. R. Wang, Reverend Tsu-Kung Chuang and his wife .

I would above all like to thank my wife, May, for her love, support, and boundless patience. She is in the fullest sense, a dearest companion. She gave up her personal ambitions to follow me, and directed her energy, patience, and unending love toward raising our children and supporting her husband. I must praise my daughter, Cindy, for never

forgetting to encourage her father at the right time and my son, little Michael, for being a generally happy boy.

I am indebted to my father-in-law and mother-in-law for their help during my second year of study. I would like to dedicate this thesis to my father: although he died when I was a child, he is always in my mind. I am deeply grateful to my mother who instilled in me a deep love and raised her children independently after my father's death.

Funding for this project, which was provided by INEEL through ASCA (Advanced System Concepts Associates), Inc., is appreciated. I am also grateful to Taiwan's National Science Council and Institute of Nuclear Energy Research (INER) for supporting me during my first three years of study. I would like to thank Dr. Der-Yu Hsia, director of INER, who sent me here for advanced study after I had been away from school for 12 years and encouraged me during the hard times of my study.

Finally, as a scientist, I do appreciate the meaning of a line in a book. It reads, "When the answers are simple, then you hear God thinking." I would like to attribute this thesis work to the God.

Author with his family (from left): Cindy, Michael, and May.

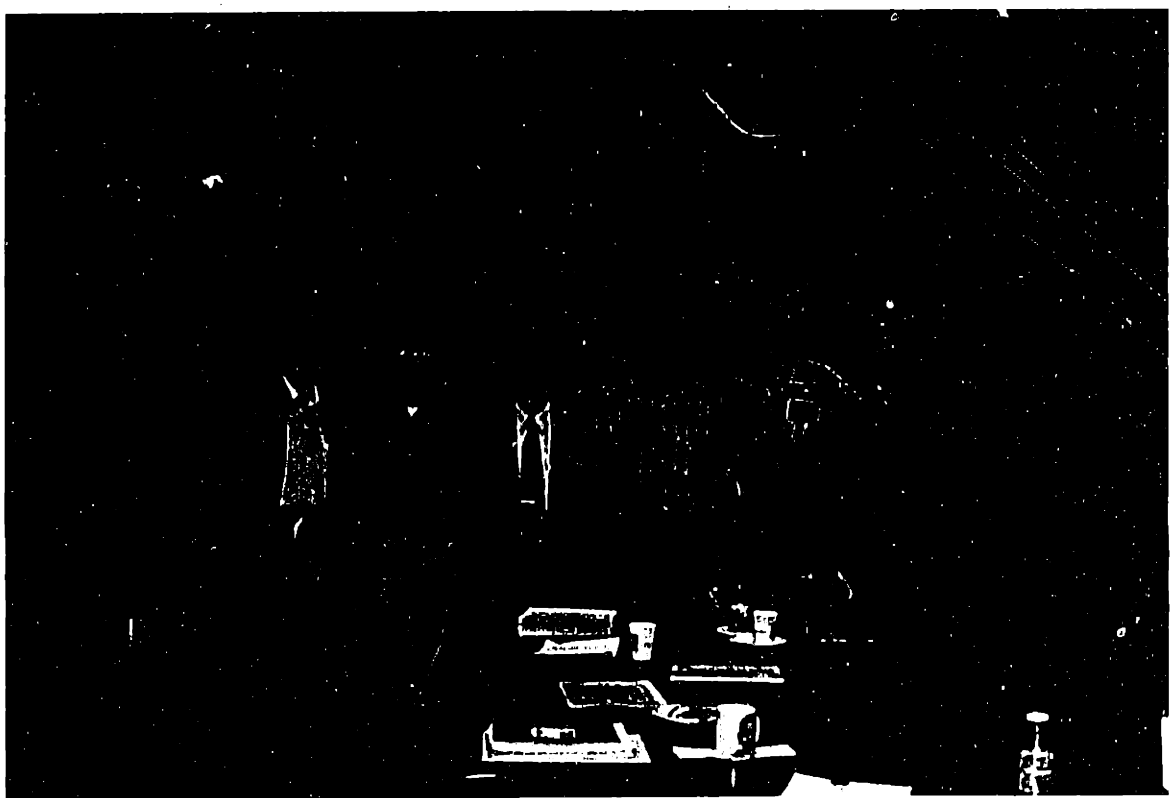

Author with his thesis committee members (from left): professors Sow-Hsin Chen, Ronald Ballinger, George Apostolakis, Michael Driscoll, and Kenneth Czerwinski.

Table of Contents

Title 1

Abstract 2

Acknowledgments 3

Table of Contents 6

List of Figures 11

List of Tables 13

Chapter 1: Introduction **Page**

1.1 Background and Motivation 14

1.2 Research Objectives 16

1.3 Previous Work 17

1.3.1 Flow-Accelerated Corrosion (FAC) 19

1.3.2 Probabilistic Risk Assessment (PRA) 22

1.4 Comparison of PRA Models 23

Chapter 2: Flow-Accelerated Corrosion (FAC) Models

2.1 Introduction 25

2.2 Review of FAC Database and Associated Models 25

2.3 Overview of Single-Phase FAC 33

2.4 Overview of Two-Phase FAC 39

2.5 Selection of FAC Empirical Models 42

2.6 Details of the KWU-Kastner-Riedle (KWU-KR) FAC Model 46

2.7 Comparison of the EPRI-CH and the KWU-KR Models 50

2.8 Comparison of the Calculated FAC Results Using Two Different Models 52

2.8.1 Comparison of results with the KWU-WATHEC Code 53

2.8.2 Comparison of results with the EPRI-CH Code 55

2.9 Application of the KWU-KR model to Four Events 57

2.10 Local and Uniform Wall Thinning Effects 58

Chapter 3: Development of Quantitative Methods **Page**

3.1 Development of Stress-Strength Interference Model 59

3.2 Determination of the Capacity 61

3.2.1 Hoop Stress Analysis 65

3.2.2 Piping Design Codes 66

3.2.3 Piping Failure Analysis 66

3.3 Determination of the Load 69

3.3.1 Steady State Load 69

3.3.2 Transient Load 69

3.4 The Monte Carlo Simulation 73

Chapter 4: Integration of FAC into Existing PRAs **Page**

4.1 Methodology for Screening and Analysis 75

4.1.1 Identification of Important FAC Scenarios 77

4.1.2 Determination of Consequences 77

4.1.3 The Role of Inservice Inspection 78

4.2 PRA models 79

4.3 General Procedure for Detailed Analysis 80

Chapter 5: Case Study

5.1 Introduction 83

5.2 The Surry IPE in SAPHIRE 83

5.3 Failure Probability Determination of Case study 85

5.4 Indirect Effects 87

5.5 Consequence Assessment 87

Chapter 6: Conclusions, and Recommendations for Future Work 94

References 96

Page

Appendix A: Four Case Studies of FAC events 105

A.1 Case 1: Surry Unit 2, a Single-Phase FAC Case 105

A.1.1 Event Description of Case 1 105

A.1.2 Additional Information Regarding Case 1 106

A.1.3 Results of Case 1 107

A.2 Case 2: Trojan, another Single-Phase FAC Case 108

A.2.1 Event Description of Case 2 108

A.2.2 Additional Information Regarding Case 2 109

A.2.3 Results of Case 2 109

A.3 Case 3: Millstone Unit 2, a Two-Phase FAC Case 111

4.3.1 Event Description of Case 3 111

4.3.2 Additional Information Regarding Case 3 111

4.3.3 Results of Case 3 111

A.4 Case 4: Fort Calhoun, another Two-Phase FAC Case 112

4.4.1 Event Description of Case 4 113

4.4.2 Additional Information Regarding Case 4 114

4.4.3 Results of Case 4 115

A.5 Determination of the Parameter Uncertainties 116

Page

A.5.1 Single-Phase Flow (Cases 1 and 2) 116

A.5.2 Two-Phase Flow (Cases 3 and 4) 117

A.6 Summary of 4 Case Studies 118

Appendix A-1: Detailed Calculations of Case 4 122

Appendix B: Detailed FAC Rate Calculations of Case Study 125

Appendix C: Detailed Failure Probability Calculations of Steady State 128

Appendix D: Detailed Failure Probability Calculations due to Transients 132

List of Figures

	Pages
Figure 1-1. Illustration of differences between traditional and aging physics PRA models.	24
Figure 2-1. Comparison of the EPRI-CH and the KWU-KR models.	34
Figure 2-2. The calculated influence of fluid temperature on the ferrous ion concentration and on mass transfer of ferrous ions.	35
Figure 2-3. Schematic of a feedwater system for a Westinghouse plant steam generators equipped with preheaters.	40
Figure 2-4. KWU-KR FAC model, comparison against single laboratory data.	44
Figure 2-5. KWU-KR FAC model, comparison against single and two-phase both laboratory and plant data.	44
Figure 2-6. EPRI-CH FAC model, comparison against single laboratory data.	45
Figure 2-7. EPRI-CH FAC model, comparison against single and two-phase both lab and plant data.	45
Figure 2-8. The factor f(t) versus t (hrs) in the KWU-KR model.	49
Figure 2-9. The Mathcad results using the KWU-KR model.	54
Figure 2-10. Results corresponding to those of Figure 4-1 using the KWU-WATHEC code.	54
Figure 2-11. Comparison of the EPRI-CH and the KWU-KR models by changing of velocity.	55
Figure 2-12. Comparison of the EPRI-CH and the KWU-KR models by changing of dissolved oxygen content.	56
Figure 2-13. Comparison of the EPRI-CH and the KWU-KR models by changing of pH.	56

Pages

Figure 3-1. Stress-strength interference model. 60

Figure 3-2. Stress-strength interference model at different times ($t_2>t_1$). 60

Figure 3-3. Comparison of values calculated by empirical model with measurements from laboratory experiments and in power stations. 62

Figure 3-4. Example of a transient load. 69

Figure 3-5. Schematic representation of steady state load (L_{ss}) and transient load (L_{tr}) processes and degradation of capacity ($t_2>t_1$). 70

Figure 4-1. Risk questions applied to FAC. 76

Figure 5-1. The selected pipe segment of the Surry NPP. 86

Figure 5-2. Results of failure probability calculations. 89

Figure 5-3. Results of failure rate calculation at transient of the Surry pipe segment. 90

Figure A-1. Pdf and cdf results of Case 1 and Case 2. 120

Figure A-2. Pdf and cdf results of Case 3 and Case 4. 121

List of Tables

Pages

Table 2-1. Main PWR components and their degradation mechanisms. 26

Table 2-2. Main BWR components and their degradation mechanisms. 27

Table 2-3. Review of the "pipe leakage" LERs for the most recent 6 years. 28

Table 2-4. Summary of 17 LER cases related to the "MSL Leakage". 31

Table 2-5. PWR plants with pipe wall thinning in the feedwater-condensate systems. 38

Table 2-6. BWR plants with pipe wall thinning in the feedwater-condensate systems. 39

Table 2-7. The major differences between the KWU-KR and the EPRI-CH models. 52

Table 3-1. E Factor Uncertainties. 64

Table 3-2. Typical stress parameter values for SA 106B and hoop strain parameter values for SA 516 Grade 70 carbon steel. 67

Table 5-1. Failure probability calculations due to steady state pressure and transients. 88

Table A-1. FAC parameters and uncertainty information in Case 1 (single phase flow). 107

Table A-2. FAC parameters and uncertainty information in Case 2 (single phase flow). 110

Table A-3. FAC parameters and uncertainty information in Case 3 (two phase flow). 112

Table A-4. FAC parameters and uncertainty information in Case 4 (two phase flow). 115

Table A-5. Parameter uncertainties estimation. 116

Table A-6. Calculated and corresponding measured quality data. 117

Table A-7. Summary of uncertainty adjustment factor, E for four cases. 119

Chapter 1: Introduction

1.1 Background and Motivation

The operation of complex systems, such as light water nuclear reactors, over long periods of time (e.g., 20-40 years) invites the potential of age-related degradation and a reduction of the strength of passive components. The U.S. Nuclear Regulatory Commission (NRC) sponsored the Nuclear Power Plant Aging Research (NPAR) program during 1985-1994 to gather information about nuclear power plant aging [Kasza, et al., 1996]. This program collected a large body of information, mainly qualitative, on plant aging. Incorporating this body of knowledge into modern probabilistic risk assessment (PRA) has been envisioned as an effective and systematic method to assess the impact on plant risk resulting from aging of SSCs (systems, structures, and components). However, this body of knowledge has not yet been formally integrated into risk assessment.

The principal objective of the NPAR program was to develop a basic understanding of age-related degradation (ARD) processes and their effect on nuclear power plant systems, structures, and components. The NRC's Project Directorate of License Renewal (PDLR) has been charged with the responsibility for developing appropriate technical criteria for addressing the aging issues related to renewal of nuclear power plant licenses. In order to carry out this responsibility, the PDLR initiated the evaluation of age-related information from all available sources, including NPAR reports, generic communications, and Licensee Event Reports (LERs) and to use the results of this assessment to determine supplemental and update license renewal guidelines. This activity was called the Generic Aging Lessons Learned (GALL) program [Kasza, et al., 1996].

More than 550 documents comprising 163 NPAR reports, 31 NRC Generic Letters, 265 Information Notices, 82 Licensee Event Reports, 5 Bulletins, and 10 NUMARC Industry Reports were reviewed under the GALL program. The review found that (1) no new issues were revealed with respect to components subject to ARD, and (2) that all ongoing significant issues were being addressed by the regulatory process. However, (3) the aging of passive components must be subjected to continued scrutiny [Kasza, et al., 1996].

A number of time-dependent, or age-related degradation mechanisms [e.g., fatigue, irradiation embrittlement, stress corrosion cracking and flow-accelerated corrosion (FAC)], not fully accounted for in original designs, have caused failures and raised questions about the safety of older nuclear power plants [Shah and Macdonald, 1993]. To better capture these age-related issues, the methods development and analysis presented in this document utilize PRA techniques and models. These will allow for modeling of aging of passive components in a PRA so that the impact of aging on core damage frequency can be estimated. From the incorporation of physical aging models into PRA models, it is expected that decisions related to plant operation and maintenance will have a stronger basis. Further, resources geared toward plant operation can be better utilized based upon the risk-informed methods presented in this work.

One question that arises concerns the assumed robustness in nuclear power plant design and the overall impact of aging mechanisms. Modern power plants were designed to operate for 40 years, and it was assumed that all aging-related wear would be accounted for in the original designs. However, it turns out that some aging effects were not accounted for in the design of many components and systems. These concerns are illustrated by Gosselin [1997]:

"Failures typically result from degradation mechanisms and loading conditions (i.e., intergranular stress corrosion cracking (IGSCC), flow-accelerated corrosion (FAC),

thermal stratification, etc.) not anticipated in the original design. Since the likelihood of a pipe failure is strongly dependent upon the presence of an active degradation mechanism in combination with service conditions and transient load conditions, it has been established that the relative rupture frequency of a pipe segment can be determined based on evaluating the type of degradation mechanism present in a pipe segment during any mode of operation and by considering associated loading and service conditions."

NRC Commissioner Nils Diaz addressed the 450th ACRS (Advisory Committee on Reactor Safeguards) meeting regarding NRC's life extension policy of nuclear power plants on March 6, 1998 and stated:

"I believe the license renewal process will be difficult unless we fully and legally incorporate risk insights into it, and I'll tell you why -- because the thing that was introduced into the rule was this aging management process, which is a difficult issue, ... and that could actually create very contentious litigations. We have the responsibility to define and clarify what we mean and if necessary to demand that certain issues be risk-informed, to be able to set them in the proper context [NRC, 1998]."

1.2 Research Objectives

The research objectives of this work are to develop methods to include FAC in PRA and to assess its impact on core damage frequency (CDF). PRA provides a convenient framework for such an assessment. However, a straightforward use of PRA is not possible at this time due to the reasons explained below.

Traditional PRA, in general, does not include passive SSCs in its models, because passive SSCs which are affected by aging are much more reliable than the active components, which are modeled in PRAs routinely.

A stress-strength interference (or reliability physics) model based on physical FAC phenomena (rather than estimating distribution parameters from lifetime data) will be proposed. We develop load and capacity (or stress and strength, respectively) probability distribution using the KWU-Kastner-Riedle (KWU-KR) [Kastner and Riedle, 1986] FAC model. The uncertainties associated with both the parameters and the model of the KWU-KR are assessed. Once this stress-strength interference methodology is developed, it is applied to several FAC case studies.

We apply the INEEL (Idaho National Engineering and Environmental Laboratory) SAPHIRE [Smith, et al., 1997] PRA models to the selected pipe segments of the Surry IPE (Individual Plant Examination) to obtain changes in core damage frequency due to FAC for different periods of time during plant life.

1.3 Previous Work

Aging issues such as IGSCC and FAC are complex, multi-parameter phenomena, and the susceptibility of a given plant or SSC cannot be determined by considering only a few parameters. Even though aging models can predict observed results fairly well in some cases, such calculations are subject to large uncertainty. Since the development of detailed aging models based on reliability physics is still in its infancy, an approximate model that modifies the failure rate directly has been proposed [Vesely, 1987]. The failure rate of a component is written as

$$\lambda(t) = \lambda_0 + \alpha t \qquad (1\text{-}1)$$

where

$\lambda(t)$: total component failure rate,

λ_0 : component random failure rate,

α : aging related factor,

t : operation time.

The linear failure rate model described in Eq. (1-1) assumes that the total failure rate, $\lambda(t)$, is the sum of two failure rates, one associated with random failures, λ_0, and the other associated with failures caused by aging, αt. This assumption of linearity in time has been questioned; in fact, it is shown in the NUREG/CR-6157 report [Sanzo et al., 1994] that the failure mechanisms discussed earlier do not necessarily lead to failure rates that are linear in time.

A general drawback of the linearly-increasing failure rate model, equally shared by the other reliability distributions that have been proposed in the literature [Sanzo, et al., 1994], is that it essentially represents a parametric approximation made at a relatively high level of failure processes and mechanisms that usually exhibit complex physical behavior. Thus, although a particular parametric reliability distribution may adequately fit the available failure data, it will nevertheless always constitute a drastic simplification when examined from the point of view of the underlying physical phenomena. The obvious danger under these conditions is that a careless or superficial choice and application of parametric reliability models may obscure the understanding of the role played by important physical processes and may inhibit the management of aging.

The Taylor expansion of the risk as proposed by Vesely et al. [Vesely, et al., 1990] is applied to the CDF calculations. The authors suggest that component aging and risk models should be analyzed separately; aging models are introduced at the component level (i.e., as discussed above) and the risk analysis is performed at the system and plant level. This approach relates the change in individual component unavailabilities due to aging to the change in the overall plant risk. The results of the analysis can, then, be used to evaluate the effectiveness of maintenance and surveillance in controlling aging and to direct resources to those SSCs are most important to nuclear power plant risk.

The Taylor expansion model technique is a better approximation for addressing aging, but still lacks sufficient detail. This model technique has several limitations; these limitation are discussed by Sanzo, et al. [Sanzo, et al., 1994]. Specifically, the Taylor expansion "masks" details of the aging process that are better represented via a physics-based model.

Besides the information that the NPAR Program has collected, there has been extensive use of expert opinions. In 1986, the Executive Director for Operations (EDO) of U.S. NRC established the TIRGALEX (Technical Integration Review Group for Aging and Life Extension) [Levy, et al., 1988] to structure a plan to integrate the NRC's aging and life-extension activities. One of the major results of the TIRGALEX plan has been the identification of the safety-related structures and components that should receive high priority in the subsequent phase of the NPAR program.

The TIRGALEX expert panel utilized a set of risk criteria to set priorities in the evaluation of aging structures and components. The same data set used in this process, which has since been called the TIRGALEX database, was also used as the database in later PRA studies under NPAR program.

1.3.1 Flow-Accelerated Corrosion (FAC)

Reviews of Licensee Event Reports (LERs), the Nuclear Plant Experience (NPE) database, and associated literature indicate that FAC is an important aging mechanism for investigation.

Flow-accelerated corrosion (FAC) is often called erosion-corrosion. It is primarily a corrosion process enhanced by chemical dissolution and mass transfer, rather than a mechanical process involving removal of the oxide layer by erosion or cavitation. A

particular FAC problem area is the wall thinning of carbon steel pipe, a passive component. FAC in carbon steel pipe systems is characterized by the simultaneous dissolution of iron from the iron oxide-fluid interface and the formation of an iron oxide film at the oxide-metal interface. Bulk flow plays a vital role in providing a sink for dissolution. Under stagnant conditions, corrosion products would concentrate in the aqueous solution reducing the concentration gradient driving force for the corrosion process. Flow inhibits this concentration process and enhances the concentration gradient. Single-phase FAC is a function of (1) pipe material, (2) fluid velocity, (3) pipe geometry, (4) dissolved oxygen concentration, (5) water chemistry, and (6) water temperature. In addition to the parameters mentioned above, two-phase FAC caused by wet steam coolant, is a function of steam quality and void fraction [Shah, et al., 1997].

For single-phase FAC, wear patches often start as "horseshoe or scallop" shapes expanding to wide troughs of dimension less than the order of the pipe. Two-phase material degradation appears as "tiger striping" occurring in bends and downstream from flow disruptions in which separate patches on the order of the pipe diameter experience significantly greater material loss than immediately adjacent sections [Chexal, et al., 1996].

An additional acceleration may occur when rapid flashing of water to vapor occurs. This phenomenon is aggravated by system pressure fluctuations. Increased fluid velocity, approaching sonic velocity, accelerates FAC [Nedelko and Kastner, 1991].

Over the past several years, three FAC models have been developed by researchers: the KWU-KR [Kastner and Riedle, 1986, and Nedelko, et al., 1991] and the EPRI-Chexal-Horowitz models (EPRI-CH) [Chexal, et al., 1996]. While the formulation of the EPRI model is not documented in detail due to its proprietary nature, the formulation of the FAC material loss rate used in the KWU-KR model [Kastner, et al., 1986] is well documented. A third empirical model, part of the BRT-Cicero code, was

developed at the Electricité de France (EDF) and is based on experimental data taken on the Cicero test loop [Chexal, et al., 1996]. The EDF's BRT-Cicero code is not documented in detail either due to its proprietary nature. Consequently, the FAC analysis presented in this work will center around the KWU-KR model.

Like any parametric model, the model's predicted rate differs from the actual corrosion rate. Potential discrepancies between model predictions and actual plant results are due to several reasons that will be addressed later.

Both the KWU and EPRI models are limited in their capability to consider the effect of complex pipe geometries. The behavior at a particular location depends not only on the geometry at that location, but also on the upstream flow geometry. A geometric enhancement factor is generally used to represent the effect of increasing turbulence on FAC. The first geometry factors recognized by Keller were developed empirically based on two-phase flow experience; the application to single-phase flows has some uncertainty [Chexal, et al., 1996].

EPRI has developed the computer code CHECWORKS (Chexal-Horowitz Engineering-Corrosion Workstation) for managing FAC in nuclear power plant piping. This program has capabilities for estimating parameters (such as local water chemistry and flow rate) that affect FAC rates, and for predicting FAC rates and helping to select inspection locations. The computer code is based on data from France, England, and Germany, and the U.S. It is claimed that the comparison between the predicted results and measurements shows that the code predicts FAC rates within ±50%. The main sources of uncertainty are associated with the original thickness and thickness profile of the pipe components, trace amounts of alloy content in the pipe material, actual number of hours of operation, plant chemistry history, and discontinuities on the inside surface of the pipe.

All PWR and BWR plants in the U.S. use the CHECWORKS code (or its predecessor code CHECMATE) for estimating FAC rates [Chexal and Horowitz, 1995]. This code is also used by many fossil plants, by the U.S. Navy, and by several overseas utilities. The code has been used to identify the sites most susceptible to FAC, to prioritize the locations that need to be inspected, to estimate remaining service life for each susceptible component, and to evaluate the effectiveness of different water chemistries and other mitigative actions.

Siemens/KWU in Germany has long been active in researching wall thinning rate estimation caused by FAC. The empirical KWU-KR model was developed in the early 1980s for the calculation of material losses due to FAC in single- and two-phase flow [Kastner and Riedle 1986]. The KWU-KR model was based on experiments carried out at Siemens/KWU and on plant data from all known single and two-phase locations (more than 6,000 data points overall), as well as on theoretical considerations. After the Surry Unit 2 accident in 1986, the WATHEC program based on the KWU-KR model was developed to perform weak-point analyses at power plants. In 1991, WATHEC was interfaced with the DASY program which handles the recording, management, evaluation, and documentation of the data obtained from non-destructive examinations. These two software packages were continuously improved in cooperation with European utilities to calibrate the predicted wall thinning rates for further plant diagnosis with increased prediction accuracy [Chexal, et al., 1996].

1.3.2 Probabilistic Risk Assessment (PRA)

FAC is a complex, multi-parameter phenomenon, and the susceptibility of a given site cannot be determined by considering only a few parameters. Even though the models can predict observed results fairly well in some cases, such calculations are subject to large uncertainty. The two models are limited in their ability to consider the effects of complex pipe geometries. The behavior at a particular location depends not only on the

geometry at that location, but also on the upstream flow geometry. These individual parameter uncertainties can be propagated through the model using Monte Carlo methods. Even if the input parameters for the model were known perfectly, the model prediction would be still imperfect. The issues associated with quantification of uncertainty in the predictions of the FAC physical model will also be included in this work. The consideration of the failure probability due to FAC causes the change of the associated initialing event frequency, and then the final impact of a level 1 PRA, the CDF change of a specified nuclear power plant will be studied in the our work.

1.4 Comparison of PRA Models

The modeling technique discussed in the remainder of this work is an extension of modern PRA techniques. To include physical aging mechanisms into the PRA model the basic events are contained in fault or event trees. As part of the incorporation of physical aging models into the PRA, it may be necessary to augment the existing fault or event trees to include the additional aging mechanisms. For example, if sections of pipe are susceptible to FAC, the system fault trees containing these sections of pipe need to be modified to account for the pipe segments. Once the pipe segments are incorporated into the PRA, the physical aging model representing FAC could be applied to the pipe segment basic events, thereby allowing an analyst access to physical parameters (e.g., fluid velocity, steam quality, temperatures, pH) that drive the FAC phenomenon. Consequently, having the physical process incorporated directly into the PRA yields risk insights based upon the aging process rather than an abstraction of failure data into a statistical probability parameter. This general concept of incorporating a physical aging model is illustrated in Figure 1-1. For aging physics model PRA, the step 1 is discussed in Chapter 2. Chapter 3 includes steps 2 and 3. Chapter 4 covers steps 4 and 5. We apply the whole methodology in a case study addressed in chapter 5.

Traditional PRA 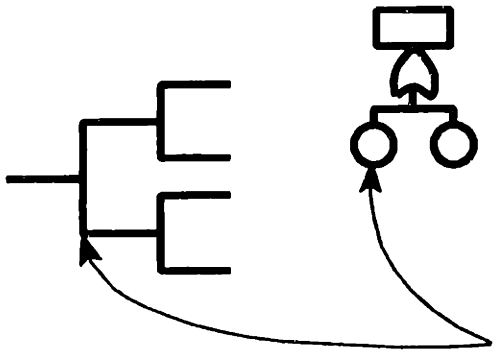	1. Obtain component failure data (active data components), generic data, or combination of both. 2. Determine appropriate component reliability model [e.g., $1 - \exp(-\lambda T)$]. 3. Use statistics (e.g., Bayes Theorem) to determine appropriate failure rate. 4. Calculate component failure probabilities. 5. Put failure rates into fault/event trees.
Aging Physics Model PRA 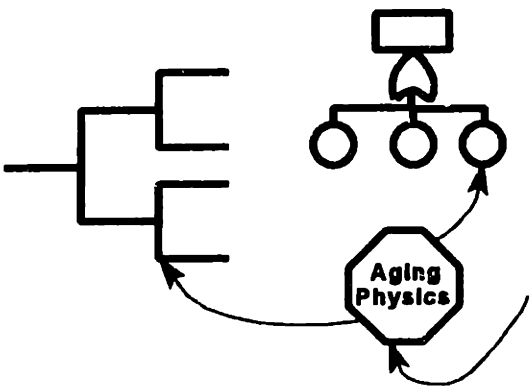	1. Determine applicable aging mechanisms and affected components. 2. Develop "aging physics" model. 3. Determine loading conditions on components. 4. Incorporate physics model and loading conditions into PRA via fault/event trees. 5. Use physics model to determine aging-related failure probabilities.

Figure 1-1. Illustration of differences between traditional and aging physics PRA models.

Chapter 2: Flow-Accelerated Corrosion (FAC) Models

2.1 Introduction

A variety of models have been proposed to describe FAC, both empirical and mechanistic. Empirical models are based on a statistical fit with laboratory data trends which are then modified as appropriate to match plant data. Mechanistic models establish a set of interrelated equations describing the physical processes occurring at particular locations within a proposed system. While empirical models may fit the data well, extrapolation of trends to the full function space may not be accurate [Chexal, et al., 1996]. For example, the effect of velocity at low and high pH may be very different because of changes in film stability. While mechanistic models allow the investigator to incorporate all relevant mechanisms, they may produce a set of equations too cumbersome to solve in a reasonable amount of time. In the beginning of model development, mechanistic models provide insight into the phenomena and direction to the experimentation. Statistical approaches based on the data, however, provide a more usable end product for industry.

2.2 Review of the FAC Database and Associated Models

Reviews of Licensee Event Reports (LERs), the Nuclear Plant Experience (NPE) database, and associated literature indicate that FAC is a candidate among aging mechanisms (see Table 2-1 and Table 2-2, main PWR and BWR components and their degradation mechanisms [Shah and Macdonald, 1993]) for investigation and modeling.

Using the SCSS (Sequence Coding and Search System) database, ORNL searched for *"Pipe Leakage"* problems to retrieve the most recent LERs (from 1990 to April 1996).

Table 2-1. Main PWR components and their degradation mechanisms

Components \ Degradation Mechanisms	Radiation Embrittle-ment	Time-Dependent Relaxation (Creep)	Hydrogen Embrittle-ment	Stress Corrosion Cracking	Low-Cycle Thermal Fatigue	High-Cycle Mechanical and Thermal Fatigue	Corrosion Fatigue	Thermal Embrittle-memt	Mechanical Wear, Fretting and Fatigue	Corrosion and FAC
Reactor Pressure Vessel (RPV)	X			X						X
Containment and Basemat		X	X	X						X
Reactor Coolant Pipe, Safe ends, and branch pipe					X	X		X	X	
Steam Generator tubes				X		X	X		X	X
Reactor Coolant Pump (RCP)						X		X		X
Pressurizer				X	X					
Control Rod Drive Mechanisms				X				X	X	
Safety-related Cables and Connections	X							X		X
Emergency Diesel Generators									X	X
Reactor Internals		X		X		X			X	
Reactor Pressure Vessel Supports	X			X						
Feedwater Pipe and Nozzles, and Steam Generator Shell				X	X	X				X

Table 2-2. Main BWR components and their degradation mechanisms

Degradation Mechanisms / Components	Radiation Embrittlement	Time-Dependent Relaxation (Creep)	Stress Corrosion Cracking	Low-Cycle Thermal Fatigue	High-Cycle Mechanical and Thermal Fatigue	Corrosion Fatigue	Thermal Embrittlement	Mechanical Wear, Fretting and Fatigue	Corrosion and FAC
Containment			X			X			X
Reactor Pressure Vessels (RPV)	X		X	X	X				X
Recirculation Pipe and Safe Ends			X				X		
Recirculation Pumps			X		X		X		
Control Rod Drive Mechanisms	X		X				X	X	X
Safety-related Cables and Connections in Containment	X	X					X		X
Emergency Diesel Generators	X							X	X
Reactor Pressure Vessel Internals	X		X		X	X	X		
Reactor Pressure Vessels Supports				X					
Feedwater and Main steam Pipe					X			X	X

Table 2-3. Review of the "pipe leakage" LERs for the most recent 6 years.

Case no.	LER no.	Type	Pipe Leakage Location	Active/ Passive
1	APL-90-010	PWR	Pipe joints and threaded connections to Check valve of air supply system to 2 dampers used for MCR normal ventilation.	P
2	DUQ-91-002	PWR	Pipe to loop 1B cold leg vent valve	P
3	DUQ-90-001	PWR	SG tube leak	P
4	APL-90-001	PWR	Reactor building cooling isolation valve keakage.	A
5	CWE-92-012	PWR	S/D, leakage of feedwater check valve	A
6	TVA-93-004	BWR	Operator error, no physical leakage	NA
7	CPL-92-008	BWR	S/D, a through-wall leak in jacket water cooler service water supply line of EDG	P
8	NEB-94-010	BWR	S/D, leakage through RHR shutdown cooling isolation valve	A
9	NEB-93-005	BWR	S/D, reactor feedwater check valve leakage	A
10	NEB-93-005	BWR	S/D, backflow through the check valve in non-regenerative heat exchanger and RWCU pipe. Design error.	A
11	FPC-91-005	PWR	Inter-stage packing leakoff of a makeup and purification system valve	A
12	PGE-92-001	PWR	VCT outlet check valve didn't test. TS violation.	NA
13	PGE-90-010	PWR	A crack in the positive displacement charging pump suction pipe. The cause of crack is vibration induced high cycle fatigue.	P
14	PGE-91-004	PWR	Calculation error in TS associated Unidentified Leakage Rate.	NA
15	CWE-94-001	BWR	The undocumented plant modification, a sampling line isolation valve leakage.	A
16	CWE-91-015	BWR	The isolation valve in a primary containment penetration line leakage.	A
17	CWE-94-002	BWR	One primary containment isolation valve didn't perform LLRT.	NA

Table 2-3. Review of the "pipe leakage" LERs for the most recent 6 years (continued).

Case no.	LER no.	Type	Pipe Leakage Location	Active/ Passive
18	CW5-92-015	BWR	LPCI testable injection check valve leakage.	A
19	FIT-95-010	BWR	A packing leak on Reactor Recirculation system valve.	A
20	PNY-92-022	BWR	S/D, failure to perform ISI in emergency service water and EDG.	NA
21	OPP-92-018	PWR	S/D, a modification revealed severe corrosion of carbon steel fasteners on the boric acid pump flanges and pipe support.	NA
22	OPP-92-002	PWR	Condensate from nearby component cooling water pipe dripping onto the inner PAL (Personnel Air Lock) door bulkhead structure and upper latch bolt bracket causing surface corrosion.	P
23	HOP-95-013	BWR	Failure to perform ISI for some pipe line.	NA
24	GPC-90-022	BWR	Operator error, no actual system leakage occurred.	NA
25	PEG-90-035	BWR	A 30" pipe section on the "A" Service Water System loop had developed minor through wall flaw (in the internal pipe epoxy coating which allowed pipe corrosion to begin and subsequent erosion to occur.)	P
26	PEG-90-025	BWR	S/D, a leak at a joint weld (vibration induced fatigue) on a reactor Recirculation instrument line.	P
27	IND-95-014	PWR	S/D, a Service Water leak was detected inside containment occurring at Fan Cooler discharge flow element weld . This transition weld resulted in galvanic interaction and corrosion of the carbon steel and stainless steel.	P
28	DPC-90-025	PWR	A packing leak of Pressurizer PORV header Hi point vent valve.	A
29	NEU-94-023	BWR	A small leakage in the Service Water discharge pipe from Reactor Building Closed Cooling Water heat exchanger.	P
30	NEU-93-021	BWR	A through wall defect in the Service Water pipe in the Turbine Building. The root cause is erosion/corrosion of carbon steel pipe.	P

There are a total of 880 LERs (740 pages) associated with leakage problems of pipe systems [Poore, 1996]. 30 cases have been reviewed. Table 2-3 shows a summary. Note that 11 cases are related to passive components, 11 cases are related to active components, and the remaining 8 cases are not related to components. Service Water Systems (SWS) play an important role in these pipe leakage locations. This was also found in the Nuclear Plant Aging Research (NPAR) program [Jarrel, et al., 1989].

Using the SCSS database [Poore, 1996], "PWR and Pipe/Pipe and Steam Leak/Leakage/Rupture/Ruptured/Crack/Fracture/Fractured" has been searched to retrieve the recent LERs (from 1980 to April 1996). There are a total of 89 LERs associated with steam leakage problems of PWRs' pipe components. Table 2-4 shows a summary of 17 LERs. The LERs are reported to the NRC within 30 days. Generally, the degradation mechanisms or root causes of LERs will be clearly identified a few months later after events. It is assumed that most of the degradation mechanisms in Table 2-4 were unclear when the LER were issued.

As applied to carbon steel pipe components, FAC can be viewed, in simple terms, as an accelerated form of corrosion due to the breakdown of a protective oxide film from the surface induced by flow. The theory behind this mechanism is complex and includes electrochemical aspects of the general corrosion phenomenon, mass transfer, and to a certain degree momentum transfer [Chexal, et al., 1996] .

FAC has been a most destructive corrosion mechanism for high-energy (fluid temperature between 212°Fto 482°F (100°C~250°C)) carbon steel pipe in light water reactors. It has caused rupture of both large-, medium-, and small-diameter pipe carrying either single phase or two-phase flow. Single-phase FAC has also caused significant wall thinning of carbon steel J-tubes and feedrings within the recirculating steam generators [Shah, et al., 1997]. A few selected events related to single-phase flow and some events related to two-phase flow are described.

Table 2-4. Summary of 17 LER cases related to the "MSL Leakage".

Case no.	LER no.	Type	Plant -Unit	Commercial Operation Date	Date of Damage	Damage Component/Extent of Damage and Comments	Degradation Mechanisms	Active/ Passive
1	APL-90-019	PWR	Arkansas Nuclear One-2	3/26/80	8/21/90	MSIV closure due to the failure of a normally energized solenoid valve. Also found S/G-A small leak later.	Not mentioned	A
2	DUQ-93-001	PWR	Beaver Valley-2	11/17/87	1/26/93	Extensive engineering analysis identified the stress of the AFW pipe to S/G-C, for combined water hammer and seismic events, exceeded the design stress allowable.	NA	NA
3	CWE-91-012	PWR	Braidwood-1	7/29/88	11/6/91	Significant leakage identified on main FW motor-operated isolation valve.	Not mentioned	A
4	CWE-90-010	PWR	Byron-2	8/21/87	12/20/90	A severe steam leak reported in main steam tunnel. The weld for main steam probe improperly repaired during outage cause a one inch hole in MSL.	SCC	P
5	NEU-94-018	PWR	Connecticut Yankee	1/1/68	7/11/94	No MSL leak. #3 RCP motor oil leak due to a cracked PVC coupling on the line caused a small fire.	SCC	P
6	NEU-93-012	PWR	Connecticut Yankee	1/1/68	7/14/93	S/D, operator error to isolate all four MSL flow transmitters. No actual MSL leakage occurred.	NA	NA
7	FPC-92-015	PWR	Crysal River-3	3/13/77	7/17/92	A steam leak occurred from the packing of a manual isolation valve associated with OTSG-A.	Not mentioned	A
8	CEC-93-010	PWR	Indian Point-2	8/1/74	8/18/93	No physical leak, an engineering analysis identified two regulating valves in instrument air system for main steam PORV & AFWS were not fully capable perform their function.	Not mentioned	A
9	TOL-94-002	PWR	Davis-Besse-1	7/31/78	7/28/94	A minor steam leak on a vent line for MFP.	Not mentioned	P

Table 2-4. Summary of 17 LER cases related to the "MSL Leakage" (continued).

Case no.	LER no.	Type	Plant -Unit	Commercial Date	Date of Damage	Damage Component/Extent of Damage and Comments	Degradation Mechanisms	Active/ Passive
10	NEU-91-012	PWR	Millstone-2	12/26/75	11/6/91	An 8 inch diameter pipe ruptured in a drain line from the first stage preheater drain tank to high pressure FW heater.	Not mentioned	P
11	VEP-92-005	PWR	Surry-1	12/12/72	4/2/92	S/D, No physical leak. TS violation for a potential leakage path from CTMT to safeguards building.	NA	NA
12	NEU-92-003	PWR	Millstone-3	4/23/86	1/30/92	No physical MSL leak. Inadequate work planning caused loss enclosure building integrity.	NA	NA
13	VEP-92-007	PWR	North Anna-2	12/14/80	8/6/92	A leak on the downstream weld of a LHSI (Low Head Safety Injection) isolation vent valve. An overstress condition when LHSI pump started caused valve weld failure.	SCC	P
14	TVA-93-001	PWR	Sequoyah-2	6/1/82	3/1/93	A steam leak on the extraction line to the feedwater heater ruptured caused a 3- by 6- inch hole in the line. The root cause of this event was a programmatic failure of the erosion/corrosion program resulting from insufficient management of the program.	Not mentioned	P
15	NEU-95-032	PWR	Millstone-2	12/26/75	8/8/95	A steam leak in a secondary system within the turbine building. The steam leakage occurred revealed a 14" vertical rupture in the 8" diameter recirculation line from the discharge of the B Heater Drains Pump (HDP) to the Heater Drain Tank.	Not mentioned	P
16	VEP-90-003	PWR	Surry-1	12/12/72	4/2/92	A leak developed downstream of a low pressure heater drain pump in Unit 2 releasing steam and water into the Unit 1 turbine building. The leak was a result of a pipe failure due to excessive thinning of the pipe wall.	Not mentioned (pipe thinning)	P
17	SCE-90-011	PWR	San Onofre-2	8/8/83	6/1/90	This voluntary licensee event report is being submitted to describe SCE's actions in response to a recent occurrence of pipe wall thinning as a result of erosion-corrosion (E-C) processes.	FAC (Flow-Accelerated Corrosion)	P

2.3 Overview of Single-Phase FAC

Single-phase FAC tests have been conducted at several British, French, and German laboratories to identify the factors affecting the FAC rates (rate of metal loss) and to provide data for development of empirical models to estimate these rates [Chexal and Jones, 1988; Chexal and Horowitz, 1995]. An evaluation of the test results and data from the operating plants has identified several factors that affect the FAC rate. These factors may be divided into three groups: (a) hydrodynamic variables - fluid velocity, pipe configuration (geometry of the flow path), and pipe roughness of pipe inside surface; (b) metallurgical variables - chemical composition including weight percentage of chromium, molybdenum and copper in the steel; and (c) environmental variables - coolant temperature and water chemistry including dissolved oxygen, ferrous ion concentration, metallic impurities in water, and pH [Shah, et al., 1997].

The hydrodynamic variables affect the rate of mass transfer of the iron ions and other corrosion products to the bulk coolant and thus affect the FAC rate. *Fluid velocity* affects the mass transfer. At a relatively low flow velocity, the FAC rate is controlled by the rate of mass transfer, whereas at higher velocity (still lower than the critical velocity above which metal removal by mechanical process takes place), the mass transfer rate is higher and the FAC rate is controlled by the chemical reactions at the oxide-coolant and metal-oxide interfaces. FAC is less frequently observed in straight lengths of pipe free from hydro-dynamic disturbances unless the bulk fluid velocity is high. Laboratory studies of the effect of bulk flow velocities, varied from 2 to 18 m/s (6.6 to 59 ft/s), on the FAC of carbon steel in 150°C (300°F) circulating water show that the FAC rate increases with an increase in the flow rate and (for a given flow rate) the FAC rate is almost constant. The variable *pipe configuration* takes into account the hydrodynamic disturbances (elbows, tees, branch connections, reducers, valves, flow control orifices, etc.) that produce high local fluid velocities and result in a further increase in mass transfer. Experiments have shown that local-flow velocities in elbows can be two to three

times the bulk-flow velocities [Bosnak, 1987; NRC, 1987a]. A rough surface produced by the FAC process can be very damaging. The micropits formed by the initial selective attack on the carbon steel microstructure grow until they touch, and thus the surface becomes rough. The dependence of mass transfer on the velocity is greater for a rough surface than for a smooth surface.

Trace amounts of chromium, molybdenum, and copper in carbon steel provide resistance to FAC. The FAC rate is most sensitive to the weight percent (wt%) of the chromium in the steel. For example, the FAC rate dependence on chromium content as predicted by the EPEI-CH model for a 90-degree carbon steel elbow is about 3.9 mm/yr (0.155 in/yr) for 0.03 wt% Cr and equal to about 0.4 mm/yr (0.016 in/yr) for 0.50 wt% Cr [Chexal and Horowitz, 1995]. Thus, a small amount of chromium significantly reduces the FAC rate. The corresponding FAC rate in the case of 0.03 wt% Cr predicted by the KWU-KR model through our calculations is about 1.14 mm/yr (0.045 in/yr), as shown in Figure 2-1. More discussions regarding Figure 2-1 are described in Section 2.8.2.

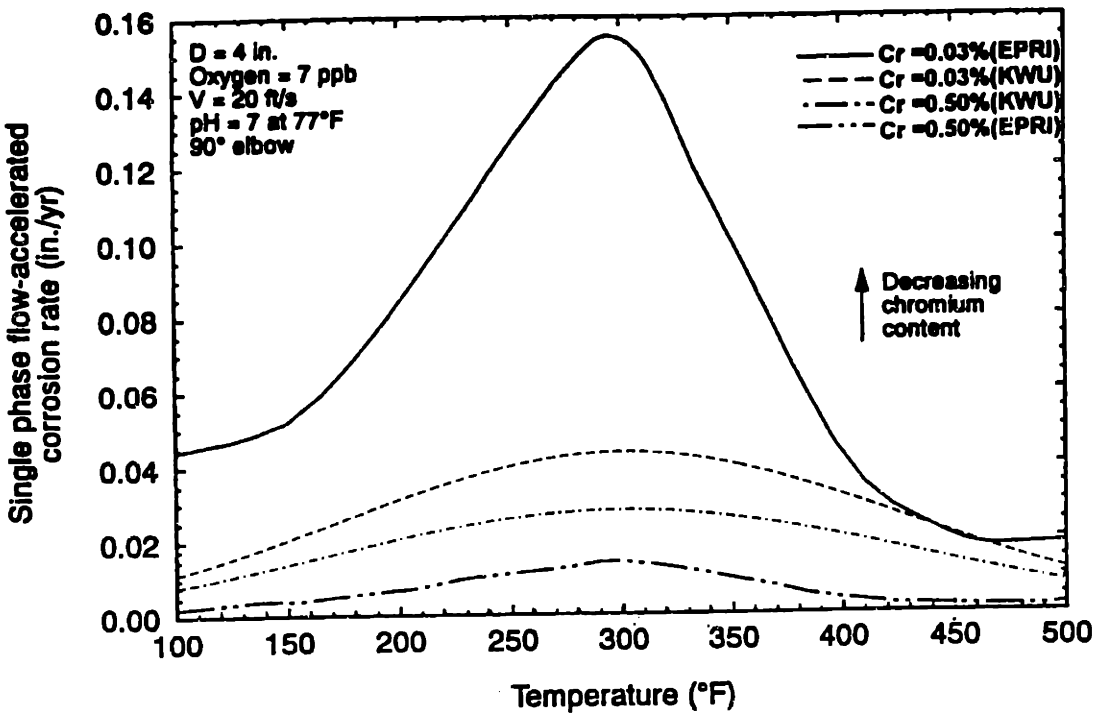

Figure 2-1. Comparison of the EPRI-CH and the KWU-KR models.

The two main environmental variables that affect the FAC rate are the fluid temperature and chemistry. The water chemistry includes dissolved oxygen, ferrous ion concentration, metallic impurities, and cold pH level. The *fluid temperature* influences both the ferrous ion production and the mass transfer of these ions into the bulk water [Remy and Bouchacourt, 1992]. As the temperature increases, the ferrous ion concentration at the oxide-water interface decreases almost linearly. On the other hand, as the temperature increases, the ferrous ion diffusivity into the coolant increases, resulting in a mass transfer coefficient that increases almost linearly. The resulting FAC rate variation with temperature is a bell-shaped curve as Figure 2-2 shows.

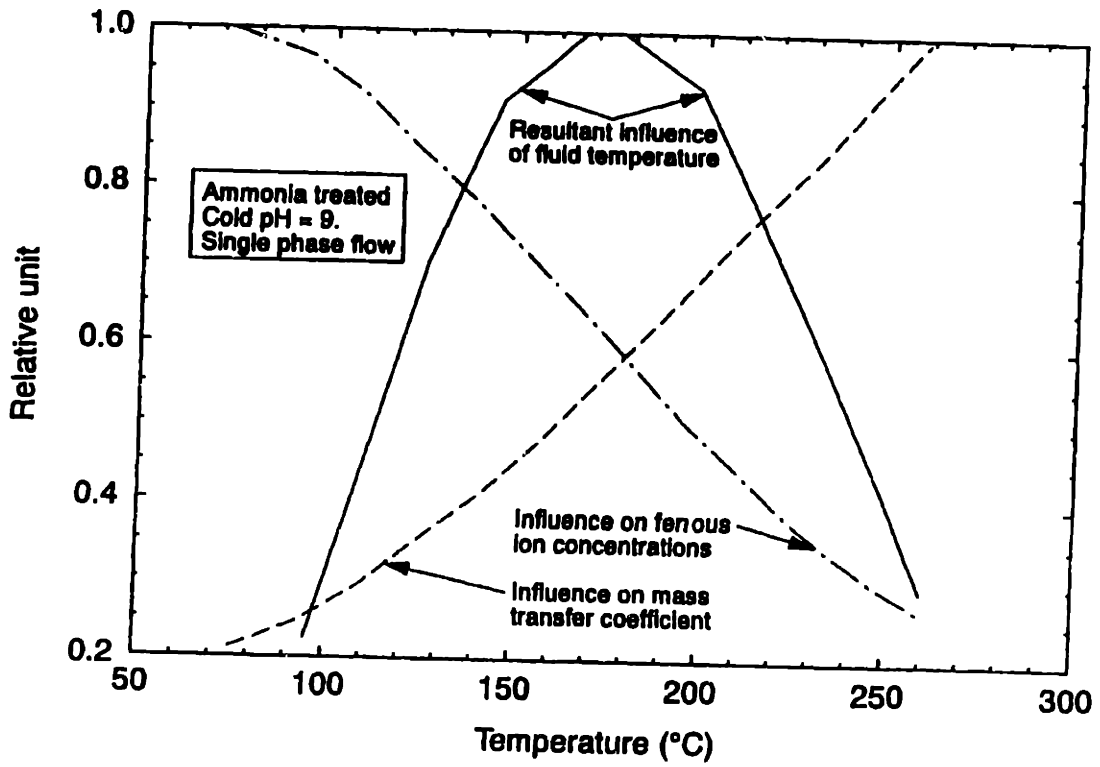

Figure 2-2. The calculated influence of fluid temperature on the ferrous ion concentration and on mass transfer of ferrous ions [Remy and Bouchacourt, 1992].

The temperature at which the maximum FAC rate occurs depends upon the other environmental conditions. For most feedwater pipe conditions, the maximum FAC rate occurs at about 150°C (300°F) [Chexal and Horowitz, 1995].

The FAC rate varies inversely with the level of *dissolved oxygen* in the fluid. As the level of oxygen increases above a threshold value, a less porous oxide layer of hematite, instead of magnetite forms. Because the solubility of hematite in the feedwater is several orders of magnitude lower than that of magnetite, the FAC rate decreases significantly. Some laboratory test results show that the threshold value for dissolved oxygen is less than 15 ppb [Remy and Bouchacourt, 1992]. Using the EPEI-CH model shows a reduction in the maximum FAC rate from about 3.2 to 0.89 mm/yr (0.125 to 0.035 in./yr) as dissolved oxygen content increases from 10 to 30 ppb.

Ferrous ion concentration and metallic impurities in the water affect the FAC rate. The increase in the *ferrous ion concentration* in the bulk fluid reduces the mass transfer of ferrous ions from the oxide-coolant interface to bulk coolant. An increased ferrous ion concentration can reduce or suppress FAC when mass transfer controls the corrosion process. FAC rates vary by an order of magnitude over the cold pH[1] range of 8.5 to 9.5, which is typical for feedwater systems [Jonas, 1988].

FAC caused the rupture of the feedwater pipe outside the containment at both the Trojan plant in 1985 [Stoller, 1985] and Surry Unit 2 in 1986 [NRC, 1987a]. A pressure transient caused the ultimate rupture of feedwater pipe already significantly degraded by FAC at both plants. In neither the Trojan nor Surry case was there a leak or any other warning signs indicating incipient failure. As a result of the Surry accident, the NRC staff asked that all utilities with operating nuclear power plants inspect their high-energy

[1] Cold pH is taken at temperature 25°C (77°F). A lower cold pH provides the same desired pH at the operating temperature.

carbon steel pipe [NRC, 1987b]. Table 2-5 lists the degraded components, fittings, and straight runs in the 27 PWR feedwater-condensate systems identified in that inspection and reported to the NRC [NRC, 1988]. Various degrees of wall thinning in the six BWR feedwater-condensate systems were also identified; these systems are reported in Table 2-6. NRC staff asked licensees and applicants to implement long-term FAC monitoring programs in 1989 [NRC, 1989].

A potential generic problem was discovered at Catawba Unit 2 in 1991 that may affect the Westinghouse Model D4, D5, and E steam generators in which a portion of the main feedwater is diverted to the auxiliary feedwater nozzle via the preheater bypass line, as shown in Figure 2-3 [Shah, et al., 1992]. The fluid velocity in the 102-mm (4-in.) diameter preheater bypass line and the connecting auxiliary feedwater line was in the range of 9 to 11 m/s (30 to 35 ft/s). The licensee detected several locations in this pipe that were at or near the minimum required wall thickness. Examinations revealed that single-phase FAC had reduced the nominal 8.56-mm (0.337-in.) wall thickness to 4.70-mm (0.185-in.) in only four operating cycles. This implies a FAC rate of about 1.0 mm/cycle (0.039-in./cycle). If the preheater bypass line had ruptured, the break would not have been insoluble and would have resulted in the steam generator coolant being released outside containment. Over 27 m (90 ft) of pipe was replaced at Catawba Unit 2.

Generally, the FAC monitoring programs concentrate on inspection of pipe elbows and tee fittings, i.e., the sites where local high velocities may be present. However, FAC has caused rupture at other feedwater pipe sites, such as in the flange of a flow measuring device downstream of an orifice at Loviisa Unit 1 in Finland and in the straight portion of a pipe, located immediately downstream of a level control valve, at Surry Unit 1 and at Millstone Unit 3. FAC has caused significant wall thinning of the feedwater control valve bypass line at both the San Onofre and Diablo Canyon plants. It was surprising to find significant wall thinning and failures of the startup feedwater

Table 2-5. PWR plants with pipe wall thinning in the feedwater-condensate systems [NRC, 1988].

Plant	Unit	Commercial operation	Degraded components (fittings, straight runs)
Arkansas Nuclear One	1	Aug-74	Elbows, drain pump discharge pipe
Arkansas Nuclear One	2	Dec-78	Undefined
Calvert Cliffs	1	Oct-74	Elbows, reducers, straight runs
Calvert Cliffs	2	Nov-76	Elbows, reducers, straight runs
Callaway		Oct-84	Recirculation line elbows
Diablo Canyon	1	Apr-84	Elbows, straight runs
Diablo Canyon	2	Aug-85	Elbows, Y
D.C. Cook	2	Mar-78	Elbows
Fort Calhoun	-	Aug-73	Elbows, straight run
Haddam Neck	-	Jul-67	Recirculation line
Millstone	2	Oct-75	Elbows, heater vent pipe
North Anna	1	Apr-78	Elbows, straight runs
North Anna	2	Jun-80	Elbows, straight runs
H. B. Robinson	2	Sep-70	Recirculation lines
Rancho Seco	-	Sep-74	Straight runs downstream of feedwater isolation valves or main feedwater pumps minimum flow valves
San Onofre	1	Jun-67	Reducers, heater drain pipe
San Onofre	2	Jul-82	Heater drain pipe
San Onofre	3	Aug-83	Heater drain pipe
Salem	1	Dec-76	Recirculation line
Salem	2	Aug-80	Recirculation line
Shearon Harris	-	Oct-86	Recirculation line
Surry	1	Jul-72	Fittings
Surry	2	Mar-73	Fittings
Sequoyah	1	Jul-80	Elbows. straight runs
Sequoyah	2	Nov-81	Elbows
Trojan	-	Dec-75	Elbows, reducers, straight runs
Turkey Point	3	Oct-72	Feedwater pump suction line fittings

Table 2-6. BWR plants with pipe wall thinning in the feedwater-condensate systems [NRC, 1988].

Plant	Unit	Commercial operation	Degraded components (fittings, straight runs)
Dresden	2	Jan-70	Elbows
Duane Arnold		Mar-74	Elbows, reducers, straight runs
Pilgrim	1	Jun-72	Elbows
Oyster Creek		May-69	Elbows
River Bend	1	Oct-85	Recirculation line
Perry		Jun-86	Straight runs

system pipe at both the Wolf Creek and Callaway plants because these systems were used for a very short time period during startup. Investigation of these failures showed that the cause was the flow resulting from the leaking valves on the pipe [Chexal, et al., 1996].

2.4 Overview of Two-Phase FAC

Examination of worn extraction pipe has identified two distinct mechanisms causing damage in the system carrying two-phase coolant: oxide dissolution and droplet-impact wear [Keck and Griffith, 1987]. The oxide dissolution mechanism is similar to the single-phase FAC mechanism discussed above with one exception. Two-phase FAC has been observed in pipe carrying wet steam. Its occurrence has not been observed in pipe carrying dry steam (100% quality). Moisture in the wet steam is essential to dissolve the oxide film. Test results show that the FAC rate in a two-phase flow varies with the quality of the steam. It is zero at 100% quality and equal to the single-phase (water) flow value at 0% quality. The FAC rate peaks at some intermediate value of quality [Chexal and Horowitz, 1990]. Field data indicated that the greatest degradation is seen in pipe containing steam with the highest moisture content, such as the turbine crossover pipe and the exhaust and extraction pipe connected to the high-pressure turbines.

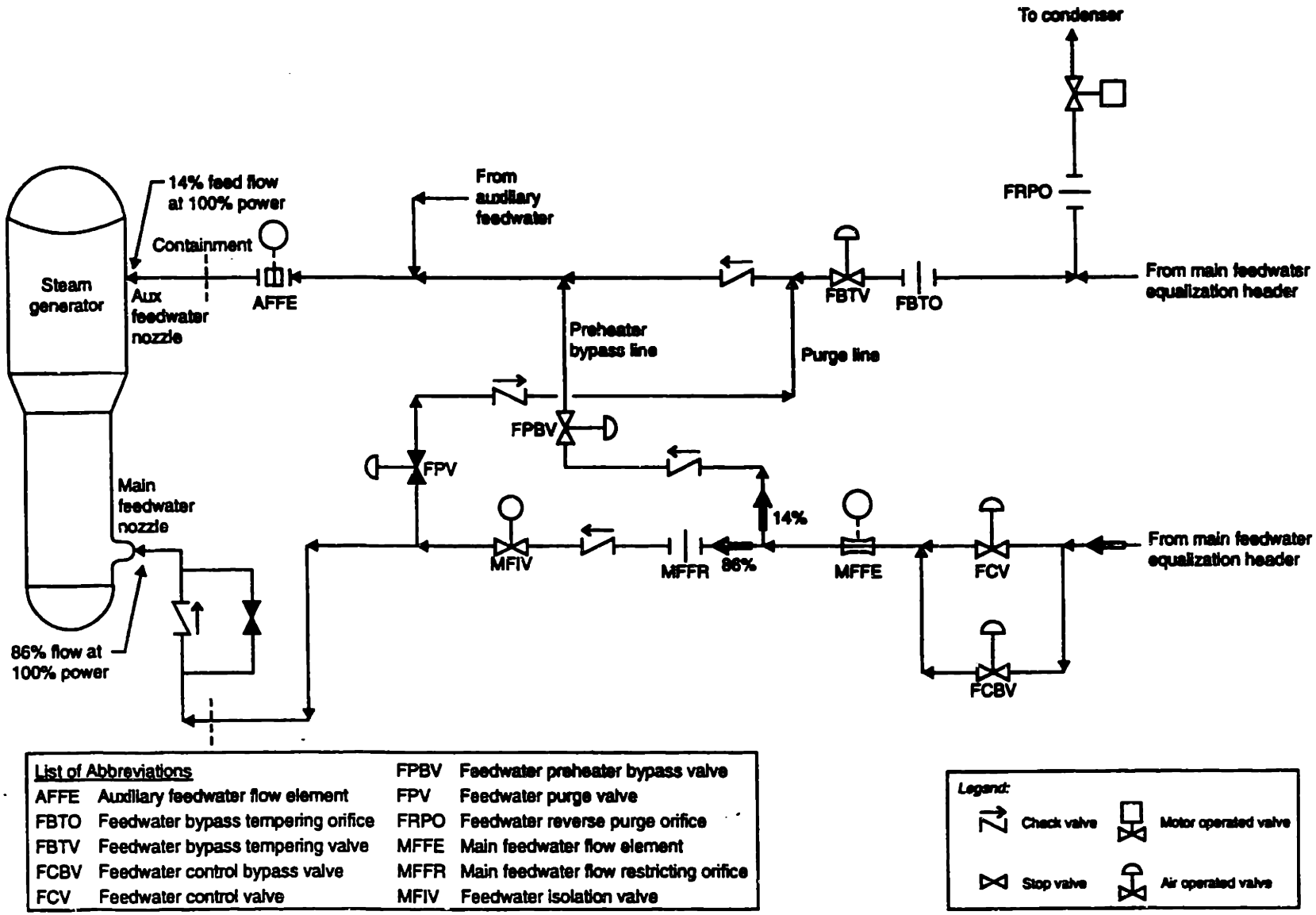

Figure 2-3. Schematic of a feedwater system for a Westinghouse plant steam generators equipped with preheaters [Shah, et al., 1997].

The droplet-impact wear mechanism may be explained as follows. The liquid phase in a steam line generally flows in a thin layer near the main steam line pipe wall, while the vapor forms the core of the flow and moves much faster than the liquid phase. This velocity difference creates shear forces at the liquid-vapor interface; if this force is greater than the surface tension force at the interface, some liquid will be sheared off the liquid layer and carried over with the vapor. This liquid will form droplets, which will be accelerated by the vapor and become entrained in the vapor core. A fraction of the entrained liquid droplets will impinge on the oxide film on the main steam line inside the surface. The impact of liquid droplets on carbon-steel oxide films can produce a matrix of cracks and subsequent fatigue failure of the films, and expose the underlying metal surfaces to the corrosive action of the coolant. The parameters that determine film failure are the oxide hardness, the critical strain to oxide failure, and the fatigue loads required to fracture the oxide film. This wear mechanism occurs under certain conditions at elbows and fittings where the flow changes direction, predominantly on the outside radius of the bend in the direction of the flow [Keck and Griffith, 1987]. In contrast, damage caused by oxide dissolution occurs on the inside radius of the bend where flow separation causes turbulence. The droplet impact wear mechanism requires the presence of droplets, so this mechanism occurs only in pipes carrying two-phase flow.

Keck and Griffith [1987] provide simple models for estimating oxide dissolution and droplet-impact wear. The model developed to describe droplet-impact erosion does not depend strongly on temperature, but does depend strongly on flow velocity (fourth power dependence). Therefore, droplet-impact wear is expected to be of importance at high flow velocities.

FAC has caused ruptures in two-phase systems at some PWRs. The following are three examples: Oconee Unit 2 in 1982 , Arkansas Nuclear One Unit 2 in 1989, and Sequoyah Unit 2 in 1993. The FAC caused a 1219-mm (4-ft) rupture of a 609.6-mm (24-in.)-diameter, long-radius elbow in the feedwater heat extraction line that is supplied steam

from the high-pressure turbine exhaust at the Oconee Unit 2 in 1982 [NRC, 1982]. The utility established a pipe inspection program for two-phase (steam/water) systems after this incident. After the feedwater pipe rupture accident at Surry Unit 2 in 1986, the utility augmented this program to include single phase systems [NRC, 1991].

In 1989, following the 18 April rupture of a 355.6-mm (14-in) diameter steam extraction line at Arkansas Nuclear One Unit 2, pipe inspections revealed significant thinning of other sections of the two-phase steam extraction pipe at the plant. The pipe wall was worn from the nominal 9.52-mm (3/8 in) thickness to a thickness of about 0.79-mm (0.031-in). The 180 degree fishmouth rupture was about 76.2-mm (3-in.) wide. That prompted the utility to replace more than 30.48-m (100 ft) of carbon steel pipe with 2.5% chrome alloy material [Stroller, 1989].

A third incident occurred at Sequoyah Unit 2, a 1,148 MWe PWR that has been in commercial operation since 1982. The extraction line to the feedwater heater ruptured and caused a 76- by 152-mm (3- by 6-in.) hole in the line. The cause of this event was a programmatic failure of the FAC program resulting from insufficient management of the program [Stoller, 1993]. To prevent recurrence, an independent review of the FAC program for adequacy and completeness was to be performed. The plant was to evaluate appropriate pipe systems on both Units 1 and 2 again. Inspections, as well as repair and replacements, were to be performed based on the results of the evaluation. This resulted in a long shutdown for both units.

2.5 Selection of FAC Empirical Models

Of the three models proposed to describe FAC, two will be briefly discussed in this section. Those models are empirical, the KWU-KR model [Kastner and Riedle, 1986 ; Kastner, 1987] and the EPRI-CH model [Chexal, et al., 1996]. The KWU-KR model is the FAC model within the WATHEC code produced by Siemens/KWU as a program to

aid utilities in managing pipe degradation caused by the FAC process. This KWU-KR model is derived from both single- and two-phase flow data. Single-phase flow data taken in the lab were used to derive the original relationships among the parameters. The derived relationships were then adjusted as needed to fit two-phase plant data [Kastner, 1987]. A similar method was used for the EPRI-CH model which is the FAC model within the CHECWORKS code, an EPRI product that competes with WATHEC. The lab data used in the KWU-KR model were generated at Siemens/KWU and the plant data used consists of approximately 6,000 single- and two-phase data points [Chexal, et al., 1996]. The data used by EPRI includes British, French and German lab data, U. S. plant data, and EPRI sponsored lab data [Chexal, et al., 1996].

Both the KWU-KR and EPRI-CH model report better model predictions when compared to laboratory single phase data than when compared to all data within the respective databases. Figures 2-4 and 2-5 give the comparison, respectively, of single phase lab data and of single and two-phase both lab and plant data to the KWU-KR model [Kastner and Riedle, 1986]. For single and two-phase both lab and plant data in Figure 2-5, the empirical calculated FAC rate in 85% of 1,049 cases are greater or equal to the measured FAC rate. Figures 2-6 and 2-7 give the comparison, respectively, of single-phase lab and of single and two-phase both lab and plant data to the EPRI-CH model [Chexal and Horowitz, 1995; Chexal, et al., 1996]. For the performance of the EPRI-CH correlation against single-phase lab data, the measured FAC rate lies within a range of ±50% compared with the predicted FAC rate. However, lab and plant data shows the measured FAC rate lies within a range of ±100%[2] compared with the predicted FAC rate.

[2] The associated plots, either in the Chexal and Horowitz 1995 paper or Chexal and et al. 1996 book, were mistaken to say "the accuracy of the wear rate predication is generally within ±50%". Actually, the two ±50% lines as indicated in Figure 2-7 were two ±100% lines.

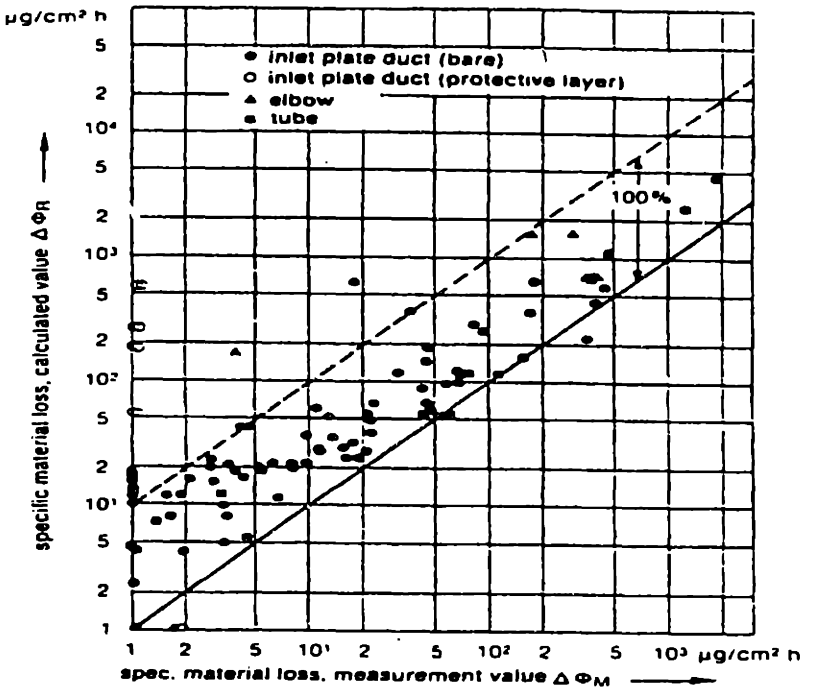

Figure 2-4. KWU-KR FAC model, comparison against single laboratory data [Kastner and Riedle, 1986].

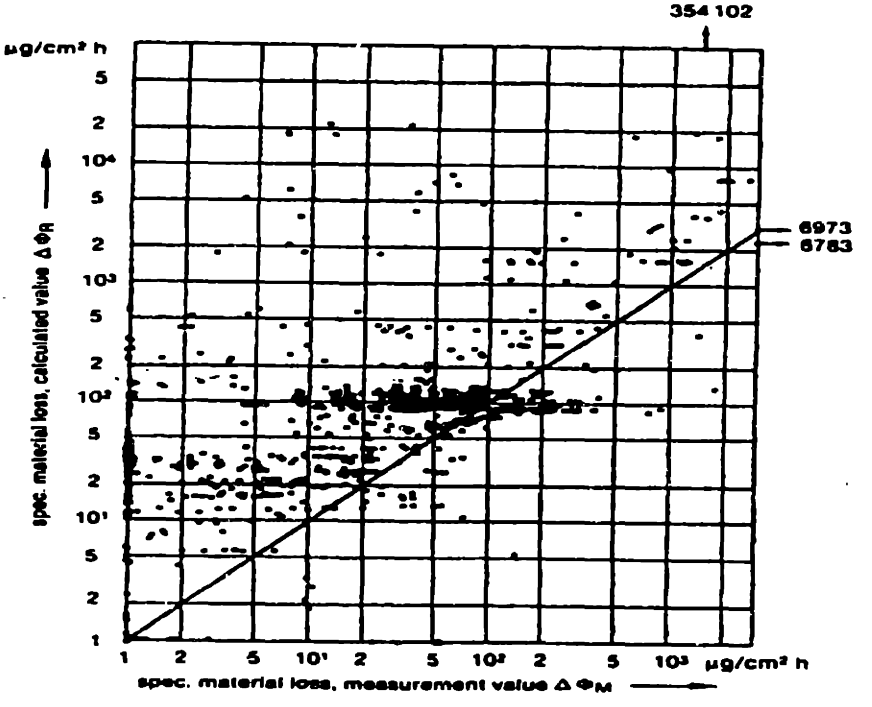

Figure 2-5. KWU-KR FAC model, comparison against single and two-phase both laboratory and plant data [Kastner and Riedle, 1986].

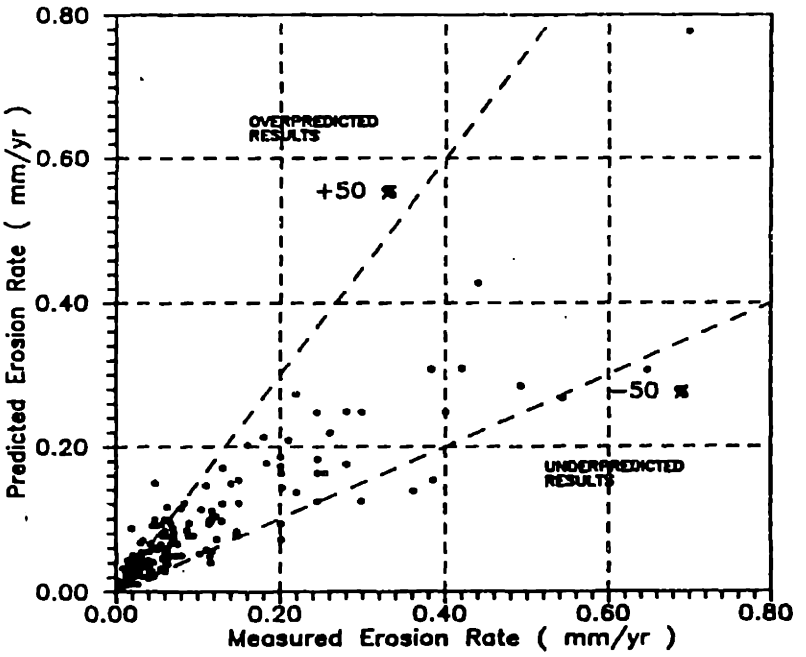

Figure 2-6. EPRI-CH FAC model, comparison against single laboratory data [Chexal and Horowitz, 1995; Chexal, et al., 1996].

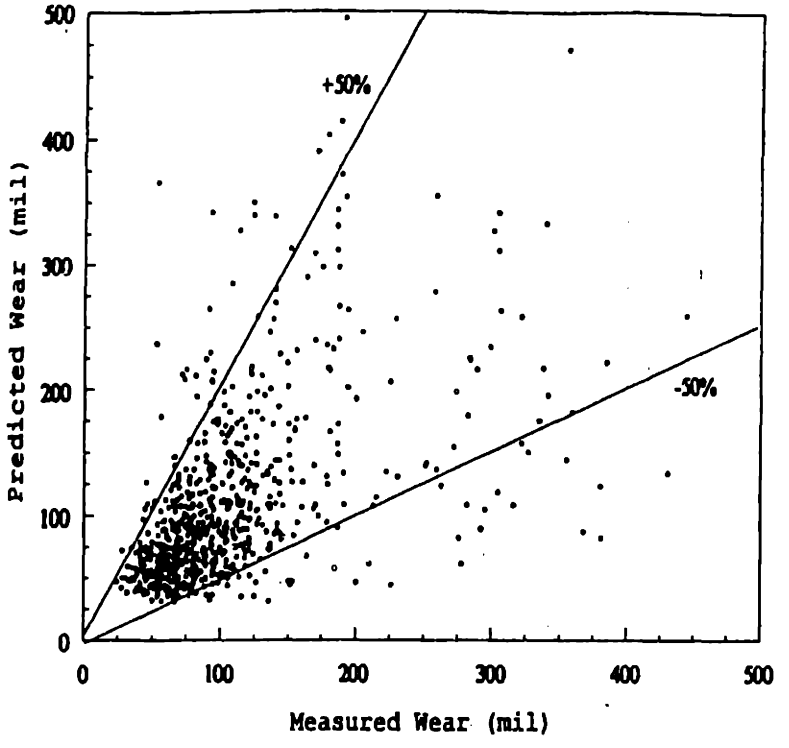

Figure 2-7. EPRI-CH FAC model, comparison against single and two-phase both lab and plant data [Chexal and Horowitz, 1995; Chexal, et al., 1996].

While the formulation of the EPRI model is not documented in detail due to its proprietary nature, the formulation of the FAC material loss rate used in the KWU-KR model is well documented. A third empirical model, part of the BRT-Cicero code, was developed at the Electricité de France and is based on experimental data taken on the Cicero test loop [Chexal, et al., 1996]. The EDF's BRT-Cicero code is not documented in detail due to its proprietary nature as well. Consequently, the FAC analysis presented in this work will center around the KWU-KR model.

2.6 Details of the KWU-Kastner-Riedle FAC Model

In its simplified form, the KWU-KR model estimates the FAC rate by way of a parametric equation of the form:

$$\text{FAC rate} = K_C \cdot F_1(V,T,h) \cdot F_2(pH) \cdot F_3(O_2) \cdot F_4(t) \cdot F_5(x) \qquad (2\text{-}1)$$

where

K_C	Keller's geometry factor,
$F_1(V,T,h)$	a complex function of velocity V, fluid temperature T, and material composition h,
$F_2(pH)$	a function of pH at $77^o F$ $(25^o C)$,
$F_3(O_2)$	a function related to the oxygen influence,
$F_4(t)$	a function of exposure time, and
$F_5(x)$	a function of the steam quality in two-phase flow.

Using the KWU-KR methodology, the pipe thickness can be estimated as a function of time. The wall erosion, $W_c(t)$, is the thickness of the pipe that has been eroded away and is a function of time. This term is calculated by

$$W_C(t) = \frac{\int_0^t \Delta\Phi_R(t) \cdot dt}{\rho_{st}} \qquad (2\text{-}2)$$

where

$\Delta\Phi_R(t)$: FAC rate ($\mu g / cm^2 hr$) and can be calculated as in equation (2-3) below,

t : the exposure time,

ρ_{st} : the density of steel.

Using the KWU-KR model, the pH, oxygen content, liquid velocity, geometrical factor, total content of chromium and molybdenum in steel, and operating temperature are assumed to be known. We can calculate the FAC rate from the following equations [Kastner and Riedle, 1986] :

$$\Delta\Phi_R(t) = 6.25 \cdot k_c \{B \cdot e^{N \cdot w} \cdot [1 - 0.175 \cdot (pH - 7)^2] \cdot 1.8 \cdot e^{-0.118 \cdot g} + 1\} \cdot [f(t)] \qquad (2\text{-}3)$$

with

$$B = -10.5 \cdot \sqrt{h} - 9.375 \cdot 10^{-4} \cdot T^2 + 0.79 \cdot T - 132.5$$

$$N = -0.0875 \cdot h - 1.275 \cdot 10^{-5} \cdot T^2 + 1.078 \cdot 10^{-2} \cdot T - 2.15 \qquad \text{for } 0 \le h \le 0.5\%$$

$$N = (-1.29 \cdot 10^{-4} \cdot T^2 + 0.109 \cdot T - 22.07) \cdot 0.154 \cdot e^{-1.2 \cdot h} \qquad \text{for } 0.5\% \le h \le 5\%$$

where

$\Delta\Phi_R$: calculated specific rate of material loss, $\mu g / cm^2 h$,

k_C : geometrical factor,

w : flow velocity, m/s,

pH : pH value,

g : oxygen content, $\mu g / kg$,

h : content of chromium and molybdenum in steel (total), %,

T : temperature, °K.

Note that the time correction factor, f(t), of the FAC rate equation is a function of the exposure time. The behavior of this factor is shown in Figure 2-8. The factor f(t) has a value of 1 in small operating periods and tends to a value of 0.79 for an operating period of $9.6 \cdot 10^4$ hrs (approximately 11 years). For longer operating periods ($t \geq 9.6 \cdot 10^4$ hrs), f(t) equals 0.79. The time correction factor is given by

$$f(t) = C_1 + C_2 \cdot t + C_3 \cdot t^2 + C_4 \cdot t^3 \qquad (2\text{-}4)$$

where

t is the exposure time (in hours); C_1, C_2, C_3, and C_4 are constants as follows:

$C_1 = 0.9999934$

$C_2 = -0.3356901 \cdot 10^{-6}$

$C_3 = -0.5624812 \cdot 10^{-10}$

$C_4 = 0.3849972 \cdot 10^{-15}$

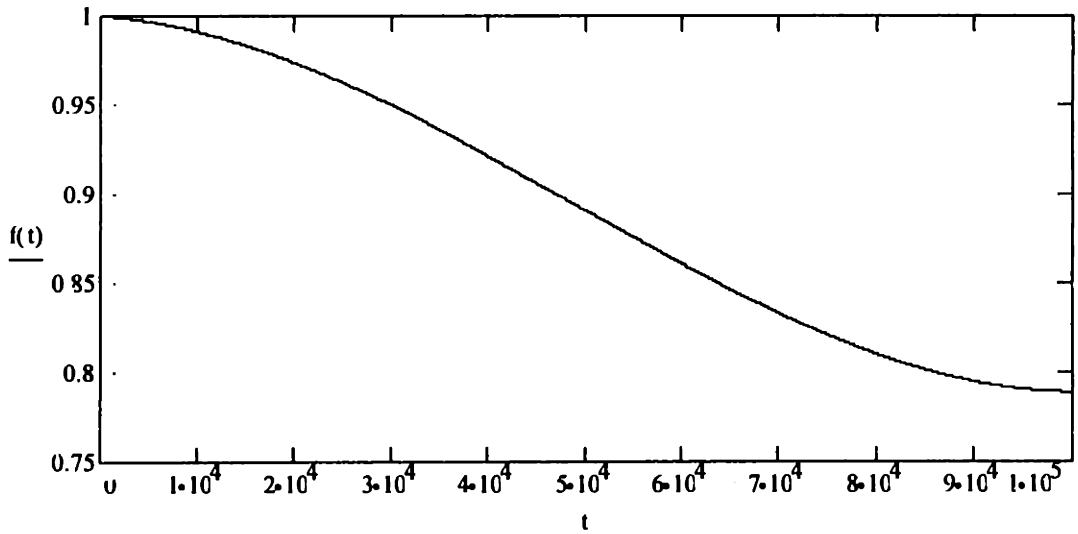

Figure 2-8. The factor f(t) versus t (hrs) in the KWU-KR model.

As with any model, a number of assumptions have been made. The KWU-KR model embodies several assumptions that impact its range of applicability [Kastner, 1987]:

1. There is no restriction on the flow velocity.

2. The material losses due to FAC are mostly to be ignored (consistent with the literature) at water temperatures greater than 240°C (464°F).

3. The pH parameter is bounded by the values of 7.0 and 9.39 on the low and high ends, respectively. If the pH is less than 7, it must be set equal to 7. If the pH is greater than 9.39, the calculated material loss is assumed to be $\Delta\Phi_R = 1\,\mu g/(cm^2 * h)$.

4. The range of oxygen concentrations is $0 \le g \le 30\mu g/kg$. For $g > 30\,\mu g/kg$, the calculated material loss is $\Delta\Phi_R = 1\,\mu g/(cm^2 * h)$.

5. The range of material content for chromium (Cr)- and molybdenum (Mo)-content is $0 \le h \le 0.5\%$. For $h > 0.5\%$, no material losses due to FAC are expected.

6. This model is valid only for operating time periods longer than 200 hours ($t \ge 200$ h). Very high material losses can occur in the start-up phase.

7. The basic condition is annular flow in two-phase flow. When applying the empirical model for water flow to water/steam flows, the reference velocity used is not the velocity of a two-phase mixture, but the mean velocity in the film of water on the wall of the component, W_F. A simplified equation for this is:

$$W_F = \frac{\dot{m}}{\rho_W} \cdot \frac{1-x}{1-\alpha} \tag{2-5}$$

where $\dot{m}$: the mass flux,

ρ_W : the density of the water at saturation condition,

x : the steam quality,

α : the void fraction.

2.7 Comparison of the EPRI-CH and KWU-KR Models

The formulation of the FAC rate used in EPRI-CH model is [Chexal, et al., 1996]:

$$\text{FAC rate} = F_1(T) \cdot F_2(AC) \cdot F_3(MT) \cdot F_4(O_2) \cdot F_5(pH) \cdot F_6(G) \cdot F_7(\alpha) \tag{2-6}$$

where

$F_1(T)$: the factor for temperature effect,

$F_2(AC)$: the factor for alloy content effect,

$F_3(MT)$: the factor for mass transfer effect,

$F_4(O_2)$: the factor for oxygen effect,

$F_5(pH)$: the factor for pH effect at temperature,

$F_6(G)$: the factor for geometry effect,

$F_7(\alpha)$: the factor for void fraction in two-phase flow.

Since the theoretical relationship between the parameters F_1 through F_7 was not evident, the formulation was developed empirically. Note that if any one of these factors becomes zero, the FAC rate goes to zero. The following are the restrictions with regard to the range of applicability of this model [Chexal and Horowitz, 1995] :

(1) The fluid temperature factor, $F_1(T)$, influences several variables. The variation of FAC rate with temperature is a bell-shaped curve with the maximum around $150^0C\,(300^0F)$. The temperature range of interest for nuclear power plants is $93.3^0C - 260^0C$ $(200^0F - 500^0F)$.

(2) The alloy content factor, F_2 (AC), includes three alloy elements: chromium, copper, and molybdenum. The substantial decrease in the rate of FAC with even small amounts of chromium is due to the increase in stability of the oxide layer. Chromium tends to drastically reduce the solubility of ion oxides in pure water and, thus, its presence greatly reduces the FAC rate.

(3) The mass transfer coefficient is one of the important factors that affects both the single-phase and the two-phase FAC rate.

(4) The FAC rate varies inversely with the amount of dissolved oxygen present.

(5) In the pH range of interest between 7 and 10 (i.e., the cold pH measured at 25^0C (77°F)), the higher the hot pH , the lower the FAC rate.

(6) The geometry factor accounts for the increased mass transfer that takes place in fittings and upstream conditions, due to local turbulence.

(7) In two-phase flow, the distribution and velocity of the liquid phase govern the FAC rate. A void fraction correlation developed by Chexal et al. is used in this model. When the void fraction is unity, i.e., there is no liquid present, $F_7(\alpha) = 1$, which means that FAC does not occur in dry steam.

In summary, the major differences between the two models are shown in Table 2-7.

Table 2-7 The major differences between the KWU-KR and the EPRI-CH models.

	KWU-KR	EPRI-CH
Material Alloy Composition Consideration	Cr and Mo	Cr, Mo, and Cu
Kinds of the Different Geometry Factors	15	48
Two-Phase pH Value Input to the Code	Set to equal 7	Measured plant data
Two-Phase Oxygen Value Input to the Code	Set to equal 0	Measured plant data
Operation Time in FAC Rate Equation	Dependent	Independent

2.8 Comparison of the Calculated FAC Results Using Two Different Models

To validate the application of the KWU-KR model in the FAC rate calculations through our computer code, we compare our calculated results with two commercial codes, the KWU-WATHEC computer code and the EPRI CHEC computer program in this section.

2.8.1 Comparison of results with the KWU-WATHEC Code

Using Mathcad [Mathsoft Inc., 1995], we obtain the predicted FAC rates for a benchmark calculation. The calculation used the following baseline parameters: 102-mm (4-in.) diameter carbon steel elbow, 7 ppb oxygen content, 6.1-m/s (20-ft/s) flow velocity, room temperature [25°C (77°F)] pH of 7, and 0.03 wt% of chromium, molybdenum, and copper[3] content; the variations are noted as appropriate. The pH level at room temperature is also referred to as cold pH. Figure 2-9 is our calculation results using the KWU-KR model for changing flow velocity from 1.5-m/s (5-ft/s) to 9.1-m/s (30-ft/s). Figure 2-10 shows the calculation results using the KWU-WATHEC computer code under the same condition. We analyzed the same problems using the WATHEC program, version 2.2, rls 4.2. The WATHEC analysis was performed by Mr. Ratkai at the PAKS plant in Hungary [Shah, 1998]. Comparing our results in Figure 2-9 with the KWU-WATHEC results in Figure 2-10 , we find that both in shape and in size, our results (change velocity, chromium content, dissolved oxygen, and pH) fit very well when compared with the KWU WATHEC Code calculated results, except for the results of later forcing the FAC rate to equal zero which means no FAC effect, when the temperature approaches 500^0F. The comparison of these results by changing the chromium content, dissolved oxygen, and pH is also shown to have similar results.

[3] Copper content isn't included in the calculation of the KWU-KR model as indicated in Chapter 2.

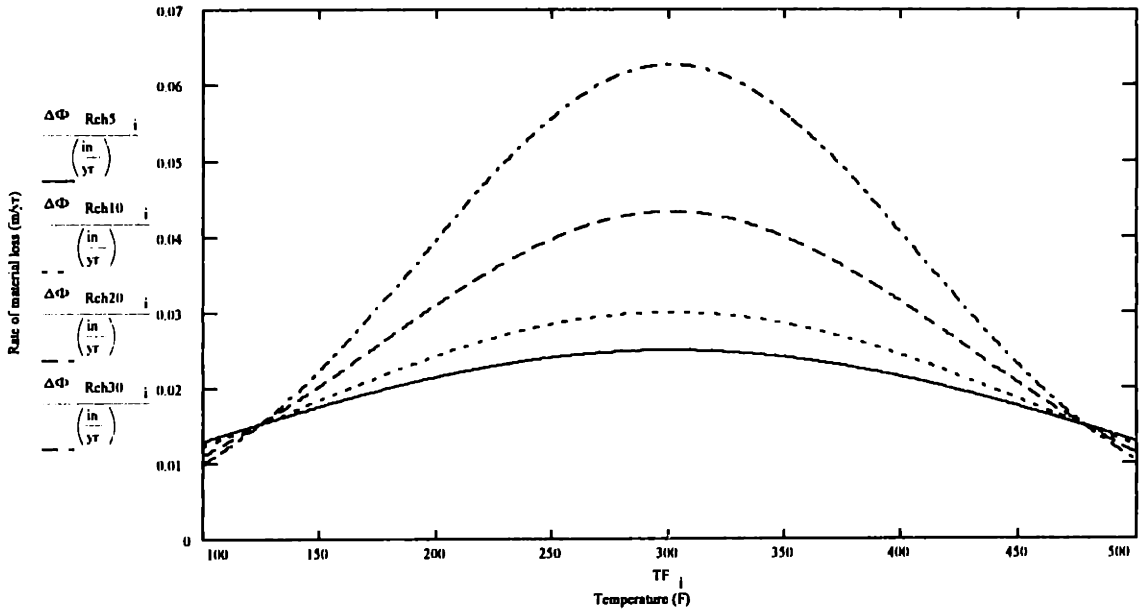

Figure 2-9 The Mathcad results using the KWU-KR model

(from the top curve, V=30 ft/sec, 20 ft/sec, 10 ft/sec, 5 ft/sec).

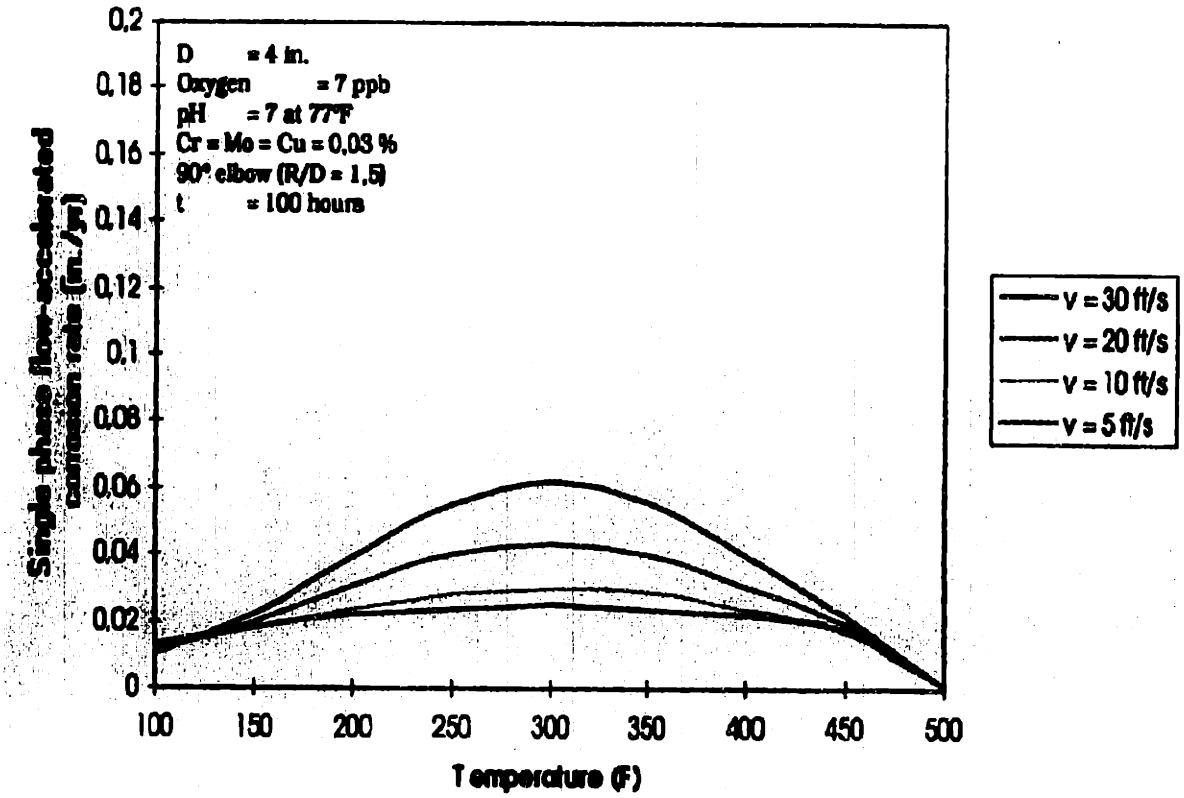

Figure 2-10. Results corresponding to those of Figure 4-1 using the KWU-WATHEC code (from the top curve, V=30 ft/sec).

2.8.2 Comparison of results with the EPRI-CH Code

Chexal and Horowitz [1995] have analyzed four simple FAC problems using the EPRI-CH model (see Figures 3, 5, 7, and 8 in the Chexal and Horowitz' paper [Chexal and Horowitz, 1995], or Figures 52, 51, 54, and 56 in the NUREG/CR-6456 report [Shah, et al., 1997]). This model has been incorporated in the CHEC computer program and other subsequent programs developed by EPRI. Comparison of the results shows that the KWU-KR results are generally significantly smaller than those of the EPRI code. A comparison of our results with those of the EPRI-CH was shown in Figure 2-1. For example, the EPRI code gives a maximum FAC rate of about 3.9 mm/yr (0.155 in/yr) for 0.03 wt% [Chexal and Horowitz, 1995]. The corresponding FAC rate in the case of 0.03 wt% Cr predicted by the KWU-KR model through our calculations is about 1.14 mm/yr (0.045 in/yr), as shown in Figure 2-1. The other three associated comparisons are shown in Figures 2-11 to 2-13. Those four cases calculated by KWU-KR are less conservative when compared with corresponding results of the EPRI-CH model.

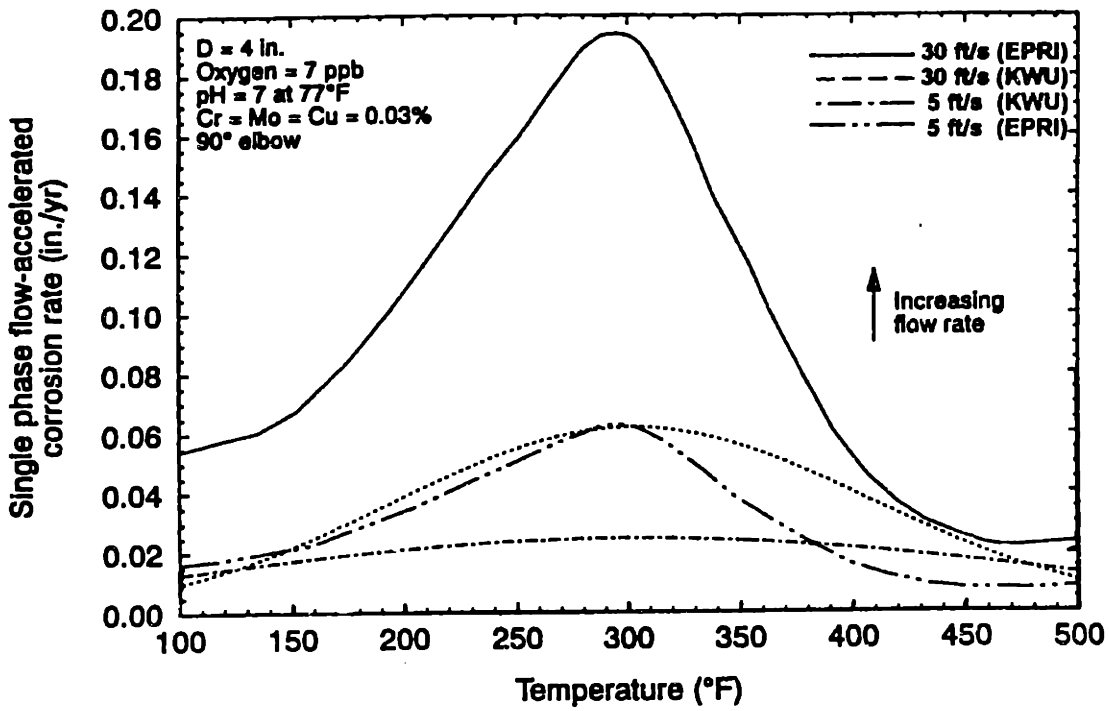

Figure 2-11. Comparison of the EPRI-CH and the KWU-KR models by changing of velocity.

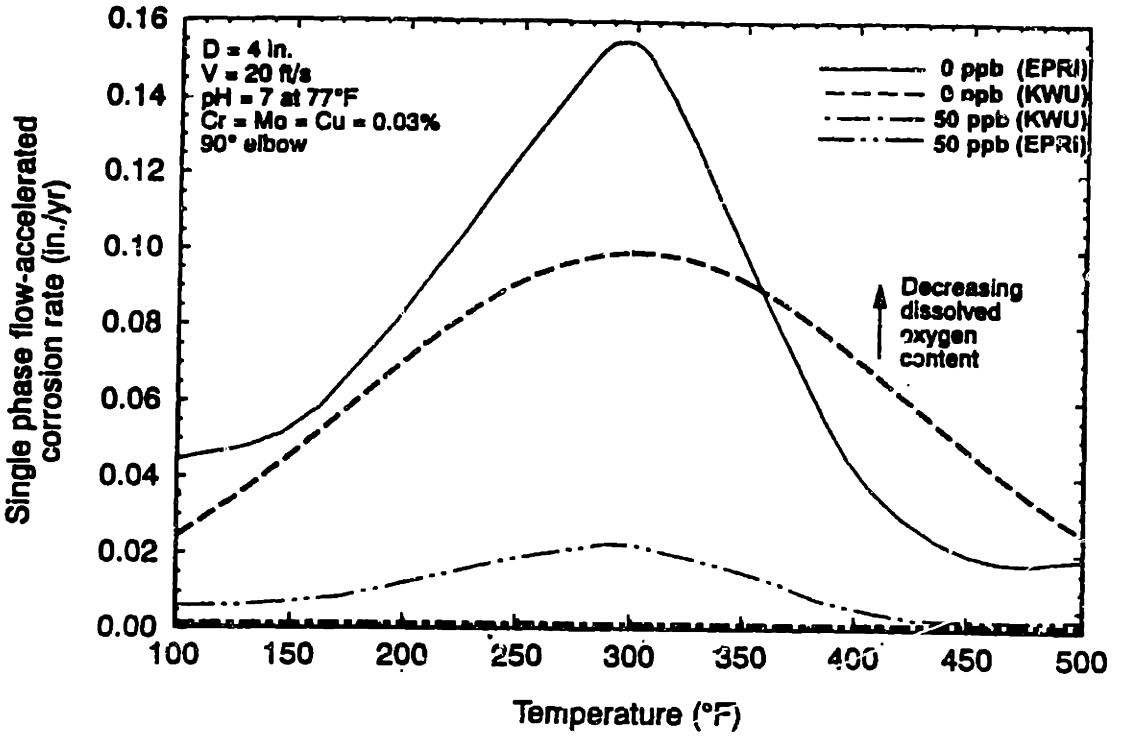

Figure 2-12. Comparison of the EPRI-CH and the KWU-KR models by changing of dissolved oxygen content.

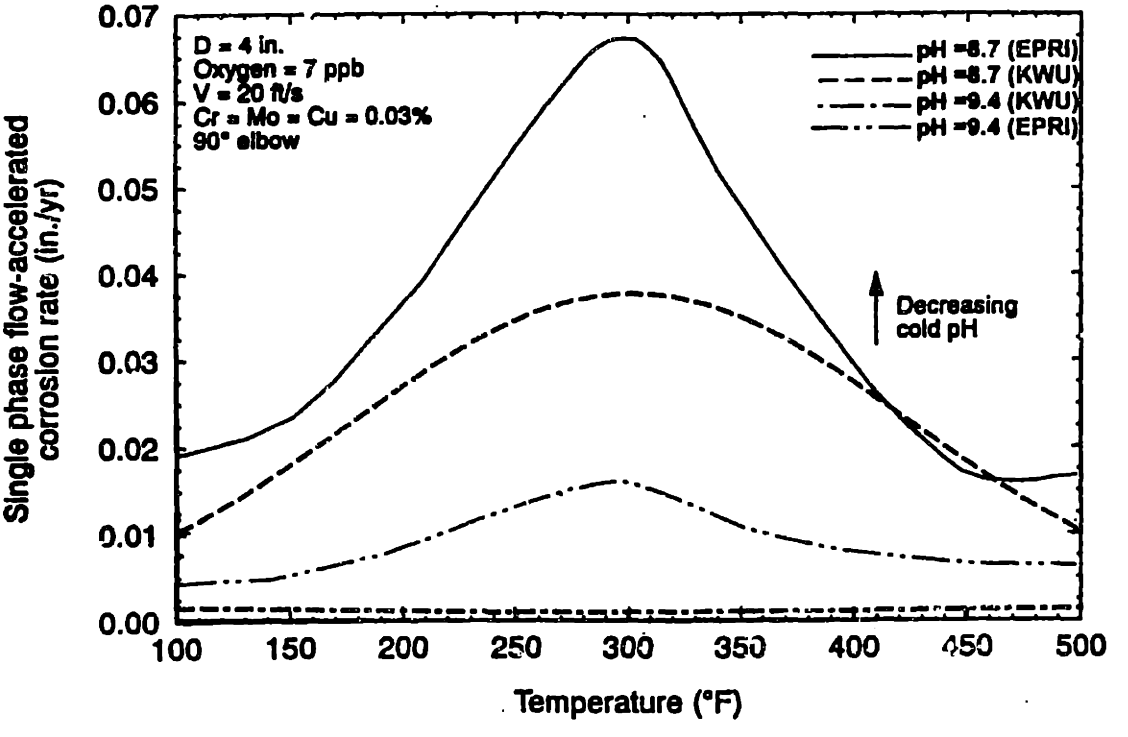

Figure 2-13. Comparison of the EPRI-CH and the KWU-KR models by changing of pH.

2.9 Application of the KWU-KR model to Four Events

To learn the KWU-KR model and to see what kind of prediction results it gives, four cases which have occurred in nuclear power plants were selected to perform detailed calculations.

When using the KWU-KR model for the FAC rate calculation, the various parameters contribute to the overall uncertainty on the resulting calculation, namely the FAC rate. The parameter uncertainties associated with this calculation should be propagated through the model in order to obtain probability distributions for the FAC rate. To explore the parameter uncertainty, four cases representing actual FAC-caused ruptures are discussed in Appendix A. These four FAC cases are:

Case 1 Surry Unit 2, ruptured elbow downstream of tee in feedwater (18 in.) pipe.

Case 2 Trojan, heater drain pump discharge (14 in.) pipe.

Case 3 Millstone Unit 2, heater 2B secondary steam (16 in.) pipe.

Case 4 Fort Calhoun, fourth stage extraction stream (12 in.) pipe.

Using these four cases, the parameter uncertainties can be investigated by using their individual distribution type, and then by using the Monte Carlo sampling methods (10,000 runs) to obtain the associated uncertainty [Decisioneering, 1996]. Cases 1 and 2 are single phase flow cases while Cases 3 and 4 are for two phase flow. The detailed calculations and results are shown in Appendix A.

2.10 Local and Uniform Wall Thinning Effects

Corrosion can be classified from the surface morphology into two types, uniform (or generalized corrosion), and localized corrosion (pitting corrosion, crevice corrosion, etc.). Under certain circumstances, it is possible to safely operate a piping system when the local wall thickness is below the minimum allowable thickness. This is true when it can be demonstrated that the thinned area is local and relatively small so that the integrity of the component is not compromised. When an area of a pipe or component has been thinned below the limit, t_{min}, it is normally declared to be unfit for further service. However, a methodology has been developed for evaluating the component for further service. This methodology defines a local acceptance thickness, t_{aloc}, that may be less than the minimum allowed wall thickness [ASME Code Case N-480, 1990].

However, we consider the uniform wall thinning effect only in our calculations. The uniform corrosion results in the relatively uniform removal of a surface and leads to relatively large thinned areas. Localized corrosion is not relevant to FAC [Chexal, et al., 1996]. From previous work used to identify and assess the severity and frequency of degradation mechanisms in nuclear power plant piping, approximately 1,000 cracking and leaking events and 100 rupture events (leakage rates greater than 50 gpm) were identified [Gosselin, et al., 1996]. Of the rupture events, 30% of the total were attributed to FAC, and 7% each to design and installation errors, maintenance errors, water hammer, and unknown mechanisms. The remaining mechanisms each were 1% to 4% of the total rupture events. FAC is the only mechanism has any significant potential for large leaks [Gosselin, et al., 1996; Gosselin, 1997]

Chapter 3: Development of Quantitative Methods

3.1 Development of Stress-Strength Interference Model

To obtain the probability that a pipe segment will rupture due to FAC, the wall thinning must be used to determine the remaining pressure capacity. This pressure capacity is then compared with the pressure loading that the pipe segment would be subjected to during operation. This type of "load versus capacity" evaluation is known in the reliability literature as stress-strength interference.

Let the pressure capacity be C (in our case, the system maximum allowable pressure is a function of time due to time dependence of the thickness of the pipe that has been eroded away). The stress or load is L, i.e., either (i) a static load from the system operation pressure at the full power, steady state operation, or (ii) a dynamic load. The probability of failure of the pipe can be computed from

$$P_f(t) = P[C(t) < L(t)] = 1 - \int_0^\infty F_L(x,t)\ f_C(x,t)\,dx = \int_0^\infty [\int_x^\infty f_L(y,t)dy] f_C(x,t)dx \quad (3\text{-}1)$$

where

$P_f(t)$	:	pipe failure probability,
C(t)	:	pressure capacity,
L(t)	:	pressure load,
$F_L(x,t)$	:	the load cumulative distribution function,
$f_C(x,t)$	:	the capacity probability density function (1/psi),
$f_L(y,t)$	:	the load probability density function (1/psi) ($= \frac{dF_L(x,t)}{dx}$),
t	:	operational time (hr).

A plot of $f_L(y,t)$ and $f_C(x,t)$ is shown in Figure 3-1.

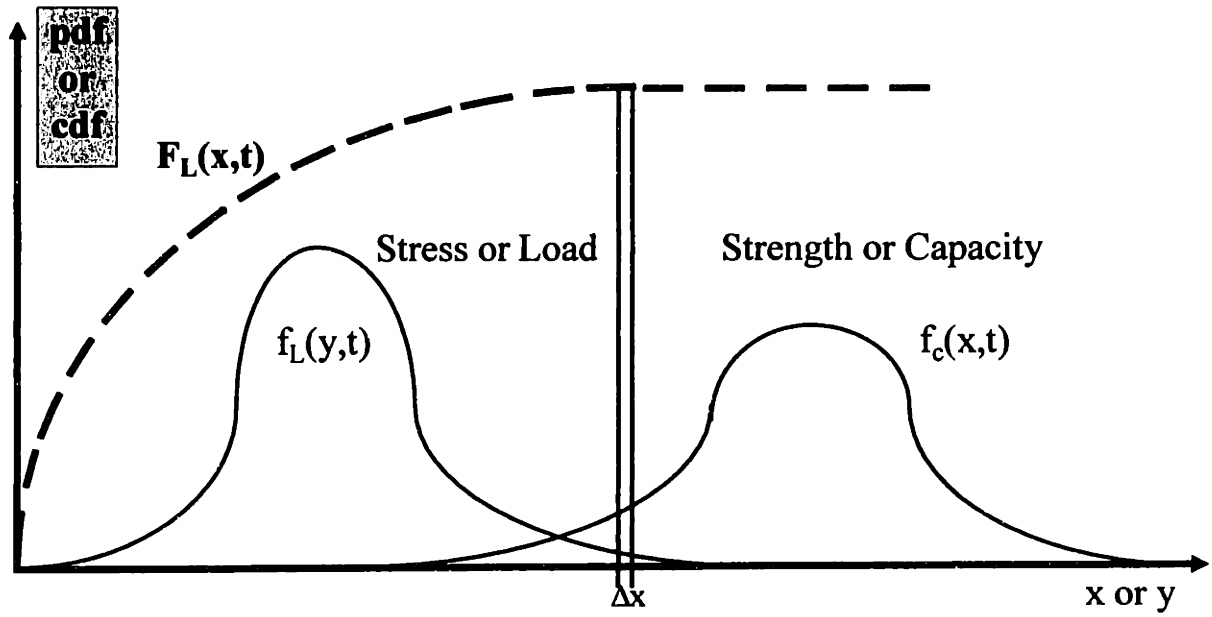

Figure 3-1. Stress-strength interference model.

The pdf $f_c(x,t)$ is expected to stretch towards lower values of the capacity as the wall thickness is reduced due to FAC (Figure 3-2).

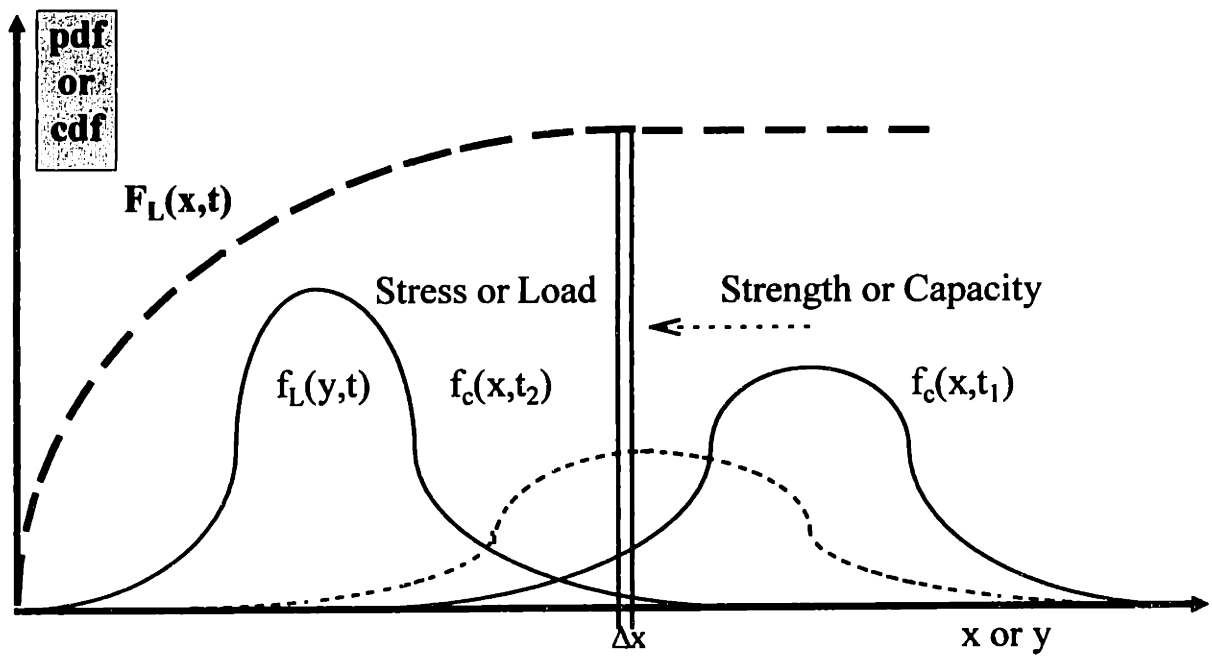

Figure 3-2. Stress-strength interference model at different times ($t_2>t_1$).

3.2 Determination of the Capacity

The capacity probability density function, $f_C(x, t)$ can be determined by estimating the FAC rate (e.g., the KWU-KR model) as a function of time and assessing the relevant uncertainties. The equation for the wall erosion, $W_c(t)$, has already been given as Equation (2-2). The pipe pressure capacity evaluation would then include the thinning wall (which is a function of time) to determine the expected pressure capacity.

From the published literature [Kastner and Riedle, 1986] (Figure 3-3), the relationship between the empirical model predictions and the measured FAC rates in laboratory studies or in power plants can be determined. From the data, it appears that the KWU-KR model was developed to overpredict the FAC rate. In other words, it is designed to err mostly on the conservative side. This feature of the model could be used to determine an "adjustment" factor that would express our uncertainty in the calculated results. Referring to Figure 3-3, there is a total of 1,049 cases where it appears that the variability reflected on individual data points is due to both parameter uncertainties and the uncertainty due to the model itself.

To express our uncertainty in the KWU-KR model predictions, we employ the "adjustment-factor" approach discussed by Zio and Apostolakis [1996; Apostolakis, 1995]. This approach takes the single available model which is called the deterministic reference model (DRM), and introduces a multiplicative factor E to modify the results obtained from the available model. In other words, to better match the actual collected data, the predicted results are adjusted by a factor. The KWU-KR model is our choice of the reference model. Thus, we write:

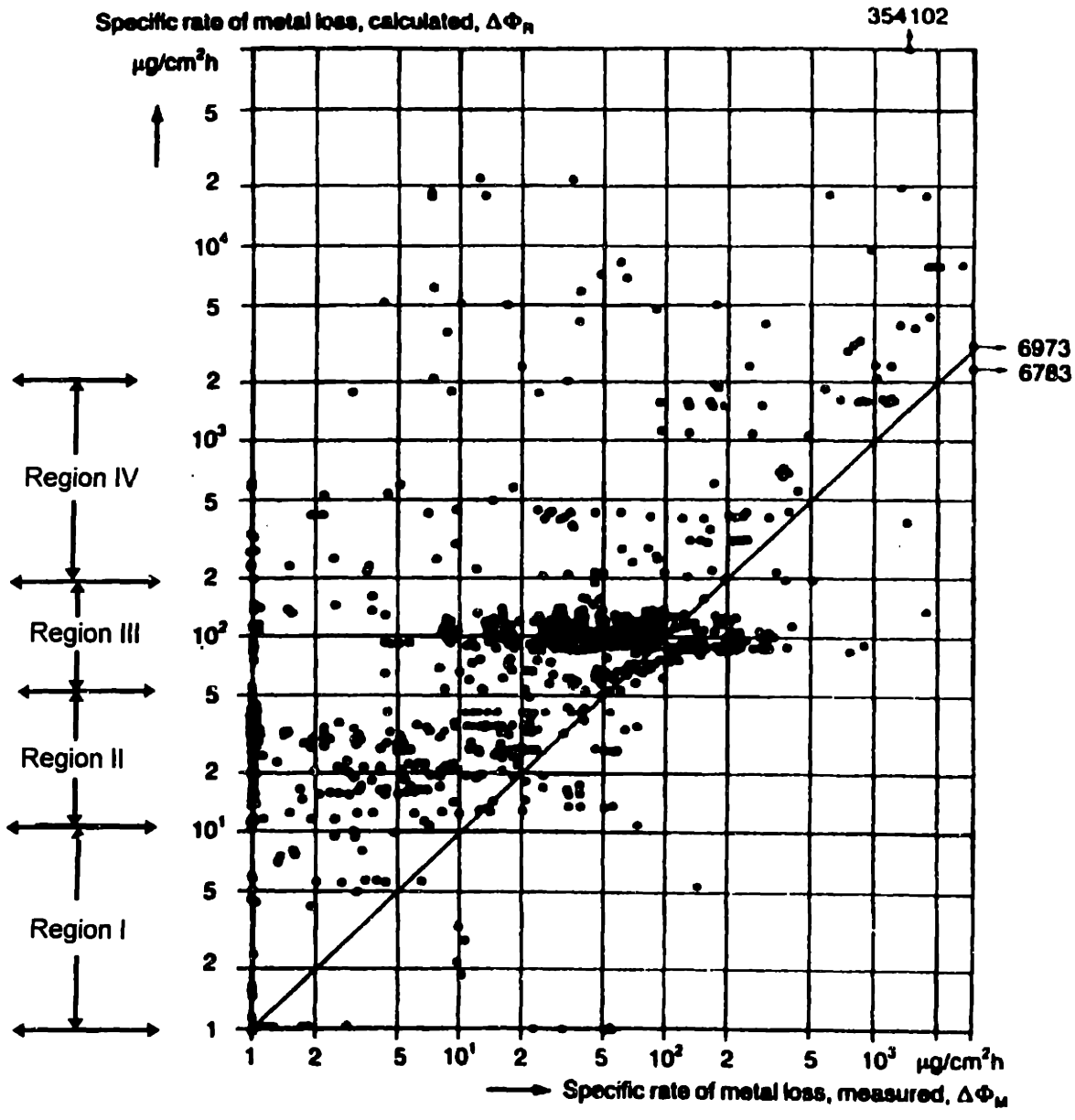

Fig. 3-3 Comparison of values calculated by empirical model with measurements from laboratory experiments and in power stations

Region I: 1 to 10 $\mu g/cm^2 hr$ (29 data points),

Region II: 10 to 50 $\mu g/cm^2 hr$ (184 data points),

Region III: 50 to 200 $\mu g/cm^2 hr$ (653 data points),

Region IV: 200 to 2,000 $\mu g/cm^2 hr$ (92 data points).

$$W = W_{DRM} * E \qquad (3\text{-}2)$$

where

W	:	actual (i.e., measured) FAC rate,
W_{DRM}	:	calculated FAC rate, using the DRM.
E	:	adjustment factor.

W is the product of its deterministic reference model prediction, W_{DRM}, and an adjustment factor E which accounts for the uncertainty in the calculated value.

To develop a probability distribution for E, divide Figure 3-3 into four regions along the axis of the calculated specific rates of metal loss $\Delta\phi_R$ ($\mu g/cm^2hr$). However, some data points above $\Delta\phi_R = 2.0 \cdot 10^3 \mu g/cm^2hr$ (along the axis of the calculated specific rates of metal loss) and some data points below $\Delta\phi_M = 1.0 \mu g/cm^2hr$ (along the axis of the measured specific rates of metal loss) were likely chopped off. We will exclude those data points from the total of 1,049 data points, thus, 958 data points are included in our calculation.

The data for each region resulted in a lognormal distribution for E by the goodness-of-fit tests [Decisioneering, 1996]. Once the distribution of the E parameter is known for the four regions, they can be introduced into the pressure capacity equation as shown in Section 3.2.3, later.

Table 3-1 shows the details of these lognormal distributions for the four regions. The lognormal distribution is shown in Equation (3-3). It has two parameters: μ (log mean) specifying its scale and ω (log standard deviation) specifying its shape. This distribution is skewed to the right.

$$f(E) = \frac{1}{\sqrt{2\pi}\omega x}\exp[-\frac{(\ln E - \mu)^2}{2\omega^2}] \quad (3\text{-}3)$$

Mean: $$m = \exp[\mu + \frac{\omega^2}{2}] \quad (3\text{-}4)$$

Standard deviation of the variable E: $$\sigma = e^{2\mu+\omega^2}(e^{\omega^2} - 1) \quad (3\text{-}5)$$

Median = $E_{50} = e^{\mu}$ (3-6)

Error Factor = $$\frac{E_{50}}{E_{05}} = \frac{E_{95}}{E_{50}} = e^{1.645\omega} \quad (3\text{-}7)$$

Table 3-1. E Factor Uncertainties.

	Region I	**Region II**	**Region III**	**Region IV**
μ	0.327	-1.169	-0.721	-2.029
ω	1.168	1.154	1.035	1.646
E_{05}	0.203	0.047	0.089	0.009
E_{50}	1.387	0.311	0.486	0.131
Mean	1.4263	0.6046	0.8307	0.5095
E_{95}	9.467	2.074	2.666	1.971
E=1	39th-Percentile	84.4th-Percentile	75.7th-Percentile	89.1th-Percentile

The distribution of E is interpreted as epistemic [Apostolakis, 1995]. This means that, for each region, E has a single value which is unknown to us. One may question this assumption and argue that, even within a region, E should exhibit variability from point to point, because the model performs better for some of the experimental conditions. Furthermore, the variability displayed in each region is due to both model and parameter uncertainties. As a first approximation, we take E to be epistemic.

3.2.1 Hoop Stress Analysis

A pipe component must be designed to withstand the internal pressure at which it will operate. The stress resulting from the internal pressure is known as the hoop stress. In many pipe systems, the hoop stress governs the required thickness. Pipe codes use a variation of the familiar equation for the stresses in a pressurized, thin-walled cylinder. Equation (3-8) is typical of the relationship used in pipe codes to calculate the minimum wall thickness needed to withstand the hoop stress in a straight pipe. This equation includes an allowance for wall thickness variability and deficiencies that may occur during installation or that result from FAC [ANSI/ASME, 1986].

$$W_{min} = W_{hoop} = \frac{P \cdot D_o}{2 \cdot (S \cdot J + P \cdot y)} + A \qquad (3\text{-}8)$$

where

W_{hoop} : the minimum wall thickness required, inches.

P : internal design pressure, psig.

D_o : outside diameter of pipe, inches.

S : maximum allowable stress in material due to internal pressure and joint efficiency at design temperature, psi.

J : longitudinal joint efficiency (or casting quality factor).

Y : a coefficient having the value of 0.4 for the temperatures of interest except for thick wall pipes where D_o / T_{hoop} is less than 6.

A : An additional thickness allowance for corrosion and/or erosion, to compensate for material removal during threading or grooving, extra mechanical strength that is required during installation, etc.

3.2.2 Pipe Design Codes

In the US, the specific pipe codes for the design of plant pipe systems depends on the age of the plant and the safety classification of the systems involved. Typically, pipe systems have been designed using either the B31.1 [ANSI, 1986] or B31.7 Power Pipe Code [ANSI, 1969] or Section III of the ASME Pressure Vessel Code [ASME, 1995] that deals with nuclear components. In older plants, B31.1 and B31.7 are used to design the power pipe. In newer plants, B31.1 was used to design the balance of plant pipe while the safety related pipe was designed using Section III. In addition, ASME Code Case N-480 [ASME, 1990] provides rules for evaluation, in-service inspection, repair, and replacement of ASME Class 1, 2, and 3 pipe susceptible to single-phase FAC.

3.2.3 Pipe Failure Analysis

The actual failure pressure of a pipe segment cannot be determined directly by Equation (3-3). To perform this evaluation, the pipe fragility analysis performed for the NRC's Inter-System Loss-of-Coolant Accident (ISLOCA) research program was used [Galyean, et al., 1993]. The ISLOCA analysis used a pipe failure analysis based upon hoop stress impacting the pipe in question. For a cylindrical vessel or pipe subjected to hoop stress, the pressure capacity that can be expected to cause failure can be calculated.

Once the E parameter is defined, it can be introduced into the pressure capacity equation as

$$C(t) = \frac{\sigma_f \{W_n - W_{DRM}(t)E\}}{[r + W_{DRM}(t)E](1+\varepsilon_f)} \qquad (3\text{-}9)$$

where

C(t)	:	pressure capacity (psi),
σ_f	:	failure stress (psi),
r	:	initial inside radius (in.),
$W_{DRM}(t)$	:	thickness of pipe eroded away at time t (in.),
W_n	:	nominal wall thickness (in.),
ε_f	:	hoop strain at failure,
E	:	uncertainty adjustment factor.

Table 3-2. Typical stress parameter values for SA 106B and hoop strain parameter values for SA 516 Grade 70 carbon steel.

Temperature (°F)	Failure stress (σ_f), ksi	Hoop strain (ε_f), %
77	61.2	6.2
400	64.8	3.7
600	62.1	5.8
800	49.5	7.9

Values for σ_f and ε_f for 304 stainless steel and SA 516 grade 70 carbon steel are listed in Wesley (1992). The parameters for SA 516 grade 70 carbon steel are shown in Table 3-2. Note that both the failure stress σ_f and hoop strain ε_f (both with 3σ uncertainty[4] less than 1%) can be treated as point values when compared with the variability of the adjustment factor E. The 3σ uncertainty of the initial inside radius and the nominal wall thickness comes from the manufacture's specified tolerance of 12.5%.

The failure pressure, C, is the pressure that would cause pipe rupture. Thus, in the capacity-load framework, the calculated failure pressure is the "capacity" of interest.

The load distribution, $f_L(y,t)$, represents the expected pressures for a particular section of pipe. Normally, the majority of the load distribution will be at the nominal system operational pressure. For example, if the nominal system pressure is approximately 370 psig and is experienced 90% of the time during operation, the load distribution would have 90% of the distribution centered at or around 370 psig. Transient pressures that cause the system pressure to exceed the nominal pressure would need to be incorporated into the load distribution. This incorporation would entail determining the anticipated pressures and their likelihood of experiencing such a pressure. A hypothetical load distribution may then look similar to the curve shown in Figure 3-4. We will consider the maximum peak pressure with uncertainty, given by a normal distribution, in the transient load calculation.

[4] This means three times of the standard deviation of a normal distribution. The interval defined by plus and minus 3σ from a mean value includes the random variable with 99.73% probability.

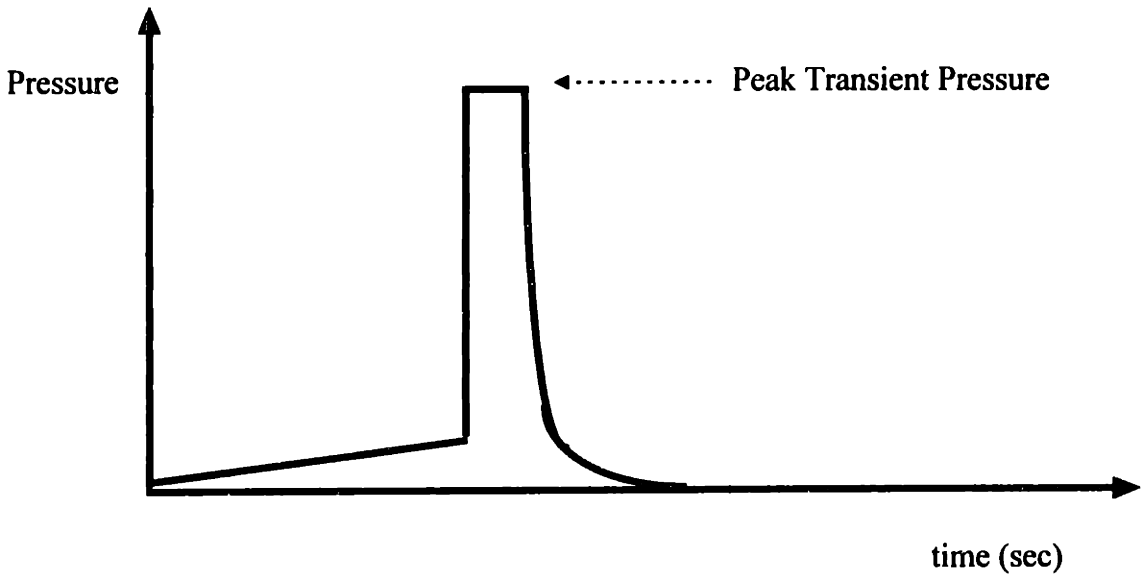

Figure 3-4. Example of a transient load.

3.3 Determination of the Load

3.3.1 Steady State Load

For static loads, $f_L(y,t)$ is a delta function and time independent. If the operating pressure of the associated system is $L_{ss,}$ we have

$$f_L(y,t) = \delta(y - L_{ss}) \tag{3-10}$$

3.3.2 Transient Loads

For transient loads, the pressure varies with time. To illustrate the basic concepts of time-dependent analysis, we consider a pipe segment subjected to a sequence of discrete and independent aleatory load events shown in Figure 3-5.

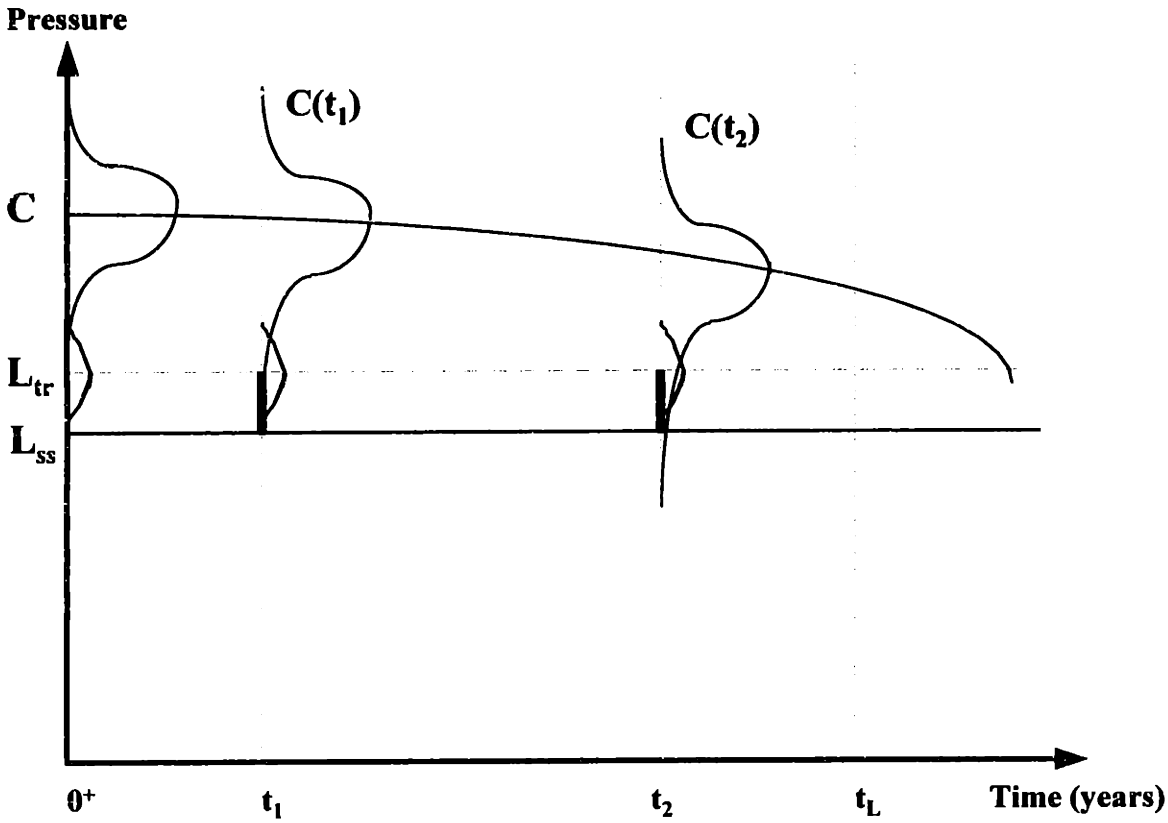

Figure 3-5. Schematic representation of steady state load (L_{ss}) and transient load (L_{tr}) processes and degradation of capacity ($t_2>t_1$).

Assume that the initial pressure capacity of the pipe segment is C(t). Suppose further that n transient loads occur within the time interval (0, t_L). Hence, the pressure capacity of pipe deteriorates with time due to FAC according to;

$$C(t)= C(t_0)g(t) \qquad (3\text{-}11)$$

where

g(t) : fraction of initial pressure capacity remaining at time t,

$C(t_0)$: random variable of the initial pressure capacity.

From Equation (3-9), we obtain

$$g(t) = \frac{r[W_n - W_{DRM}(t)E]}{W_n[r + W_{DRM}(t)E]} \tag{3-12}$$

If n transient loads occur within the time interval (0, t_L), at times t_j, j = 1,...,n, the reliability function is represented as follows [Ellingwood and Mori, 1993; Ellingwood, et al., 1996]:

$$R(t_L) = P[\{ C(t_0)\, g(t_1) > L(t_1) \} \cap ... \cap \{ C(t_0)\, g(t_n) > L(t_n) \}] = \prod_{j=1}^{n} F_L[C(t_0) g_j] \tag{3-13}$$

where $g_j = g(t_j)$ and $t_1 < t_2 < ... < t_n$. In general, the load occur randomly at times $\underline{T} = \{T_1, ..., T_n\}$ described by the joint pdf $f_{\underline{T}}(t)$. The time-dependent reliability function becomes,

$$R(t_L) = \int_{t_{n-1}}^{t_L} \cdots \int_0^{t_1} \{ \prod_{j=1}^{n} F_L[C(t_0) g_j] \} f_{\underline{T}}(t)\, dt \tag{3-14}$$

The number of loads within (0, t_L) is random. The number of events is governed by a Poisson process within the time interval (0, t_L). Their occurrence times, T, are the n-order of the random variable, $\underline{T}^* = \{T_1^*, ..., T_n^*\}$. These are uniformly distributed in (0, t_L) and are statistically independent. Since the intensities of the loads are statistically independent and identically distributed, we have

$$\prod_{j=1}^{n} F_L[C(t_0) g(T_j)] = \prod_{k=1}^{n} F_L(C(t_0) g(T_k^*)] \tag{3-15}$$

The joint pdf of the occurrence times is,

$$f_{\underline{T^*}}(t) = (1/t_L)^n \left[\frac{(\lambda t_L)^n \exp(-\lambda t_L)}{n!}\right] \tag{3-16}$$

and Equation (3-13) can be rewritten as,

$$R(t_L) = \sum_{n=0}^{\infty} \left[\int_0^{t_L} F_L\{C(t_0)g(t)\}\frac{1}{t_L}dt\right]^n \left[\frac{(\lambda t_L)^n \exp(-\lambda t_L)}{n!}\right] \tag{3-17}$$

where λ is the mean occurrence rate of transient pressure loads.

The conditioning on the initial pressure capacity is removed in order to take into account the epistemic uncertainty in the initial capacity: accordingly,

$$\overline{R(t_L)} = \int_0^{\infty} \exp\left[-\lambda t_L\left[1 - \frac{1}{t_L}\int_0^{t_L} F_L\{C(t_0)g(t)\}dt\right]\right] f_{C0}(x)dx \tag{3-18}$$

where $f_{C0}(x)$ is the pdf of the initial capacity, $C(t_0)$.

The probability of failure of the pipe during $(0, t_L)$ can be computed from $P_{fi}(t_L) = 1 - \overline{R(t_L)}$. The total failure probability of the pipe segment due to FAC caused by both the steady state and the transient loads can be obtained by summing the individual failure probabilities. We select a specific pipe segment due to FAC and perform a detailed stress-strength interference calculation in Chapter 5.

3.4 The Monte Carlo Simulation

Once both the load and capacity distributions are known, a simple Monte Carlo routine can be used to determine the failure probability of Equation (3-1). For the steady-state load, the Monte Carlo routine can be determined as follows:

Step 1. For a particular set of FAC parameters (e.g., flow rate, temperature, pH, etc.) at their best estimate value, use the KWU-KR model to determine FAC rate at time t_j, $\Delta\phi_R(t_j)$ by Equation (2-3), and the thickness of pipe eroded away at time t_j, $W(t_j)$, as shown in Equation (2-2).

Step 2. For a particular set of $\Delta\phi_R(t_j)$, find the corresponding adjustment factor $E_{i,j}$ distribution from Figure 3-3 and Table 3-1.

Step 3. For a particular set of $W(t_j)$, σ_f, ε_f, and with uncertainty distributions assigned to the adjustment factor $E_{i,j}$, the initial inside radius r_i, and the nominal wall thickness Wn_i, we plug them into Equation (3-9) to determine the capacity pressure C_i.

Step 4. Compare C_i with the steady-state load pressure for each iteration. Note that for each iteration, the capacity pressure will be different since it is a random variable. For those iterations where the load pressure is greater than the capacity pressure the pipe fails. Consequently, this iteration will increase the "pipe-failure count" by one.

Step 5. To calculate the overall pipe failure probability, take the "pipe-failure count" divide it by the total number of iterations.

Step 6. Repeating Step 1 through Step 5 by changing the time t_j, we obtain from year 1 to year j the time-dependent pipe failure probability at steady-state.

For transient loads, we use the Latin Hypercube sampling method to divide the associated probability distributions into 20 intervals of equal probability and consider the transient load variations in our calculations. The detailed computer program based on Mathcad code [Mathsoft, 1995] is shown in Appendix D. Equation (3-18) is directly applied to our calculations.

Chapter 4: Integration of FAC into Existing PRAs

4.1 Methodology for Screening and Analysis

The development of a methodology relies on the three general questions regarding risk that Kaplan and Garrick [1981] posed (see Figure 4-1).

Step 1 *Identification of important FAC scenarios*: What can go wrong due to FAC? We identify pipe segment failures due to FAC that can cause a transient or LOCA?

Step 2 *Assessment of the failure probability due to FAC*: How likely is an accident to occur due to FAC? We evaluate probabilities of pipe segment failure due to FAC vulnerabilities.

Step 3 *Determination of FAC consequences*: If FAC happens, what are the consequences? The consequences can be direct and indirect.

Step 1 uses information in existing plant-specific PRA/IPE models to estimate the risk-significance of plant pipe segments due to FAC effects, and screens out a significant number of pipe segments for which the consequences are too low to be worthy of further analysis. Step 2 estimates the failure probability of a pipe segment due to FAC aging effects from the analysis described in Chapter 3. Initiating events, event trees, and fault trees are reviewed and updated based on the findings from the screening analysis and the physical models. The spatial (or indirect) effects (Step 3) of the failure of pipe segments are included by reviewing the internal flooding report and a plant walkdown.

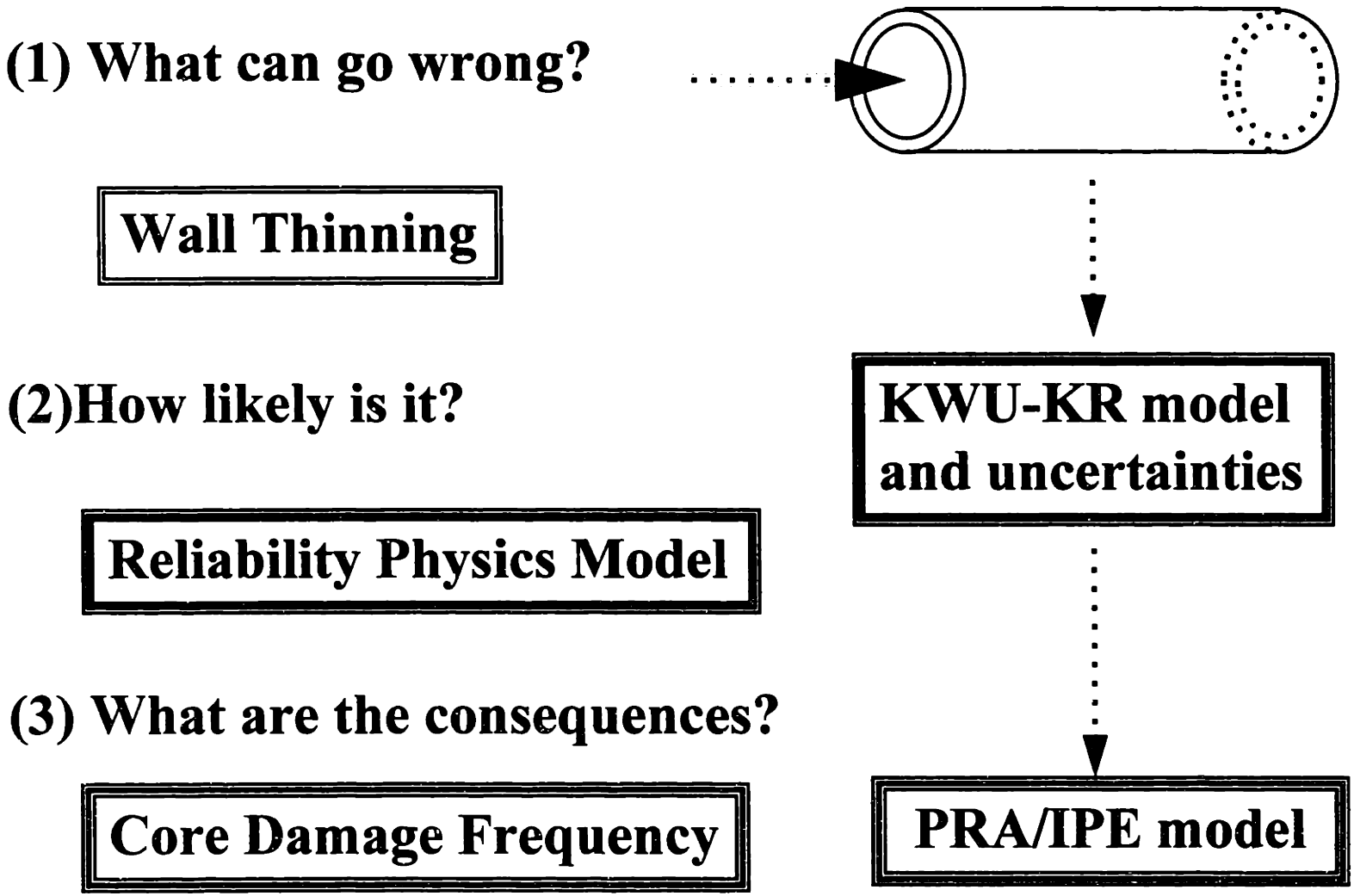

Figure 4-1. Risk questions applied to FAC.

4.1.1 Identification of Important FAC Scenarios

The following is a list of nuclear power plant systems that often experience FAC problems [Chexal, et al., 1996]:

Single phase systems: condensate and feedwater, auxiliary feedwater, heater drains, moisture separator drains, steam generator blowdown, reheater drains, and other drains.

Two-phase systems: high and low pressure extraction steam lines, flashing lines to condenser (miscellaneous drains), and feedwater heater vents.

The main feedwater pipe, auxiliary feedwater pipe, and main steam line are the three systems most likely to be affected by FAC in a PWR plant. The main feedwater pipe and main steam line are the two systems susceptible to FAC aging mechanisms in BWR plants.

The locations susceptible to FAC are observed in straight pipes downstream of components or obstacles causing turbulence (such as downstream of flow control orifices and valves). Other locations include elbows, pipe bends, reducers, tees, and pipe entries [Chexal, et al., 1996].

4.1.2 Determination of Consequences

The direct effects of pipe segment failure to be considered include [Vo, et al., 1997; Balkey, et al., 1997]:

(1) Failures that cause an initiating event, such as a transient or a LOCA,
(2) Failures that disable a single component, train, or system,
(3) Failures that disable multiple components, trains, or systems, and
(4) Failures that cause any combination of the above.

The indirect consequence analysis identifies potential effects resulting from pipe failures. The following pipe failure-induced conditions are considered: flooding, water spray, pipe whip, and jet impingement [Balkey, et al., 1997]. The first two conditions are usually analyzed in the internal flooding PRA. A high energy pipe has the potential to whip following a postulated failure. A whipping pipe has the potential to develop a through-wall crack of the associated pipe. The evaluation of fluid jets emanating from postulated breaks on nearby structures and components should consider the effect of jet loading, fluid temperature and moisture on the targets impinged upon. It is necessary to conduct the evaluation of the various areas of the Balance of Plant (BOP) area that could be impacted by indirect effects.

An example of FAC induced indirect or spatial effects (Case 4 of Appendix A) is the Fort Calhoun Station accident:

The steam line rupture damaged a nonsafety-related electrical load center in the vicinity of the pipe break. Additionally, collateral damage was experienced in several cable trays and pipe hangers, and insulation containing asbestos was blown throughout the turbine building. Certain portions of the fire protection system activated in response to the melting of fusible links in the sprinkler heads due to high temperature. Because there were no personnel in the immediate vicinity of the rupture, no one was injured. [NRC, 1997].

4.1.3 The Role of Inservice Inspection

SSCs of NPPs are subject to the effects of various degradation mechanisms during plant operation. The effect of significant degradation mechanisms on the condition, properties, and performance of SCCs with time or usage must be understood and provided for both in the design process and in the associated maintenance program.

Inservice inspection (ISI) focuses on the condition and properties of aspects of SSCs, while inservice testing (IST) focuses on the performance of systems and components [The research task force on risk-based inservice testing technology, 1996].

Risk-informed ISI (RI-ISI) are used to improve the effectiveness of the inspection of components and to reduce the overall operation and maintenance costs while maintaining regulatory compliance and maintaining or enhancing plant safety. The ISI interval is 10 years [Balkey, 1997].

4.2 PRA models

In general, PRA models do not include passive pipe failures. To include physical aging mechanisms into the PRA model the basic events contained in fault or event trees must be augmented. For example, if sections of pipes are susceptible to FAC, the system fault trees containing these sections of pipes need to be modified to account for the their failure. Once the pipe segments are incorporated into the PRA, the physical aging model representing FAC could be applied to the pipe segment basic events, thereby allowing the analyst to evaluate the impact of physical parameters (e.g., fluid velocity, steam quality, temperatures, pH) that drive the FAC phenomenon. Consequently, having the physical process incorporated into the PRA yields risk insights based on the aging process.

Modern PRAs consist of complex logic models that are developed to various degrees of detail. The SAPHIRE (Systems Analysis Programs for Hands-on Integrated Reliability Evaluations) code has the capability to define passive pipe segments. Furthermore, these pipe segments can be generated as part of the cut set generation processes and show up as normal basic events in the cut set results.

In this study, the SAPHIRE code is used. The SAPHIRE has been developed by INEEL (Idaho National Engineering and Environmental Laboratory) for the Nuclear

Regulatory Commission. The current version, 6.53, of SAPHIRE was released in June of 1998. INEEL has over 20 full-scope PRA available in the SAPHIRE software.

A single plant may have multiple, different PRA models available in SAPHIRE. There are three different SAPHIRE PRA models: the NUREG-1150 model[5], the Simplified Risk Model (SRM)[6] used for the Accident Sequence Precursor (ASP) program, and the utility IPE (Individual Plant Examination). These three models vary with respect to the level of modeling detail. The SRM includes a limited number of initiating events. Only the dominant risk contributors were explicitly evaluated and documented in the NUREG-1150 model. Recovery analysis and cut set generation for non-dominant accident sequences were routinely ignored in the NUREG-1150 model.

The absence of non-dominant sequences and a limited number of initiating events limits a SRM or a NUREG-1150 PRA models' usefulness in analyses such as FAC aging study. The plant IPE model generally reflects the current plant configuration. The model allows all accident sequences to be quantified, including the non-dominant sequences. The IPE model will be appropriate for our FAC case study. After selection of the appropriate PRA model, it can be used directly for FAC analysis.

4.3 General Procedure for Detailed Analysis

The general procedure of how to incorporate the specified plant systems associated with FAC effects is as follows:

[5] The Surry NUREG-1150 database contains adequate treatment of only the dominant sequences. The non-dominant sequences are not included.

[6] The SRM includes a limited number of initiating events (SGTR, small LOCA, transients, and loss of offsite power) only and a simplified modeling structure (train level events and little support system modeling).

Step 1: Select the systems to be addressed. Review industry experience. We may use NPP results from the associated FAC inservice inspection (ISI) program. For the selected specific systems, review the isometric drawings, pipe and instrumentation drawings (P&ID), and BOP heat balance diagram of the associated system. Identify the pipe segment boundaries.

Step 2: Select candidate pipe segments within the system to be analyzed. Locations susceptible to FAC are elbows, pipe bends, reducers, tees, pipe entries, and straight pipes where downstream of components or obstacles turbulence occurs (e.g., downstream of flow control orifices, valves). We may adopt the detailed component level risk prioritization results and the results suggested by the expert panel review for individual plant.

Step 3: Gather data for the failure probabilistic analysis. Use the KWU-KR model and the E factor to determine the capacity at specific time intervals for each relevant pipe segment. Determine the load conditions of the associated pipe segment.

Step 4: Calculate the failure probability from the first year to the tenth (t_L) year. We conservatively assume that the pipe is not inspected for 10 years. The total failure probability of a relevant pipe segment due to FAC, FP_{FAC} is as follows:

$$FP_{FAC} = FP_{ss} + FP_{tr} \qquad (4\text{-}1)$$

where

FP_{ss} : failure probability at steady state,

FP_{tr} : failure probability due to transients.

Step 5: Use the plant PRA/IPE to select the sequences associated with the initiating events (IEs) of Step 4. Determine the contribution to core damage frequency (CDF) from

these sequences, CDF_{IE}, and the mean frequency of the associated IE, $FREQ_{IE}$. Calculate the conditional core damage probability given the occurrence of this IE as follows:

$$CCDP_{IE} = CDF_{IE} / FREQ_{IE} \quad (4\text{-}2)$$

Step 6: Add the failure probability due to FAC to the probability of the IEs and calculate the CDP_{FAC} due to FAC as follows:

$$CDP_{FAC} = FP_{FAC} * CCDP_{IE} \quad (4\text{-}3)$$

Step 7: Calculate the product of the contribution to the CDF from the relevant IE, CDF_{IE} in Step 5 and for a ten year (t_L) time period. Assess the impact due to FAC on the core damage probability contribution from this IE.

Step 8: Compare with the total plant CDF.

Chapter 5: Case Study

5.1 Introduction

To perform a feasibility demonstration to incorporate FAC effects into PRA, a case study has been defined and is discussed in this chapter. The case study will provide a test bed to explore the use of the reliability physics model described in Chapter 3 and should build upon existing PRA models described in Chapter 4.

5.2 The Surry IPE in SAPHIRE

In order to select an appropriate model to investigate FAC consequences, our decision to use the Surry IPE model is based on three considerations as follows.

(1) Quality: the Surry IPE generally reflects the current plant configuration with the last update to the model from 1994. The model also allows all accident sequences to be quantified, including the non-dominant sequences.

(2) Ease of use: the model quantification time is short (less than a few minutes, including the application of recovery actions) which would allow for multiple analyses to be run in a short time.

(3) Representativeness : A desirable feature of the Surry IPE model is the existence of predefined passive pipe segments. The desirable pipe segments can be generated as part of the cut set generation process and show up as normal basic events in the cut set results. These pipe segment definitions were developed for a NRC investigation into a risk-based ISI program.

Surry has three different SAPHIRE PRA models: the NUREG-1150 model, the Simplified Risk Mod(SRM) used for the Accident Sequence Precursor (ASP) program, and the utility IPE (Individual Plant Examination). These three models vary with respect to the level of modeling detail (e.g., the NUREG-1150 model has approximately 1100 basic events, the SRM has 150 basic events, and the IPE has 2300 basic events). The Surry NUREG-1150 model was completed about 10 years ago and does not reflect the current configuration of the plant. Only the dominant risk contributors were explicitly evaluated and documented. Recovery analysis and cut set generation for non-dominant accident sequences were routinely ignored in the Surry NUREG-1150 model.

The absence of non-dominant sequences limits this model's usefulness to analyses such as FAC aging study. It is determined that the Surry IPE model is the most appropriate for our FAC case study. After selection of the PRA model, the Surry IPE model is modified to include associated pipe segments not currently in the model. There is a total of 19 IEs out of Surry's specified IEs, e.g., for LMFW (Loss of main feedwater), SLOCA (Small LOCA), MLOCA (Medium LOCA), etc.

In a more advanced application, once both the load and capacity distributions are known as described in Chapter 3, a simple Monte Carlo routine is used to determine the fraction of time that the load pressure is larger than the capacity pressure. It is envisioned that this calculation could be incorporated into the Surry IPE code via the "compound"[7] event type [Smith, 1997]. Consequently, the parameters that are contained in the capacity-load calculations (e.g., time, pipe wall thickness, adjustment factor E, and pressure loads due to the steady state and transients) can be accessible directly in the PRA model.

[7] In SAPHIRE, a "compound" event is a basic event that is linked to a user-defined calculation program (i.e., a compiled dynamic link library). This basic event can be used in any fault tree or event tree that may exist in the PRA database.

5.3 Failure Probability Determination of Case study

The selected pipe segment in our case study is the same as the particular segment that failed in December of 1986 (13.6 years after commercial operation). It is shown in Figure 5-1. The 18 inch suction line to the main feedwater pump A of Unit 2 failed in a catastrophic manner. The condensate feedwater system flows from a 24 inch header to two 18 inch suction lines each of which supplies one of two feedwater pumps.

In accordance with our choice to analyze the MFW system, we specifically model the single pipe segment failure due to FAC in Surry's MFW system, because this event also caused two main feedwater pumps to lose suction heads at the same time. Thus, we may assume that the event was a loss of the MFWs (corresponding to the T2 Initiating Event in the Surry-IPE) which caused a plant transient [Virginia, 1991].

The failed 18 inch suction line in the P&ID drawing number "1-FW-03" and the associated "Flow/Valve Operating Numbers Diagram number 11448-FM-067B, sheet 1" were reviewed and identified. The pipe segment is identified as "FW-04". This identification number is necessary as an input to SAPHIRE.

The normal operating system pressure, 370 psig, as the steady-state load pressure, is used. The pressure during the transient caused by the valve closure was approximately 440 psig.

The Mathcad and Crystal Ball codes are used to calculate for year 1 through 10 to estimate the annual, time-dependent pipe segment failure probability. The detailed FAC rate calculations are shown in Appendix B. The detailed failure probability

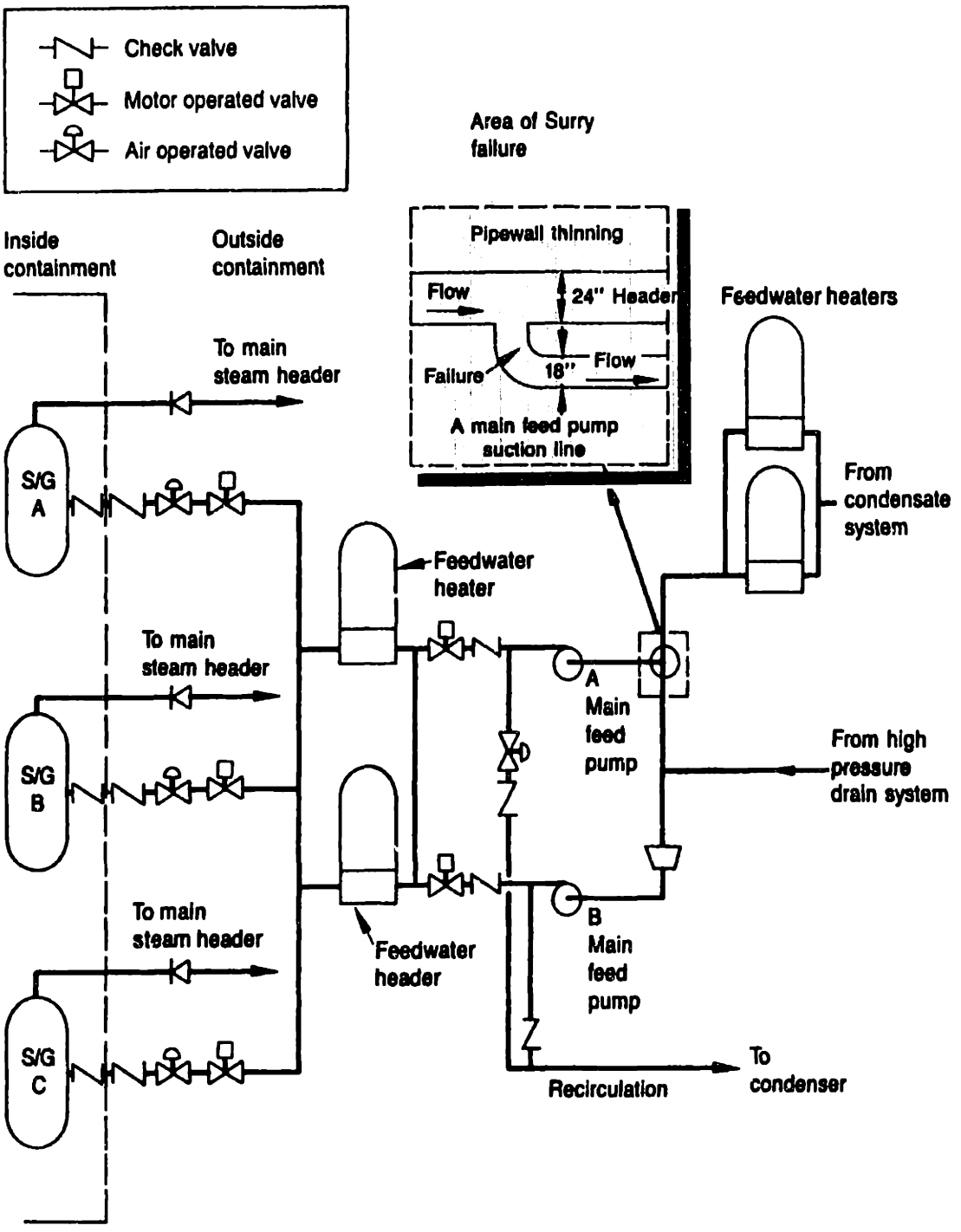

Figure 5-1. The selected pipe segment of the Surry NPP [Shah, et al., 1992] (modified).

calculations for steady state and transient conditions are shown in Appendix C and Appendix D. A summary of these calculations is shown in Table 5-1. Figure 5-2 shows the results for total, steady state, and transient failure probability within a 10 year period. Figure 5-3 shows the results of the failure rate (or the hazard function) calculations for transients.

5.4 Indirect Effects

The indirect impacts due to failure of the "FW-04" pipe segment are considered in this section. For the Surry NPP, flooding in the Turbine Building (91% contribution to CDF) was a significant plant vulnerability. Flooding may occur as a result of failures in the Circulating Water (CW) and Service Water (SW) Systems in the Turbine Building. Both the CW and SW systems are gravity fed from the intake canal (20 feet above the Turbine Building basement floor) [Virginia, 1991].

The "FW-04" pipe segment is located in the basement of the turbine building. There are no safety related equipment in the area [Smith. 1998]. Hence the indirect effects do not contribute to our case study.

5.5 Consequence Assessment

For Surry, we get from the PRA as follows:

(a) $CDF = 7.3 \times 10^{-5}$/year : total core damage frequency,

(b) $CDF_{IE\text{-}T2} = 4.8 \times 10^{-7}$/year : the CDF contribution from the occurrence of transient IE-T2, the LMFW,

Table 5-1. Failure probability calculations due to steady state pressure and transients.

Year	1	2	3	4	5	6	7	8	9	10
Calculated FAC Rate ($\mu g/cm^2h$)	**136.9**	**136.9**	**136.1**	**135.1**	**133.6**	**131.8**	**130.2**	**128.7**	**127.1**	**125.4**
Calculated Wall Thinning (in)	**0.059**	**0.118**	**0.176**	**0.233**	**0.288**	**0.341**	**0.393**	**0.444**	**0.493**	**0.541**
5th-Percentile from E Factor (in)	0.005	0.010	0.016	0.021	0.026	0.030	0.035	0.039	0.044	0.048
Median FAC (in) from E Factor	0.029	0.057	0.086	0.113	0.140	0.166	0.191	0.216	0.240	0.263
95th-Percentile from E Factor (in)	0.157	0.315	0.470	0.622	0.769	0.910	1.049	1.185	1.316	1.444
Reliability Using Monte Carlo Simulation (%)	***99.67***	***97.53***	***94.34***	***90.68***	***87.07***	***83.57***	***79.79***	***75.32***	***72.32***	***69.63***
Failure Probability at Steady-State	**0.0033**	**0.0247**	**0.0566**	**0.0932**	**0.1293**	**0.1643**	**0.2021**	**0.2468**	**0.2768**	**0.3037**
Failure Probability due to Transients	**0.00696**	**0.01301**	**0.02478**	**0.04012**	**0.05611**	**0.07543**	**0.09828**	**0.12270**	**0.14750**	**0.17360**
Total Failure Probability	**0.01026**	**0.03771**	**0.08138**	**0.13332**	**0.18541**	**0.23973**	**0.30038**	**0.36950**	**0.42430**	**0.47730**

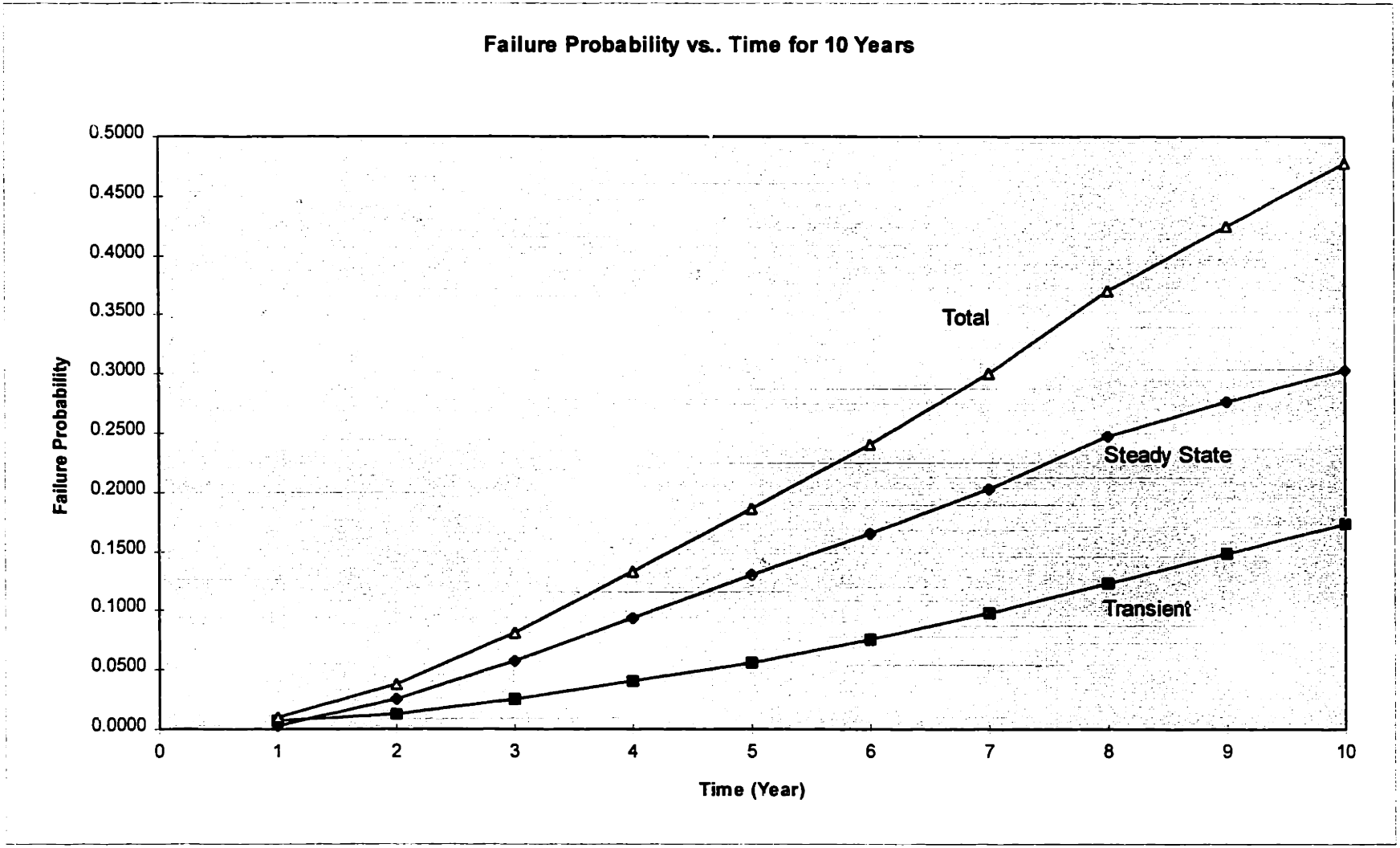

Figure 5-2. Results of failure probability calculations.

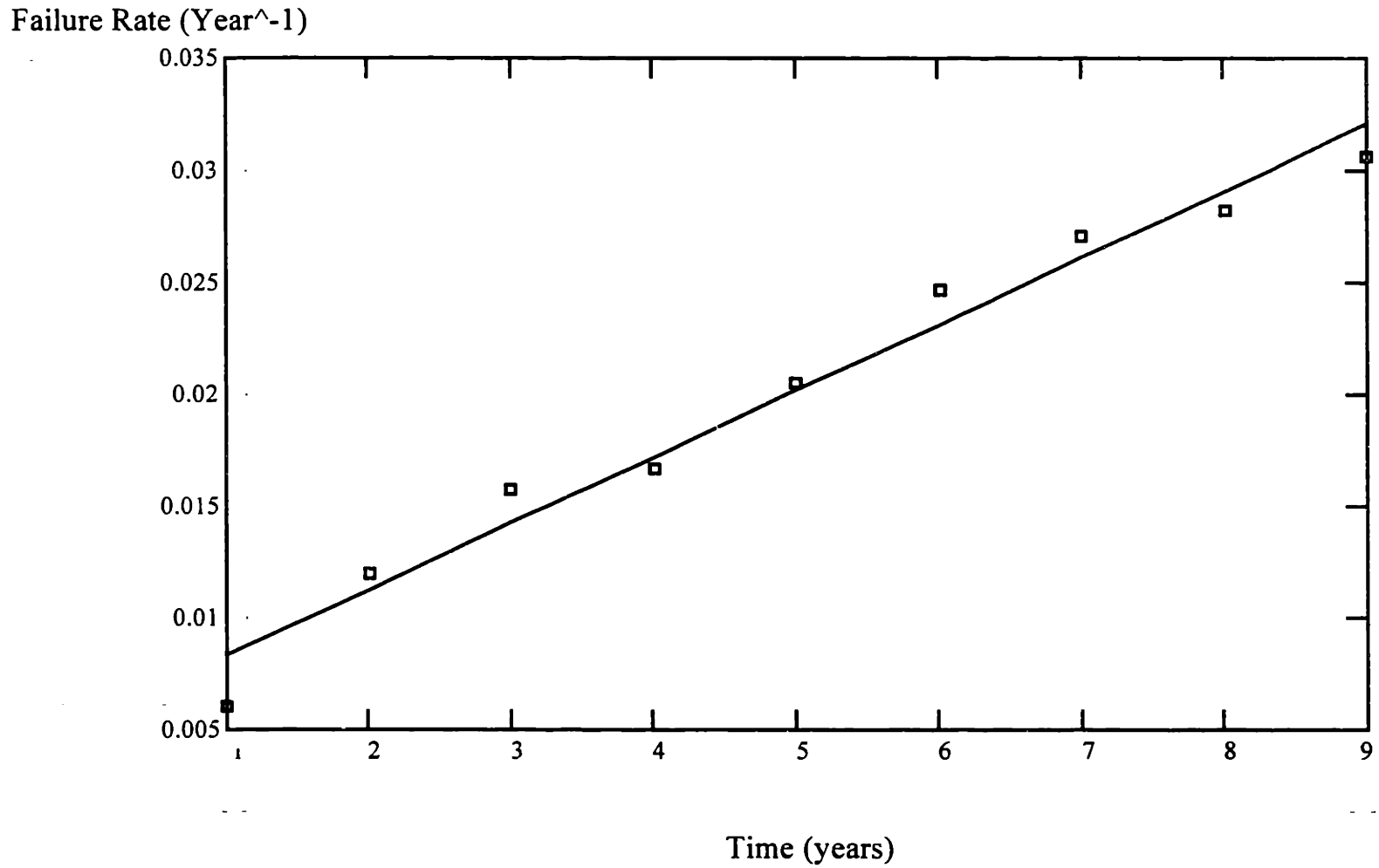

Figure 5-3. Results of failure rate calculation at transient of the Surry pipe segment.

(c) $FREQ_{IE-T2} = 0.15$ /year : The frequency of transient IE-T2, and

(d) $FP_{FAC} = 0.48$: The pipe failure probability due to FAC within a 10 year ($=t_L$) period.

According to Section 4.3, we obtain:

(1) $CCDP_{IE-T2} = CDF_{IE-T2}/FREQ_{IE-T2} = 3.2x10^{-6}$: conditional core damage probability given the occurrence of transient IE-T2,

(2) $CDP_{FAC} = FP_{FAC}*CCDP_{IE-T2} = 1.5x10^{-6}$: the core damage probability given the pipe failure probability due to FAC on the CCDP contribution from transient IE-T2,

(3) $CDP_{FAC}/ (CDF_{IE-T2} * t_L) = 31\%$ (significant) : the impact of the CDP due to FAC on the CDP contribution from the occurrence of transient IE-T2 within a t_L period,

(4) $CDP_{FAC}/ (CDF * t_L) = 0.21\%$ (insignificant) : the impact of the CDP due to FAC on the total base CDP within a t_L period.

There are two types of models of the world (MOW), deterministic and probabilistic [Apostolakis, 1990; 1995]. An example of a deterministic model is the KWU-KR methodology to calculate the FAC rate as described in Equation (2-1). An example of a probabilistic model is the occurrence of transients. This uncertainty described by the MOW is sometimes referred to as "randomness," or "aleatory uncertainty." Each MOW is conditional on the validity of its model assumptions and on the numerical values of its parameters. Since there may be uncertainty associated with these conditions, we introduce the epistemic probability model which represents our knowledge regarding the numerical values of parameters and the validity of the model assumptions.

We introduce the adjustment factor E as defined in Equation (3-2). Its variability is due to both parameter and model uncertainties. The uncertainties at the steady state in our case study are primarily due to model uncertainty. The model uncertainty at the steady state is purely epistemic as discussed in Section 3-2. Thus, the capacity of the failure probability calculation at steady state is dominated by epistemic uncertainties. Since the hazard function is meaningful for aleatory failures, we cannot obtain a hazard function (failure rate[8]) directly from our failure probability calculations. For transient loads, we use the Latin Hypercube sampling method to divide the associated probability distributions into 20 intervals of equal probability. Note that we fix the capacity at certain probability intervals for transient calculation as described in Appendix D and consider random variations of the transient load in our calculations. Now we can obtain the failure rate directly for transients, because they involve aleatory uncertainties. Figure 5-3 shows that the failure rate due to transients can be approximated by a straight line, as

[8] The hazard function or failure rate is the conditional probability density of failure in (t, t+dt) given that component has survived up to t. It defined as

$$h(t) \equiv \frac{f(t)}{R(t)}$$

where f(t): failure distribution, R(t)=1-F(t)=reliability, F(t): failure distribution.

the linear aging model postulates [Vesely, 1987]. We point out that this is not the total impact of FAC, since the failure due to the steady-state pressure is not included.

The aging related factor, α, of Equation (1-1) is 2.96×10^{-3}/year^2 ($=3.38 \times 10^{7}$/hr/year) as calculated from Figure 5-3. This number maybe compared with the α value of 3.0×10^{-9}/hr/year, for all aging mechanisms of the component, "large other safety pipe (a 10 to 24 inch pipe)", listed in the TIRGALEX (Technical Integration Review Group for Aging and Life Extension) report [Levy, et al., 1988]. It is almost two orders of magnitude higher.

We note that stainless steel used in most of safety-related pipe segments is not susceptible to FAC, so the comparison of two values of α is not meaningful. Of course, the principal conclusion from our analysis is that the linear aging model fails for the steady state case because the uncertainties are purely epistemic. It works for the transients, because the uncertainties are both aleatory (occurrence of transients) and epistemic (distribution of capacity). It is the presence of aleatory uncertainties for transients that allow us to define a failure rate.

The core damage probability due to FAC for 10 years has some impact (31%) on the 10-year failure probability due to transient IE-T2, the LMFW. However, the CDP due to FAC has insignificant impact (0.21%) on the 10-year total CDP. The main reason is that the contribution to the total core damage frequency from LMFW in Surry is small, less than 1%. The impact on the total CDP due to FAC for other NPPs has not been evaluated and needs further investigations. In conclusion, FAC effects can be included in PRA through reliability physics models.

Chapter 6: Conclusions, and Recommendations for Future Work

We have incorporated FAC effects into PRA using reliability physics. This methodology can be applied to other SSCs and aging mechanisms, for example, fatigue.

Employing the E factor uncertainties introduced in Section 3-2 and following the detailed procedure described in Section 4-3, the piping failure probability due to FAC in a NPP can be evaluated. Plant engineers can use this probabilistic model to develop their own aging management strategies. This will point out critical locations where inspection resources should be concentrated.

Even though the main benefit of the linear aging reliability model [Vesely, 1987] is its simplicity and ease of application, we point out that this is not the total impact of FAC, since the failure probability due to the steady-state pressure is not included.

The pressure capacity at steady state is dominated by epistemic uncertainties. Since a hazard function is defined for random failures, we cannot obtain the hazard function directly from our failure probability calculations. The data that we used to assess the variability of the adjustment factor E included uncertainties due to the KWU-KR model itself and due to the numerical values of its parameters. These uncertainties were impossible to separate. We made the assumption that the dominant cause of variability of the factor E was model uncertainty. In the future, when similar data are collected, an effort should be made to separate the two types of uncertainty (model and parameter), so that more accurate calculations can be obtained.

The CDP due to FAC for 10 years has some impact on the 10-year probability of the accident sequence initiated by LMFW (Loss of Main Feedwater). However, the CDP due to FAC has insignificant impact on the 10-year total CDP. The main reason is that the contribution to the total plant core damage probability from LMFW in Surry is small.

This methodology can be applied to other SSCs. For example, to evaluate the potential for FAC in the preheater-equipped steam generators as described in Chapter 2, the auxiliary feedwater (AFW) system of the Surry IPE model can be modified. This modification will be accomplished via a "change set" in the SAPHIRE software so that the modification can be turned off or on as needed. To accomplish the modification, several piping segments can be incorporated directly into the AFW fault trees. These modifications represent the preheater bypass line and can be utilized to explore the potential wall-thinning from the high-velocity feedwater flow during normal, at-power operation [Shah, et al., 1997].

Considering the contribution to the total core damage probability, the indirect effects discussed in Section 4.1.2 may become more important than in our case study. It would be worthwhile to select a piping segment located in an area susceptible to flooding indirect effects and to find its impact on the total core damage probability.

References

ANSI/ASME, 1986, *"Power Piping Code, B31.1,"* American National Standards Institute/American Society of Mechanical Engineers.

ANSI/ASME, 1969, *"Nuclear Power Piping Code, B31.7,"* American National Standards Institute/American Society of Mechanical Engineers.

Apostolakis, George E., 1990, *"The Concept of probability in Safety Assessment of Technological Systems,"* Science, Vol. 250, pp. 1359-1364, 7 December.

Apostolakis, George E., 1995, *"A Commentary on Model Uncertainty,"* in: *Proceedings of Workshop on Model Uncertainty: Its Characterization and Quantification.* A Mosleh, et al. Eds., Annapolis, MD, October 20-22, 1993, Center for Reliability Engineering, University of Maryland, College Park, MD, 1995 (also published as Report NUREG/CP-0138, Nuclear Regulatory Commission, Washington, D. C., 1994).

ASME, 1995, *"Section III, Boiler and Pressure Vessel Code,"* American Society of Mechanical Engineers, New York.

ASME Code Case N-480, 1990, *"Examination Requirements for Pipe Wall Thinning Due to Single Phase Erosion and Corrosion,"* Section XI, Division 1, American Society of Mechanical Engineers, New York, May 10.

Balkey, K. R., N. B. Closky, R. A. Bishop, P. K. Perdue, R. L. Haessler, R. A. West, E. A. Oswald, G. A. Gardner, Y. F. Khalil, G. E. Miemiec, T. L. Hamlin, A. McNeill, D. M. Bucheit, L. L. Spain, N. J. Shah, and A. Afazali, 1997, *"Westinghouse Owners Group*

Application of Risk-Informed Methods to Piping Inservice Inspection Topical Report," WCAP-14572, Revision 1, Westinghouse Energy System, Pittsburgh, October.

Bishop, B. A., 1997, *"Westinghouse Structural Reliability and Risk Assessment (SRRA) Model for Piping Risk-Informed Inservice Inspection."* WCAP-14572, Revision 1, Supplement 1, Westinghouse Energy System, Pittsburgh, October.

Chen, C. C., 1997, Personal Communication with C. C. Chen, a Chief Engineer at Maanshan Nuclear Power Station, Taipower Company, Taiwan, Oct. 9.

Chexal, B and R L. Jones, 1988, *"Implications of the Surry Piping Failure for Other Nuclear and Fossil Units,"* International Journal of Pressure Vessels & Piping, 34, pp. 331-343.

Chexal, V. K. and J. S. Horowitz, 1990, *"Flow Assisted Corrosion in Carbon Steel Piping, Parameters and Influences,"* Proceedings of the Fourth International Symposium on Environmental Degradation of Materials in Nuclear Power Systems—Water Reactors, D. Cubicciotti (Editor), National Association of Corrosion Engineers, Houston, pp. 9-1 to 9-12.

Chexal, B and J. S. Horowitz, 1995, *"Chexal-Horowitz Flow-Accelerated Corrosion Model-Parameters and Influences,"* Current Perspectives of International Pressure Vessels and Piping Codes and Standards, PVP-Vol. B, pp. 231-243. American Society of Mechanical Engineers, New York.

Chexal, B., J. S. Horowitz, R. Jones, B. Dooley, and C. Wood, 1996, *"Flow-Accelerated Corrosion in Power Plants,"* EPRI TR-106611, Electric Power Research Institute, Palo Alto.

Observed FAC thickness	0.277 in.
Calculated FAC thickness	0.0611 in. (5th percentile)
Calculated FAC thickness	0.0761 in. (mean value)
Calculated FAC thickness	0.0921 in. (95th percentile)

Table A-2. FAC parameters and uncertainty information in Case 2 (single phase flow).

Parameter	Mean value	Standard deviation	Distribution
Operational time (hr)	76,320	N/A	constant
Piping Material (Cr + Mo in %)	0.02	0.0013	normal
Piping geometry (straight pipe after pump)	0.16	N/A	constant
Fluid velocity (m/sec)	7.26	0.05	normal
Dissolved oxygen concentration (ppb)	10	0.67	normal
Water chemistry (pH)	8.7	0.09	normal
Water temperature (°K)	449.7	0.75	normal
Steam quality	0	N/A	none

A.3 Case 3: Millstone Unit 2, a Two-Phase FAC Case

A.3.1 Event Description of Case 3

Millstone 2 is an 863 MWe PWR that has been operating since 1975. In October 1986, a serious thinning of a 40.64-cm [16-inch]-diameter piping of the heater 2B secondary steam fourth stage extraction steam was found during refueling outage. The associated operation of the system is 215 psig.

A.3.2 Additional Information Regarding Case 3

The pipe material was normal for A 106 Grade C material which contained the measured Mo 0.005%, Cr 0.012%, and Cu 0.011%. Flow velocity is 255.5 kg/m^2sec and its temperature is 390^0 F (199^0 C).

A.3.3 Results of Case 3

Evaluating the Case 3 analysis (see results below), we see that there is a 100% probability that the calculated FAC thickness will be larger than the actual damaged piping loss thickness. The KWU-KR model predicts FAC rate conservatively for this case, but there is a marked absence of an uncertainty variation in the results. The results of the uncertainty analysis are shown below:

Observed FAC thickness	0.35 in.
Calculated FAC thickness	0.539in. (5th percentile)
Calculated FAC thickness	0.543 in. (mean value)
Calculated FAC thickness	0.548 in. (95th percentile)

Table A-3. FAC parameters and uncertainty information in Case 3 (two phase flow).

Parameter	Mean value	Standard deviation	Distribution
Operational time (hr)	94,320	N/A	constant
Piping Material (Cr + Mo in %)	0.02	0.0013	normal
Piping geometry (elbow)	0.3	N/A	constant
Fluid velocity (Kg/(sec*m^2))	255.5	1.7	normal
Dissolved oxygen concentration (ppb)	0	N/A	none
Water chemistry (pH)	7	N/A	constant
Water temperature (°K)	472	0.79	normal
Steam quality	0.890	0.068	normal

A.4 Case 4: Fort Calhoun, Another Two-Phase FAC Case

The Port Calhoun plant has a long operating history of 24 years, but is a somewhat unique Combustion Engineering 2-loop design with a large dry (60 psig design pressure) containment. The rated electrical output of the plant is 502 MWe. The plant design is not typical of PWR. As an example of the uniqueness of Fort Calhoun, the AFW system has three diverse pumps, two of which are safety related while the third is non-safety related. The AFW system consist of one motor driven pump, one turbine driven pump, and one non-safety diesel driven pump.

A.4.1 Event Description of Case 4

On April 21, 1997, Omaha Public Power District's Fort Calhoun Station, while operating at 100 % power, experienced an approximate 0.56 m^2 (6 ft^2) rupture of a 30.5-centimeter (12-inch)-diameter sweep elbow (radius equal to 4.64 times the pipe diameter) in the fourth-stage extraction steam piping. The operator, upon hearing steam noise and observing steam rising from the turbine deck, believed that a steam line had broken and manually scrammed the reactor. As a precaution, emergency boration was initiated. The main turbine tripped automatically as a result of the reactor trip. The turbine trip had the effect of isolating the rupture. Plant systems and related parameters responded as expected during the event.

The steam line rupture damaged a non-safety related electrical load center in the vicinity of the pipe break. Additionally, collateral damage was experienced in several cable trays and pipe hangers, and insulation containing asbestos was blown throughout the turbine building. Certain portions of the fire protection system actuated in response to fusible links in the sprinkler heads melting because of high temperature. Because there were no personnel in the immediate vicinity of the rupture, no one was injured.

The fourth-stage extraction steam system emanates from the outlet of the high-pressure turbine and preheats the feedwater heaters. The design operating conditions in the piping are 2,068 kilopascal gauge [300 psig] and 218°C [425°F], with a steam quality of approximately 92 %. The piping is fabricated of A-106B carbon steel and has a nominal wall thickness of 0.953 centimeter [0.375 inch]. The licensee's root cause assessment attributed the failure to FAC in the extraction steam piping. Initial indications of degradation in the extraction steam line at the Fort Calhoun facility were first discovered in 1985, when the furthest upstream long-radius elbow (radius equal to one

and a half times the pipe diameter) was replaced because of a pinhole leak. At that time the next upstream sweep elbow was also replaced. [NRC-IN-97-84,1997].

A.4.2 Additional Information Regarding Case 4

The fourth-stage extraction steam system had been recognized as a system that was susceptible to erosion and/or corrosion. It was, therefore, being monitored by the licensee's erosion and corrosion control program. Part of the licensee's program was utilizing the CHECWORKS computer code to identify high-wear-rate areas to be selected for inspection [NRC-IN-97-84,1997].

The CHECWORKS model for the fourth-stage extraction steam piping predicted that long-radius elbows would wear at a higher rate than the sweep elbows when exposed to similar conditions. Using CHECWORKS predictions, the licensee inspected and replaced all four long-radius elbows, but the failed sweep elbow was never inspected.

Part of the licensee's corrective actions following the rupture included inspecting all sweep elbows that had not been previously inspected. The measured wall thickness (0.112 centimeter (0.044 inch)) of the furthest downstream sweep elbow in the fourth-stage extraction piping was also significantly below the minimum wall thickness (0.272 centimeter (0.107 inch)) specified by code requirements and had to be replaced. Additionally, another sweep elbow in the fourth-stage extraction piping was also replaced because the wear (measured wall thickness of 0.394 centimeter (0.155 inch)) was considered excessive, even though it was not below the minimum allowable thickness.

The CHECWORKS predictions of the wear in the fourth-stage extraction steam system were not consistent with the actual observed wear rates as measured on the components; that is, sweep elbows showed substantially greater wear than predicted [NRC-IN-97-84,1997]..

A.4.3 Results of Case 4

Evaluating Case 4 analysis, we see that there is a 100% probability that the calculated FAC thickness will be larger than the actual damaged piping loss thickness. Again, the KWU-KR model predicts the FAC rate conservatively for this case, but there is a notable absence of an uncertainty variation in the results. The results of the uncertainty analysis are shown below:

Observed FAC thickness	0.321 in.
Calculated FAC thickness	0.618 in. (5h percentile)
Calculated FAC thickness	0.629 in. (mean value)
Calculated FAC thickness	0.639 in. (95th percentile)

Table A-4. FAC parameters and uncertainty information in Case 4 (two phase flow).

Parameter	Mean value	Standard deviation	Distribution
Operational time (hr)	145,000	N/A	constant
Piping Material (Cr + Mo in %)	0.068	0.0045	normal
Piping geometry (large radius elbow)	0.23	N/A	constant
Fluid velocity (Kg/(sec*m^2))	513.8	3.42	normal
Dissolved oxygen concentration (ppb)	0	N/A	none
Water chemistry (pH)	7	N/A	constant
Water temperature (°K)	482.7	0.80	normal
Steam quality	0.9167	0.0684	none

A.5 Determination of Parameter Uncertainties

A.5.1 Single-Phase Flow (Case 1 and 2)

The major parameters in Equation (2-3) of the KWU-KR model includes flow velocity, content of chromium and molybdenum in the piping material, oxygen content, fluid pH value, fluid temperature, piping geometry, and exposure time. We will not include the uncertainties in the last two items in our calculations. The rest of the five parameter uncertainties come from investigation of existing a BWR-6 [Niu 1997; Su 1997] and a PWR [Chen, 1997; Niu 1997] nuclear power plants. We assume that the associated instrumentation tolerances are equal to plus minus three standard deviations which bind 99.73% of the data points. It is reasonable to assume that the parameter uncertainties have a normal distribution. Table 4-5 shows the individual parameter uncertainties. We also perform a sensitivity study of the parameter uncertainties. The variations of the dissolved oxygen concentration and pH shown in Table 4-5 are the most sensitive parameters to FAC rate calculations in the KWU-KR model.

Table A-5. Parameter uncertainties estimation.

Parameters	Uncertainties	Sensitivities to FAC rate	Distribution Type
(1) Trace amounts of alloying elements (Mo+Cr) that are present in the piping (measured errors)	10~20% (20% in Case 3)	increasing 1.58% (Case 3)	Normal
(2) Flow velocity (Mlbs/hr)	2%	increasing 0.45% (Case 3)	Normal
(3) Uncertainties in the plant chemistry dissolved oxygen concentration (ppb)	10~20% (20% in Case 2)	increasing 25.4% (Case 2)	Normal
(4) Uncertainties in the plant chemistry pH Sampling	2~3% (3% in Case 2)	increasing 26.9% (Case 2)	Normal
(5) Temperature (F)	0.50%	increasing 0.68% (Case 3)	Normal

A.5.2 Two-Phase Flow (Case 3 and 4)

The FAC models in the two phase flow cases have important changes due to two constraints. The first constraint is an additional parameter, the quality x, to be considered in the calculation. From plant data [Chexal, 1996], a total of 7 data sets included values for x. Both the calculated and measured quality, x values are shown in Table A-6. Since the calculated values are always higher than the measured values, the first step is to subtract the difference of the calculated and measured mean values (8.28%) and set the expected standard deviation (6.84%) as the square root of the summation of the calculated square standard deviation and the measured square standard deviation [Rao, 1992] to generate this parameter's distribution type. The second constraint of the two phase flow cases is that the inputs of pH and O_2 content in the KWU-KR model are fixed in a conservative way (e.g., pH = 7 and dissolved O_2 content = 0), and treated as point values. Even after accounting for these two changes, the resulting uncertainty obtained via propagating the parameter uncertainty through the model was relatively small.

Table A-6. Calculated and corresponding measured quality data.

	Calculated Quality (%)	Measured Quality (%)
1	88.75	80.5
2	90.7	78.6
3	93.1	83.2
4	88.75	81.5
5	90.7	73.8
6	93.1	90.1
7	93.2	92.7
Mean of Normal Distribution	91.19	82.91
Standard Deviation of Normal Distribution	1.99	6.54

A.6 Summary of 4 Case Studies

We have selected the KWU-KR model for our FAC rate calculation. Parameter uncertainties associated with this calculation were propagated through the model to obtain probability distributions for the FAC rate. Using the four cases discussed previously, we estimate parameter uncertainties by investigating their individual distribution types, as shown in Tables A-1 to A-4, and then use Monte Carlo sampling methods (10,000 runs) to obtain the associated parameter uncertainty in the model [Decisioneering, 1996]. The corresponding pdf and cdf are shown in Figures A-1 and A-2. From Case 1 of Figure A-1, there is around 99% probability that the calculated FAC thickness will be larger than the actual damaged piping loss thickness. Case 2 of Figure A-1, there is a 100% probability that the calculated FAC thickness will be smaller than the actual damaged piping loss thickness. Note that Case 2 is an exception to the prediction of the FAC loss of the pipe wall thickness. FAC can affect straight pipes downstream of components that produce turbulence which may causes the KWU-KR model to underestimate the FAC rate (see Table A-7). We may conclude that either the KWU model cannot be applied in Case 2 or that the calculated FAC thickness is smaller than the actual damaged piping loss thickness in a non-conservative prediction. From Figure A-2, there is a 100% probability that the calculated FAC thickness will be larger than the actual damaged piping loss thickness in Cases 3 and 4.

The calculated cumulative thickness loss of Cases 1, 3 and 4 are higher than the corresponding measured loss thickness of damaged piping (see Table 4-7). This indicates that the KWU-KR model is a conservative and that it will overestimate the cumulative thickness loss, unlike Case 2 which was underestimate the cumulative thickness loss. An example of detailed calculation of Case 4 using Mathcad code [Mathsoft, 1995] is shown in Appendix A-1.

The corresponding E factors introduced in Equation (3-2) are obtained from the calculation and measured FAC rate of our four cases as Table A-6 shown. Refer to Figure 3-3, Case 2 is in Region II and Cases 1, 3, and 4 are in Region III.

Table A-7. Summary of uncertainty adjustment factor, E for four cases.

Case #	W_{actual} (in.)	W_{DRM} (in.)	$E = \frac{W_{actual}}{W_{DRM}}$	Calculated specific rate of metal loss $\Delta\phi_R$ ($\mu g / cm^2 hr$)
1	0.452	0.710	0.637	121.1
2	0.277	0.075	3.69	19.8
3	0.35	0.542	0.646	105.7
4	0.321	0.624	0.514	87.4

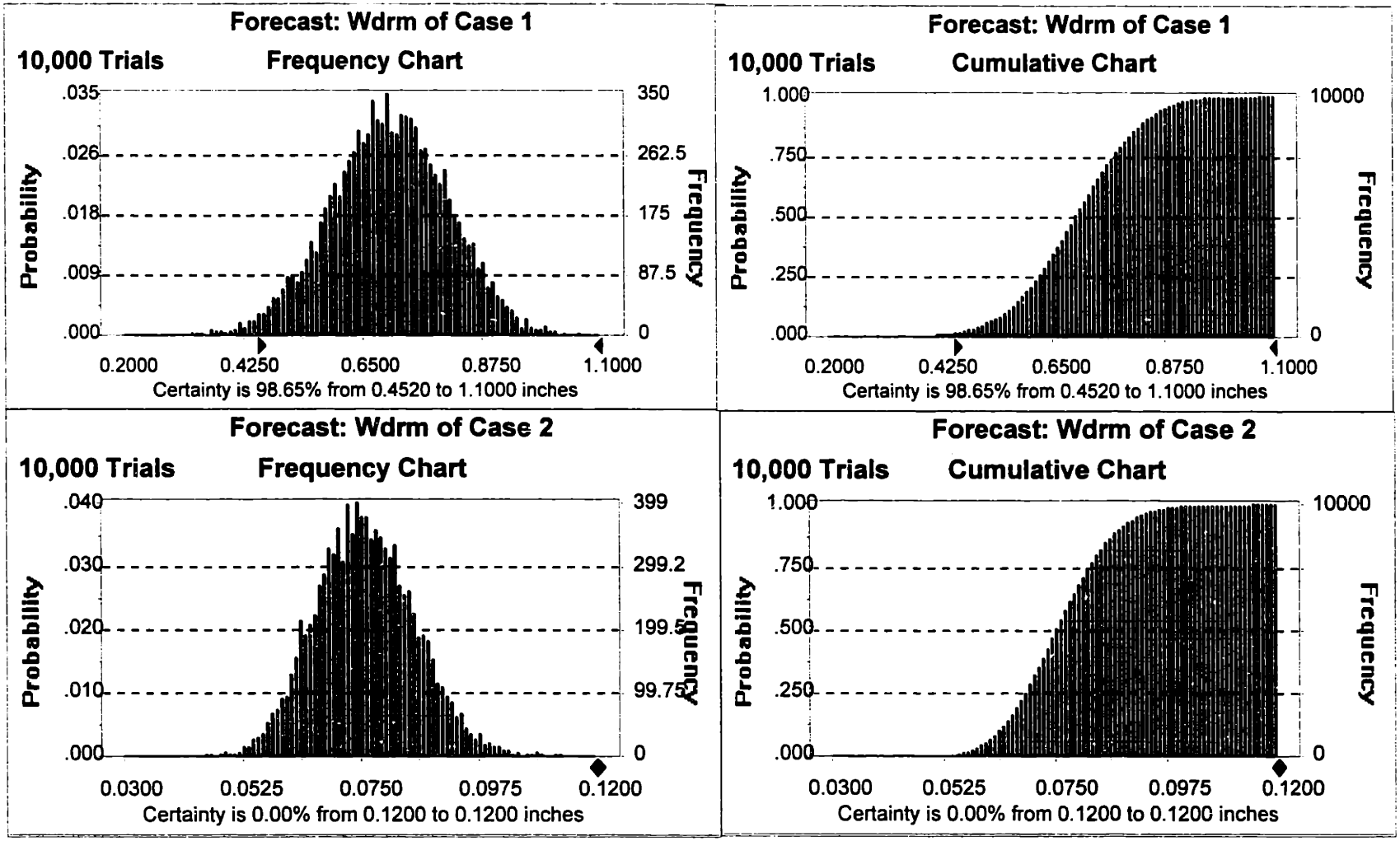

Figure A-1. Pdf and cdf results of Case 1 and Case 2.

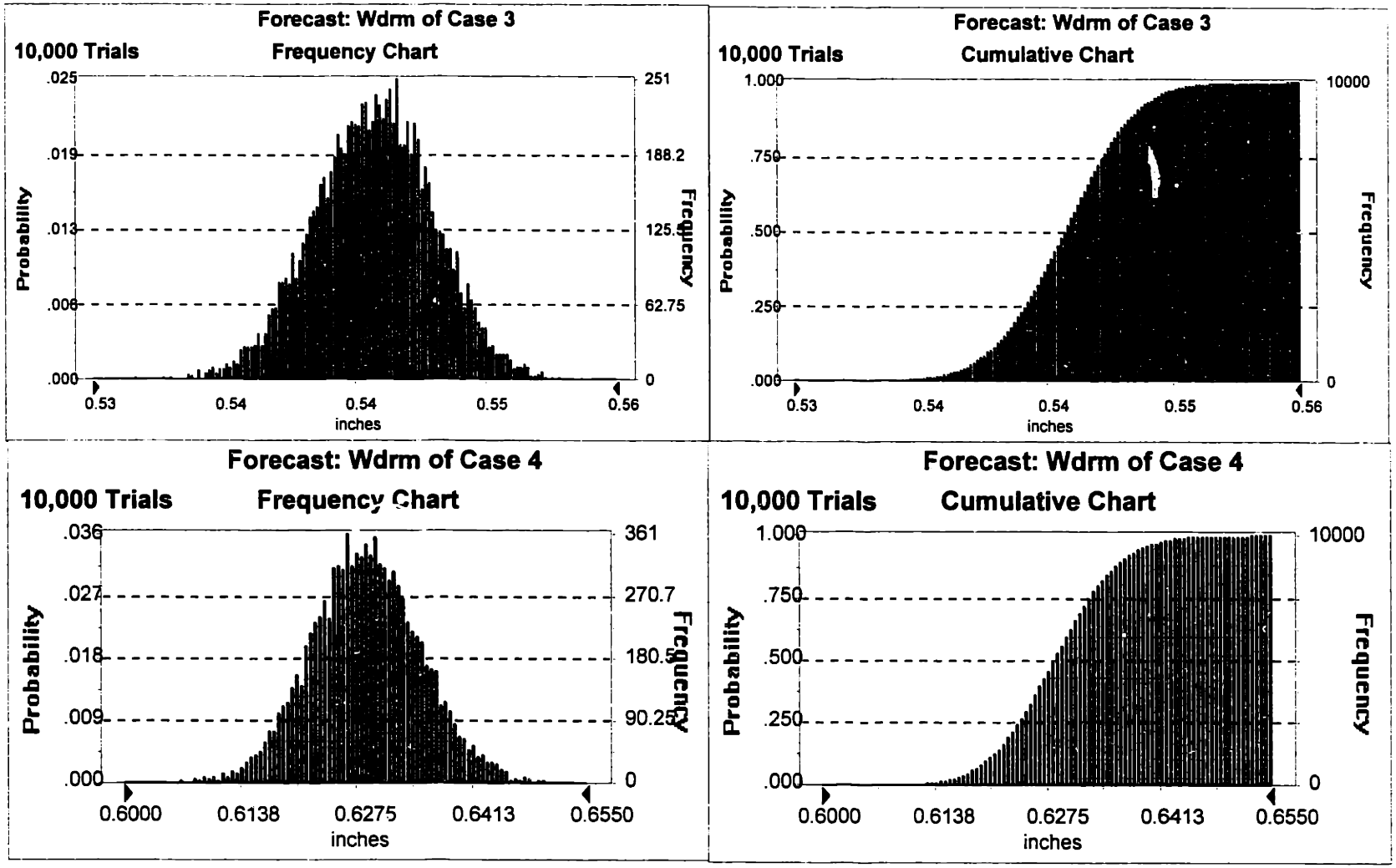

Figure A-2. Pdf and cdf results of Case 3 and Case 4.

Appendix A-1: Detailed Calculations of Case 4

Case 4: Empirical KWU- Model (Two Phase Flow)

Fort Calhoun: 4th Stage Extraction Steam Line

Operating Temperature and Pressure

$T_F := 409.5 \quad F \qquad p := 275 \cdot psi$

units conversion $T_K := \frac{T_F + 459.4}{1.8}$ gravitational constant: $g_c := 9.8 \cdot \frac{m}{sec^2}$

$p = 1.896 \cdot 10^6 \cdot Pa \qquad N := kg \cdot \frac{m}{sec^2}$

Operation time (1.45*10E5 =16.55 years):

in hours $t := 1.45 \cdot 10^5$

Pipe characteristics: alloy content taken from 0 to 5.0%

alloy content $i := 1 .. 500$ pipe diameter $D_i := 12.75 \cdot in$

$h_i := \frac{i}{100}$ $D := 12.75 \cdot in$

steel density $\rho_{st} := 8000 \cdot \frac{kg}{m^3}$

geometry factor $k_c := 0.23$

2 phase water properties at saturation conditions designated above:

pH $pH := 7$

Note that the Kastner model designates that for 2 phase flow pH be taken as 7 (real pH=9.44) and oxygen content as 0 ppb

oxygen content $g_o := 0$

flow quality $x := 0.9167$

water surface tension $\sigma := 35.6 \cdot 10^{-3} \cdot \frac{N}{m}$

liquid density $\rho_w := \frac{1}{(1.172 \cdot 10^{-3})} \cdot \frac{kg}{m^3}$

vapor density $\rho_d := \frac{1}{0.10496} \cdot \frac{kg}{m^3}$

Appendix A-1: Detailed Calculations of Case 4 (Continued)

Two phase flow calculation: computing liquid velocity.

Given:

mass flux: $m_{fl} := 372102 \cdot \frac{lb}{hr \cdot ft^2}$ $m_{fl} = 504.656 \cdot kg \cdot m^{-2} \cdot sec^{-1}$

relative vapor to liquid velocity $w_{rel} := \frac{1.18}{\sqrt{\rho_w}} \cdot \left| g_c \cdot \sigma \cdot (\rho_w - \rho_d) \right|^{0.25} \cdot (1 - x)$

void fraction calculation for this relative velocity $C := 1 + 0.12 \cdot (1 - x)$

$$\alpha := \frac{x}{\rho_d} \cdot \left| C \cdot \left(\frac{x}{\rho_d} + \frac{1 - x}{\rho_w} \right) + \frac{w_{rel}}{m_{fl}} \right|^{-1}$$

liquid film velocity calculation $w_f := \frac{m_{fl}}{\rho_w} \cdot \frac{1 - x}{1 - \alpha}$

Kastner Model: The pH is 9.44, bot oxygen content for the specimen is unknown. The Kastner model for 2 phase flow, however, designates that oxygen content should be taken as 0 μg/kg and pH=7.

Temperature alloy content factor $B_i := -10.5 \cdot \sqrt{h_i} - 9.375 \cdot 10^{-4} \cdot T_K^2 + 0.79 \cdot T_K - 132.5$

$$N_H(h) := \left(-1.29 \cdot 10^{-4} \cdot T_K^2 + 0.109 \cdot T_K - 22.07 \right) \cdot 0.154 \cdot \exp(-1.2 \cdot h) \cdot \frac{sec}{m}$$

$$N_L(h) := \left(-0.0875 \cdot h - 1.275 \cdot 10^{-5} \cdot T_K^2 + 1.078 \cdot 10^{-2} \cdot T_K - 2.15 \right) \cdot \frac{sec}{m}$$

$N_{h_i} := if(h_i > 0.5, N_H(h_i), N_L(h_i))$

Time factor $C_1 := 0.9999934$ $C_3 := -0.5624812 \cdot 10^{-10}$

$C_2 := -0.3356901 \cdot 10^{-6}$ $C_4 := 0.3849972 \cdot 10^{-15}$

$f(t) := if(t < 96000, C_1 + C_2 \cdot t + C_3 \cdot t^2 + C_4 \cdot t^3, 0.79)$

Material loss calculation: a nominal estimation of residual Mo and Cr is 0.068%

$$\Delta\Phi_{R_i} := \frac{\int_0^t 6.25 \cdot 10^{-9} \cdot \frac{kg}{cm^2 \cdot hr} \cdot k_c \cdot \left| B_i \cdot \exp(N_{h_i} \cdot w_f) \cdot \left\{ 1 - 0.175 \cdot (pH - 7)^2 \right| \cdot 1.8 \cdot \exp(-0.118 \cdot g_o) \ldots \right| + 1 \cdot f(t)\, dt}{t}$$

$\Delta\Phi_{R_7} = 87.395 \cdot 10^{-9} \cdot \frac{kg}{cm^2 \cdot hr}$ at 0.068% Mo and Cr (Measured Cr=0.068%, and Mo is unknown; assume Mo+Cr=0.068%)

Appendix A-1: Detailed Calculations of Case 4 (Continued)

Figure below in units of μg/cm^2/hr

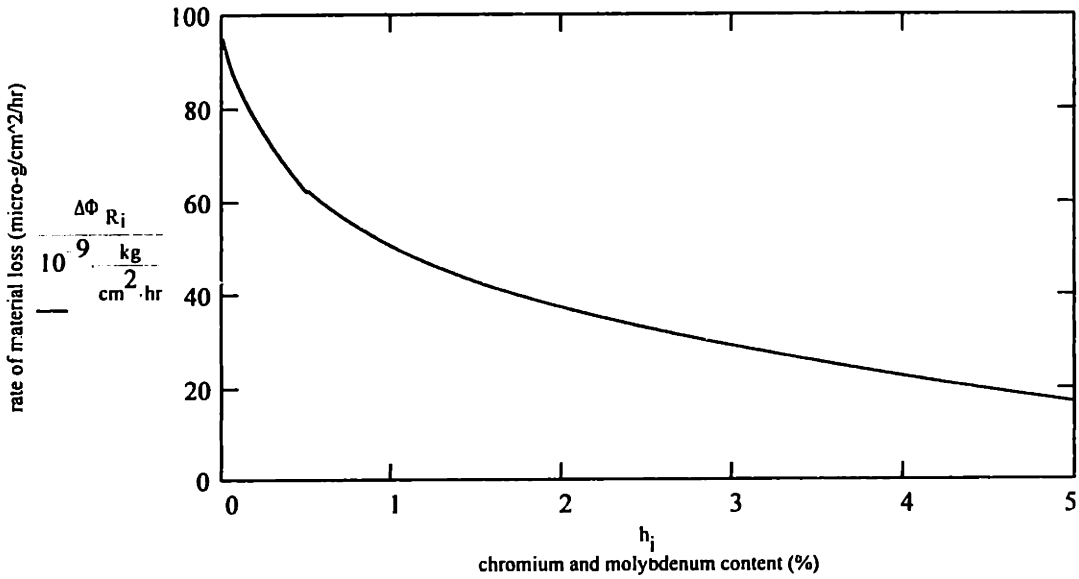

$\Delta\Phi_{Rch_i} := \frac{\Delta\Phi_{R_i}}{\rho_{st}}$ $\Delta\Phi_{Rch_7} = 0.038 \cdot \frac{in}{yr}$ at 0.068% Mo and Cr $\frac{m}{sec} = 1.242 \cdot 10^9 \cdot \frac{in}{yr}$

Operation for 16.55yrs

$\Delta\Phi_{Rchtot} := \Delta\Phi_{Rch} \cdot 16.55 \cdot yr$ $\Delta\Phi_{Rchtot_7} = 0.624 \cdot in$ at 0.068% Mo and Cr

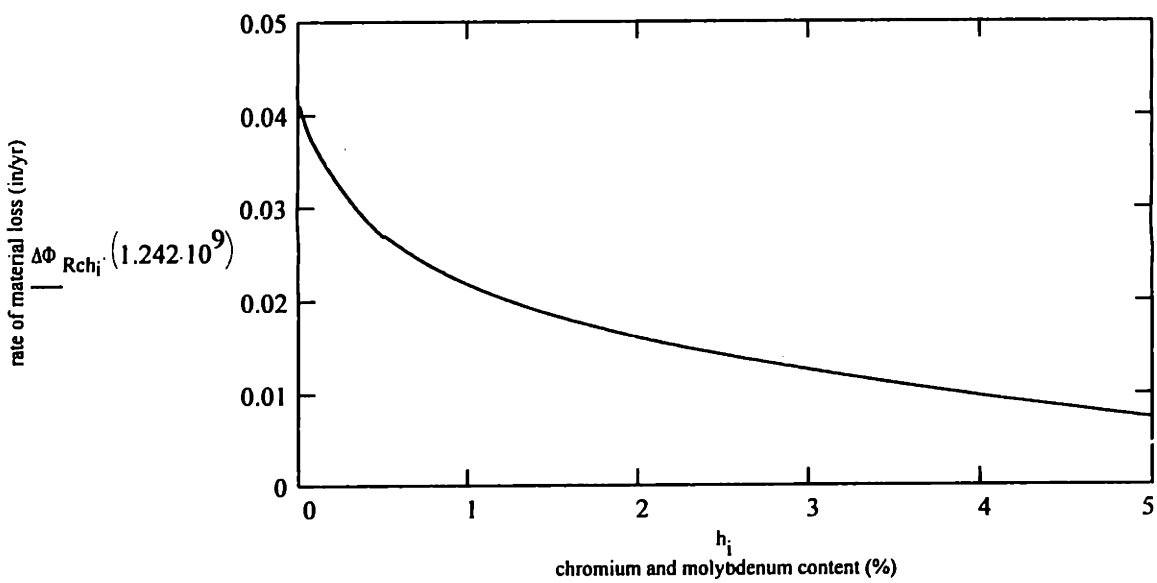

Appendix B: Detailed FAC Rate Calculations of Case Study

Surry Unit #2: A Rupture Elbow Downstream of Tee in Feedwater Piping

From the specific data of Surry-2 [Cragnolino, et. al., 1988; Janas,1988] , we may find the associated data to calculate FAC rate.

Operating Temperature and Pressure

$T_F := 374 \quad F \qquad p := 370 \cdot psi$

units conversion

$T_K := \frac{T_F + 459.4}{1.8} \qquad N := kg \cdot \frac{m}{sec^2}$

Operation time (10 years) :

in months $tm := 120$

in hours $t := tm \cdot 30 \cdot 24$ $D := 18 \cdot in$

Pipe characteristics: alloy content taken from 0 to 5.0%

alloy content $i := 1..500$ pipe diameter

$h_i := \frac{i}{100}$

steel density $\rho_{st} := 8000 \cdot \frac{kg}{m^3}$

geometry factor $k_c := 0.75$

pH $pH := 8.9$

oxygen content $g_o := 1.2$

liquid velocity = 17fps $w_f := 5.18 \cdot \frac{m}{sec}$

Using Kastner model, the pH, oxygen content, liquid velocity, geometrical factor, total content of chromium and molybdenum in steel, and operating temperature are known. We can calculate FAC rate as the following equations [Kastner, 1986].

Appendix B: Detailed FAC Rate Calculations of Case Study (Continued)

Temperature alloy content factor

$$B_i := 10.5\cdot\sqrt{h_i} - 9.375\cdot10^{-4}\cdot T_K^2 + 0.79\cdot T_K - 132.5$$

$$N_H(h) := \left(1.29\cdot10^{-4}\cdot T_K^2 + 0.109\cdot T_K - 22.07\right)\cdot 0.154\cdot\exp(1.2\cdot h)\cdot\frac{sec}{m}$$

$$N_L(h) := \left(-0.0875\cdot h - 1.275\cdot10^{-5}\cdot T_K^2 + 1.078\cdot10^{-2}\cdot T_K - 2.15\right)\cdot\frac{sec}{m}$$

$$N_{h_i} := if(h_i>0.5, N_H(h_i), N_L(h_i))$$

Time factor

$$C_1 := 0.9999934 \qquad C_3 := 0.5624812\cdot10^{-10}$$

$$C_2 := 0.3356231\cdot10^{-6} \qquad C_4 := 0.3849972\cdot10^{-15}$$

$$f(t) := if(t<96000, C_1 + C_2\cdot t + C_3\cdot t^2 + C_4\cdot t^3, 0.79)$$

Material loss calculation: a nominal estimation of residual Mo and Cr is 0.08%

$$\Delta\Phi_{R_i} := \frac{\int_0^t 6.25\cdot10^{-9}\cdot\frac{kg}{cm^2\cdot hr}\cdot k_c\cdot\left|B_i\cdot\exp(N_{h_i}\cdot w_f)\cdot\left|1 - 0.175\cdot(pH - 7)^2\right|\cdot 1.8\cdot\exp(-0.118\cdot g_o) \ldots\right| + 1\cdot f(t)\,dt}{t}$$

$$\Delta\Phi_{R_8} = 125.35\cdot10^{-9}\cdot\frac{kg}{cm^2\cdot hr}$$ at 0.08% Mo and Cr In units of μg/cm^2/hr

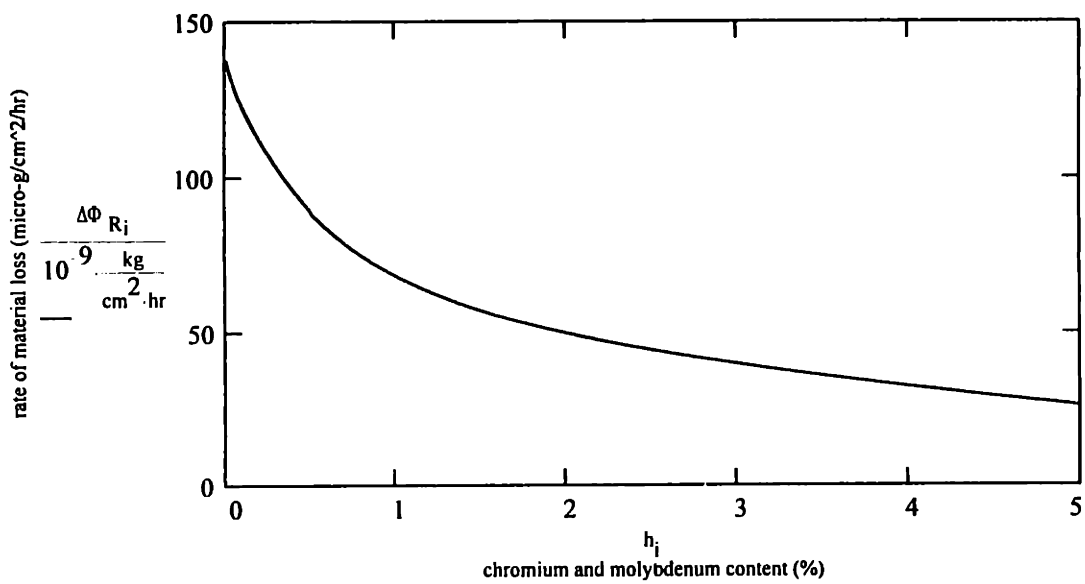

Appendix B: Detailed FAC Rate Calculations of Case Study (Continued)

$\Delta\Phi_{Rch_i} \quad \frac{\Delta\Phi_{R_i}}{\rho_{st}}$ $\quad \Delta\Phi_{Rch8} = 0.054 \cdot \frac{in}{yr}$ $\quad \frac{m}{sec} = 1.242 \cdot 10^9 \cdot \frac{in}{yr}$

Operation for 10 years $\quad \Delta\Phi_{Rch8} = 1.373 \cdot \frac{mm}{yr}$ at 0.08% Mo and Cr

$\Delta\Phi_{Rchtot} \quad \Delta\Phi_{Rch} \cdot \frac{tm}{12} \cdot yr \quad \Delta\Phi_{Rchtot8} = 0.541 \cdot in$ at 0.08% Mo and Cr

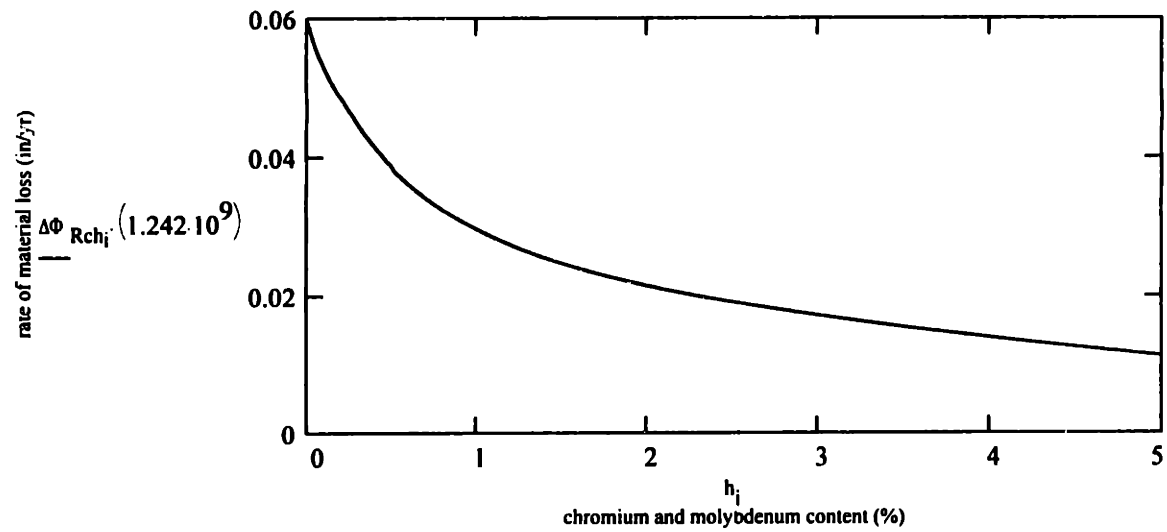

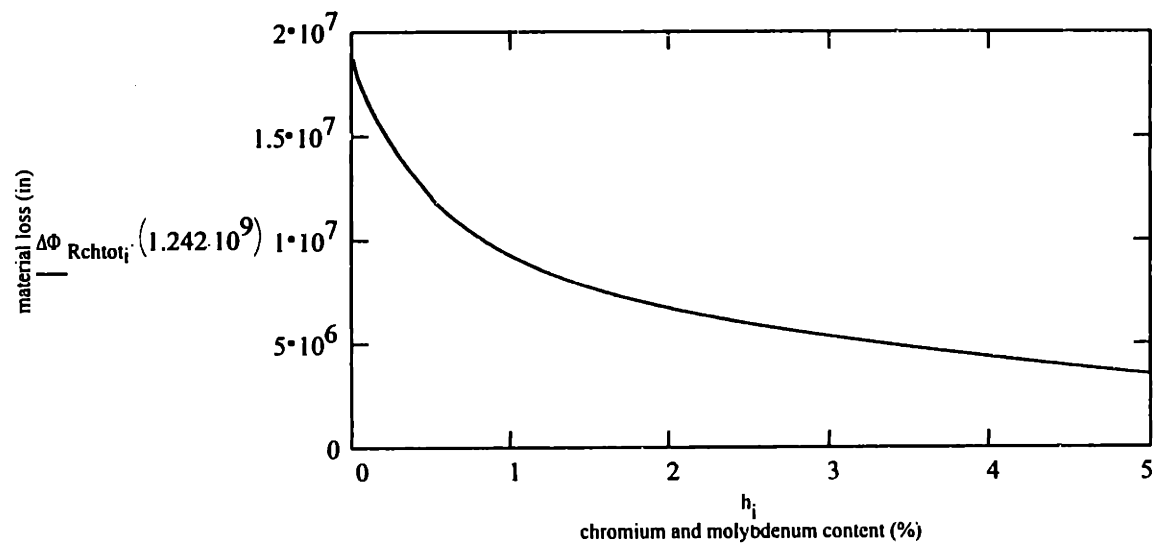

Appendix C: Detailed Failure Probability Calculations of Steady State

Year	0	1	2	3	4	5	6	7	8	9	10
σ_f (10^3 psi)	64.50	64.50	64.50	64.50	64.50	64.50	64.50	64.50	64.50	64.50	64.50
Wn (in.)	0.500	0.500	0.500	0.500	0.500	0.500	0.500	0.500	0.500	0.500	0.500
W_{DRM} (in.)	0.000	0.059	0.118	0.176	0.233	0.288	0.341	0.393	0.444	0.493	0.541
r (in.)	9.000	9.000	9.000	9.000	9.000	9.000	9.000	9.000	9.000	9.000	9.000
ε_f (%)	3.90	3.90	3.90	3.90	3.90	3.90	3.90	3.90	3.90	3.90	3.90
C (psi)	3548.73	3109.60	2676.14	2255.47	1847.20	1458.01	1087.30	727.65	378.77	47.10	-274.50
1-FP_{ss}	1	0.9967	0.9753	0.9434	0.9068	0.8707	0.8357	0.7979	0.7532	0.7232	0.6963
FP_{ss}	0	0.0033	0.0247	0.0566	0.093[illegible]	0.1293	0.1643	0.2021	0.2468	0.2768	0.3037

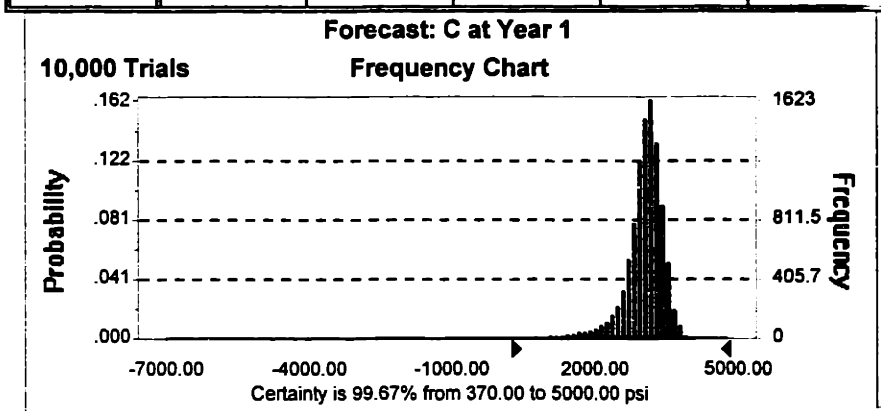

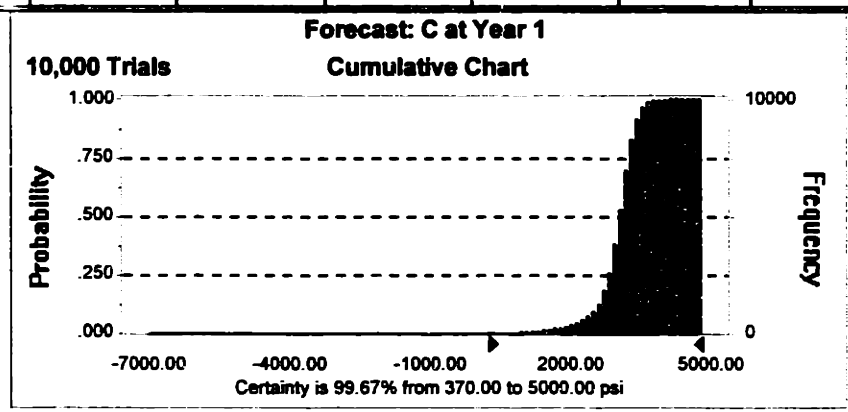

Appendix C: Detailed Failure Probability Calculations of Steady State (Continued)

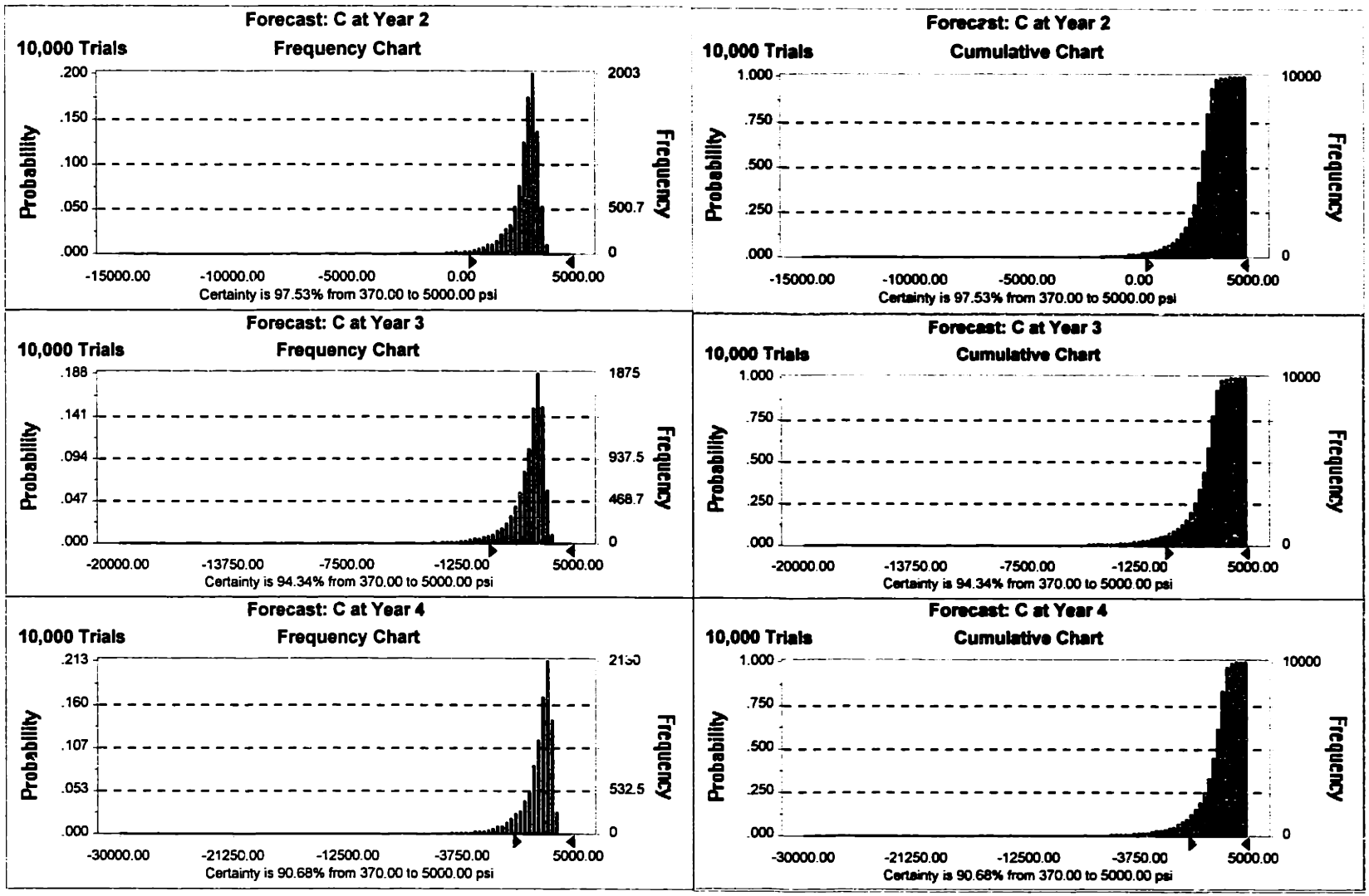

Appendix C: Detailed Failure Probability Calculations of Steady State(Continued)

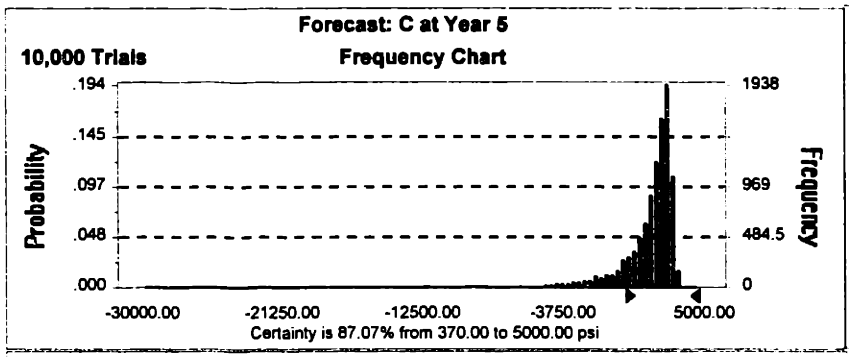

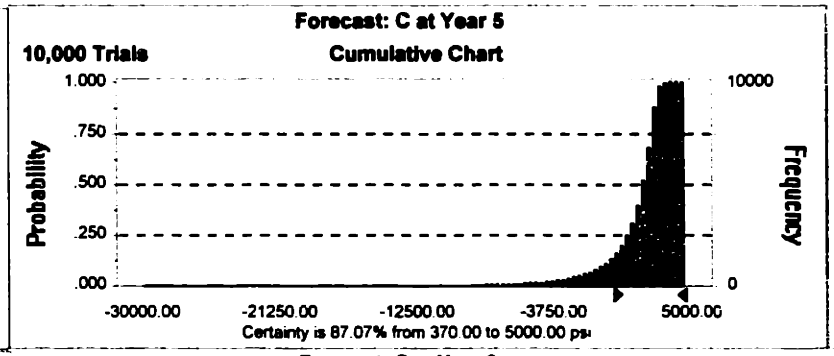

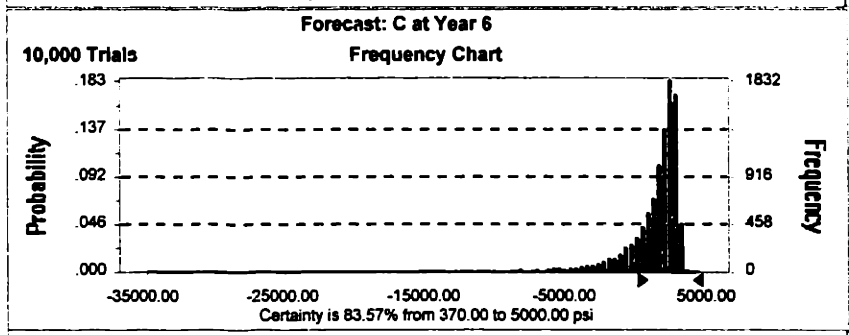

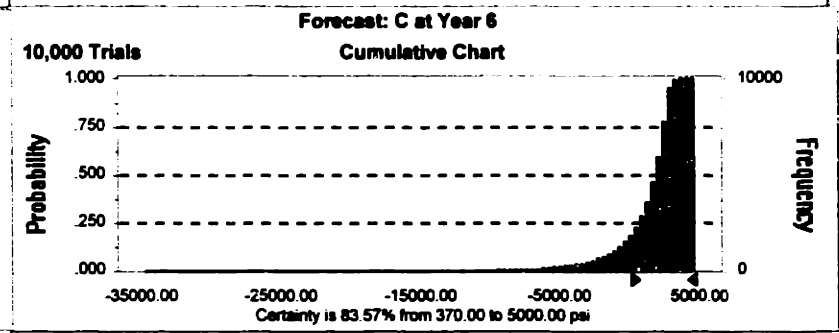

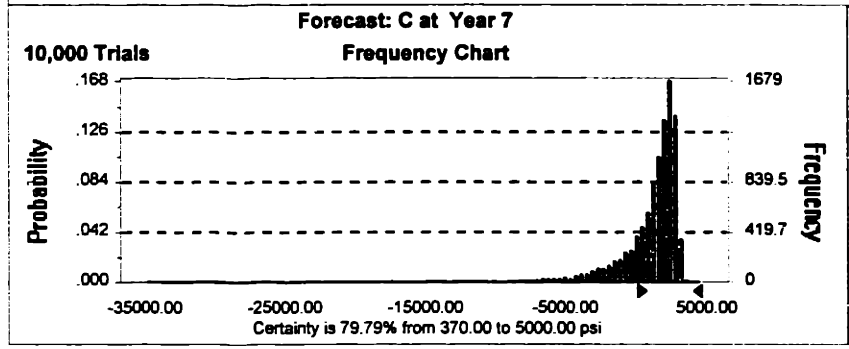

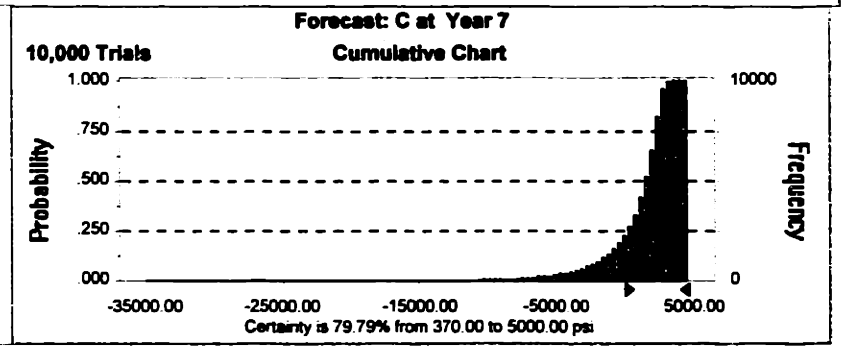

Appendix C: Detailed Failure Probability Calculations of Steady State (Continued)

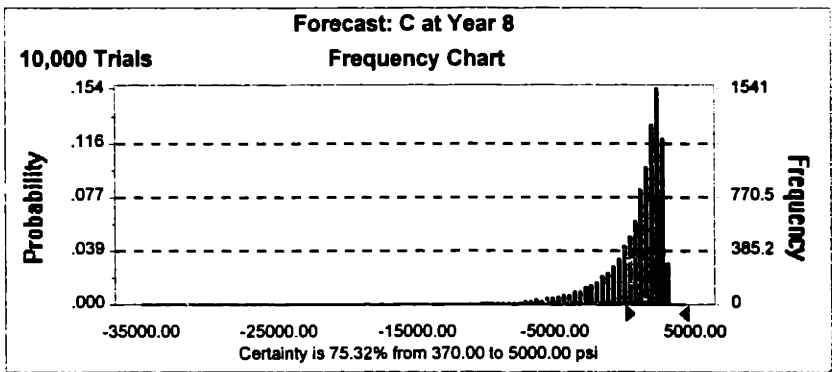

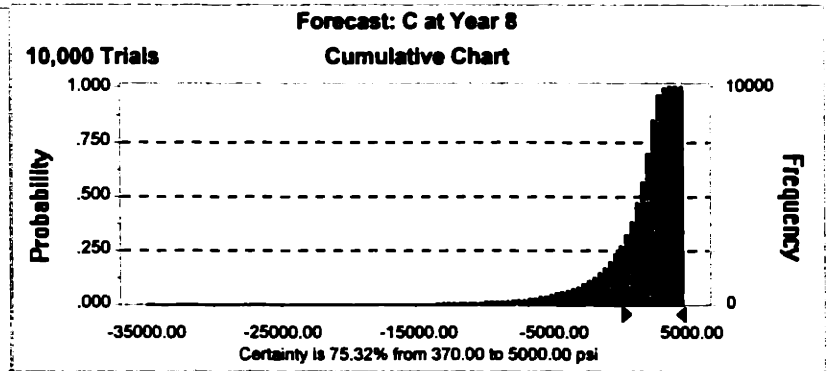

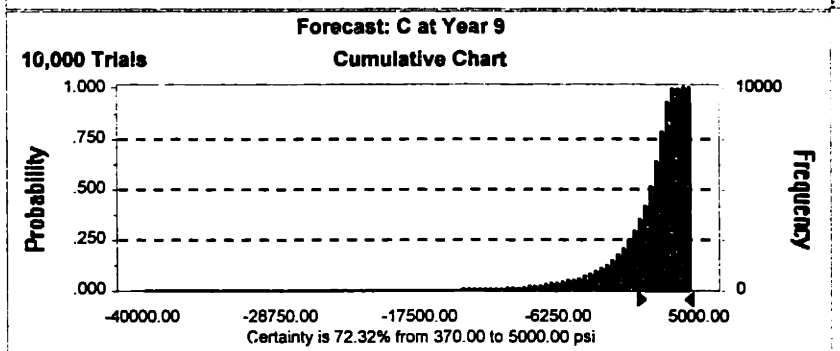

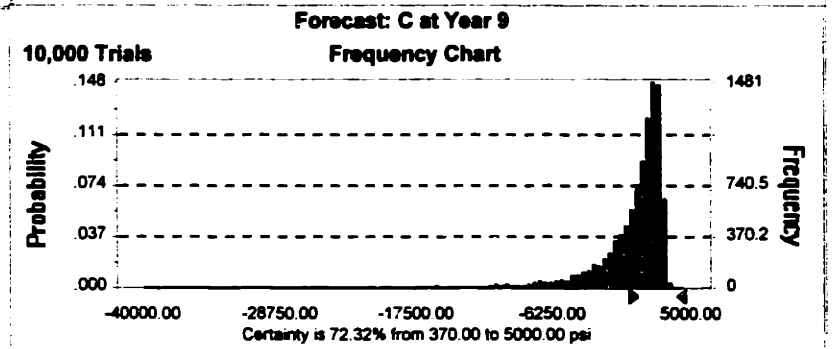

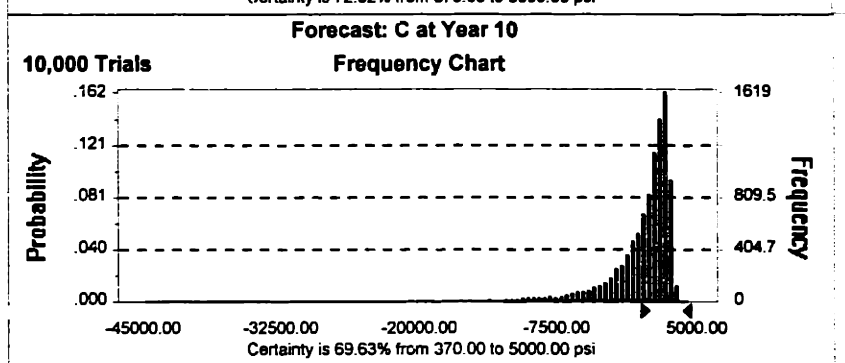

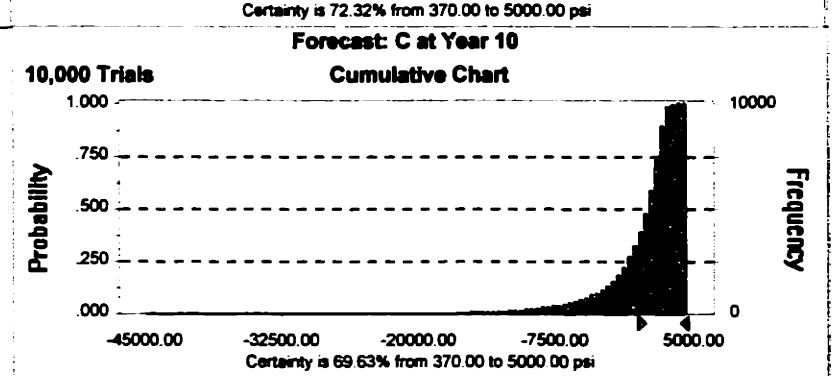

Appendix D: Detailed Failure Probability Calculations due to Transients

Using the Latin Hypercube sampling method. For a lognormal distribution, we may use the mean value of each interval (a total of 20 intervals) as a value representative of that interval (10 years). Using the special function, "dlnorm(x,μ,ω): Returns the probability density for the lognormal distribution". Using 10^3 to express infinite due to Mathcad code's constraint.

$n := 20$

$i := 1..19$

$P_i := P_{i-1} + \frac{1}{n}$

$e_{20} := 10^3$

$e_i := qlnorm(P_i, 0.721, 1.035)$

$i := 0..19$

$$EA_i := \frac{\int_{e_i}^{e_{i+1}} x \cdot dlnorm(x, 0.721, 1.035)\, dx}{\int_{e_i}^{e_{i+1}} dlnorm(x, 0.721, 1.035)\, dx}$$

$\sigma f := 64.5 \cdot 10^3$ $r := 9$

$Wn := 0.500$ $\varepsilon f := 0.039 \cdot 0.25$ $E := EA_{14}$

$Wc1 := 0.059$ $Wc2 := 0.118$ $Wc3 := 0.176$ $Wc4 := 0.233$ $Wc5 := 0.288$

$Wc6 := 0.341$ $Wc7 := 0.393$ $Wc8 := 0.444$ $Wc9 := 0.493$ $Wc10 := 0.541$

$Wm1_i := \frac{Wc1}{2} \cdot E$ $Wm2_i := \frac{Wc1 + Wc2}{2} \cdot E$ $Wm3_i := \frac{Wc2 + Wc3}{2} \cdot E$

$Wm4_i := \frac{Wc3 + Wc4}{2} \cdot E$ $Wm5_i := \frac{Wc4 + Wc5}{2} \cdot E$ $Wm6_i := \frac{Wc5 + Wc6}{2} \cdot E$

$Wm7_i := \frac{Wc6 + Wc7}{2} \cdot E$ $Wm8_i := \frac{Wc7 + Wc8}{2} \cdot E$

$Wm9_i := \frac{Wc8 + Wc9}{2} \cdot E$ $Wm10_i := \frac{Wc9 + Wc10}{2} \cdot E$

Appendix D: Detailed Failure Probability Calculations due to Transients (Continued)

$j := 1..19 \qquad k := 20 \qquad S_0 := 0$

$S_j := S_{j-1} + \frac{1}{k} \qquad Wn_{20} := 100$

$Wn_j := qnorm(S_j, 0.5000, 0.0208)$

$j := 0..19$

$$WN_j := \frac{\int_{Wn_j}^{Wn_{j+1}} x \cdot dnorm(x, 0.5000, 0.0208)\, dx}{\int_{Wn_j}^{Wn_{j+1}} dnorm(x, 0.5000, 0.0208)\, dx}$$

$r_j := r + (0.5 - WN_j)$

$$C1_i := \frac{\sigma f \cdot (Wn_{19-i} - Wm1_i)}{(r_{19-i} + Wm1_i) \cdot (1 + \varepsilon f)} \qquad C2_i := \frac{\sigma f \cdot (Wn_{19-i} - Wm2_i)}{(r_{19-i} + Wm2_i) \cdot (1 + \varepsilon f)} \qquad C3_i := \frac{\sigma f \cdot (Wn_{19-i} - Wm3_i)}{(r_{19-i} + Wm3_i) \cdot (1 + \varepsilon f)}$$

$$C4_i := \frac{\sigma f \cdot (Wn_{19-i} - Wm4_i)}{(r_{19-i} + Wm4_i) \cdot (1 + \varepsilon f)} \qquad C5_i := \frac{\sigma f \cdot (Wn_{19-i} - Wm5_i)}{(r_{19-i} + Wm5_i) \cdot (1 + \varepsilon f)} \qquad C6_i := \frac{\sigma f \cdot (Wn_{19-i} - Wm6_i)}{(r_{19-i} + Wm6_i) \cdot (1 + \varepsilon f)}$$

$$C7_i := \frac{\sigma f \cdot (Wn_{19-i} - Wm7_i)}{(r_{19-i} + Wm7_i) \cdot (1 + \varepsilon f)} \qquad C8_i := \frac{\sigma f \cdot (Wn_{19-i} - Wm8_i)}{(r_{19-i} + Wm8_i) \cdot (1 + \varepsilon f)} \qquad C9_i := \frac{\sigma f \cdot (Wn_{19-i} - Wm9_i)}{(r_{19-i} + Wm9_i) \cdot (1 + \varepsilon f)}$$

$$C10_i := \frac{\sigma f \cdot (Wn_{19-i} - Wm10_i)}{(r_{19-i} + Wm10_i) \cdot (1 + \varepsilon f)}$$

$C1_i := if(C1_i < 0, 0, C1_i)$

$C2_i := if(C2_i < 0, 0, C2_i)$

$C3_i := if(C3_i < 0, 0, C3_i)$

$C4_i := if(C4_i < 0, 0, C4_i)$

$C5_i := if(C5_i < 0, 0, C5_i)$

$C6_i := if(C6_i < 0, 0, C6_i)$

$C7_i := if(C7_i < 0, 0, C7_i)$

$C8_i := if(C8_i < 0, 0, C8_i)$

$C9_i := if(C9_i < 0, 0, C9_i)$

$C10_i := if(C10_i < 0, 0, C10_i)$

$E = 0.90417$

Appendix D: Detailed Failure Probability Calculations due to Transients (Continued)

$\lambda := 0.15$

$TL := 10$

$$Q_i := \exp(\lambda \cdot TL) \cdot 1 \cdot \frac{1}{TL} \cdot \left(\begin{array}{l} \text{pnorm}(C1_i, 440, 14.7) + \text{pnorm}(C2_i, 440, 14.7) + \text{pnorm}(C3_i, 440, 14.7) \ldots \\ + \text{pnorm}(C4_i, 440, 14.7) + \text{pnorm}(C5_i, 440, 14.7) + \text{pnorm}(C6_i, 440, 14.7) \ldots \\ + \text{pnorm}(C7_i, 440, 14.7) + \text{pnorm}(C8_i, 440, 14.7) + \text{pnorm}(C9_i, 440, 14.7) \ldots \\ + \text{pnorm}(C10_i, 440, 14.7) \end{array} \right)$$

$$R := \sum_{i=0}^{19} Q_i \cdot \frac{1}{20}$$

$E = 0.90417$

$R = 0.80209$

$FPtr := 1 - R$

$FPtr = 0.19791$

Q
0.97066
0.86119
0.86071
0.86071
0.86071
0.86071
0.86071
0.86071
0.86071
0.86071
0.86071
0.86043
0.85333
0.80972
0.75345
0.74108
0.74082
0.74082
0.74082
0.22313

e
0
0.08862
0.12907
0.16634
0.2035
0.24193
0.28259
0.32634
0.37411
0.42696
0.48627
0.55381
0.63205
0.72456
0.83674
0.97736
1.16192
1.42149
1.832
2.66825
1000

r
9.0429
9.0301
9.02399
9.01947
9.01573
9.01245
9.00945
9.00663
9.00394
9.00131
8.99869
8.99606
8.99337
8.99055
8.98755
8.98427
8.98053
8.97601
8.9699
8.95709

Wn
0
0.46579
0.47334
0.47844
0.48249
0.48597
0.48909
0.49199
0.49473
0.49739
0.5
0.50261
0.50527
0.50801
0.51091
0.51403
0.51751
0.52156
0.52666
0.53421
100

WN
0.4571
0.4699
0.47601
0.48053
0.48427
0.48755
0.49055
0.49337
0.49606
0.49869
0.50131
0.50394
0.50663
0.50945
0.51245
0.51573
0.51947
0.52399
0.5301
0.54291

Appendix D: Detailed Failure Probability Calculations due to Transients (Continued)

C1 =	C2 =	C3 =	C4 =	C5 =
3608.75572	3210.38472	2820.00629	2440.70317	2075.41887
3549.96633	3152.50546	2763.01242	2384.56342	2020.09596
3511.37926	3114.41412	2725.4038	2347.4209	1983.39959
3480.8819	3084.2942	2695.65149	2318.02362	1954.34223
3454.79425	3058.52369	2670.18988	2292.86038	1929.46468
3431.41263	3035.42323	2647.36329	2270.29834	1907.15597
3409.77852	3014.04729	2626.23885	2249.41686	1886.50713
3389.27543	2993.78745	2606.21598	2229.62291	1866.9324
3369.46024	2974.20621	2586.86267	2210.48978	1848.01015
3349.97904	2954.95403	2567.83361	2191.67629	1829.4031
3330.51688	2935.71975	2548.82133	2172.8785	1810.81073
3310.76048	2916.19372	2529.51977	2153.79379	1791.93372
3290.36128	2896.03136	2509.58816	2134.08513	1772.4386
3268.8869	2874.80506	2488.60359	2113.33412	1751.91129
3245.74089	2851.92484	2465.98236	2090.96313	1729.78
3220.00399	2826.48115	2440.82439	2066.08126	1705.16259
3190.06011	2796.87453	2411.54643	2037.12091	1676.5065
3152.48456	2759.71422	2374.79084	2000.75647	1640.51682
3097.05858	2704.87648	2320.52659	1947.04662	1587.33826
0	0	0	0	0

Appendix D: Detailed Failure Probability Calculations due to Transients (Continued)

C6	C7	C8	C9	C10
1726.97133	1391.71476	1066.15667	753.17309	452.44796
1672.42237	1337.90563	1013.06144	700.75999	400.68638
1636.14911	1302.03718	977.58392	665.65631	365.94006
1607.41416	1273.61075	949.45551	637.81294	338.3692
1582.80762	1249.26357	925.35888	613.95596	314.74138
1550.73924	1227.42519	903.74271	592.55236	293.54102
1540.31112	1207.20832	883.72994	572.73484	273.91021
1520.94439	1188.04068	864.75464	553.94354	255.29487
1502.2222	1169.50999	846.40898	535.77489	237.2955
1483.81103	1151.2863	828.36645	517.90567	219.59203
1465.41358	1133.07543	810.33584	500.04754	201.89884
1446.73363	1114.58413	792.02683	481.91293	183.93101
1427.44114	1095.4856	773.11572	463.18114	165.37073
1407.12611	1075.37378	753.20027	443.45357	145.82286
1385.22228	1053.6877	731.72462	422.17927	124.74113
1360.85584	1029.56155	707.83067	398.5075	101.28189
1332.48852	1001.47069	680.00701	370.93953	73.95849
1296.85453	966.17731	645.04284	336.29043	39.6108
1244.18039	913.98628	593.31887	285.01356	0
0	0	0	0	0